JPL PUBLICATION 84-5

N84-28355

Satellite-Derived Sea Surface Temperature: Workshop-II

June 22-24, 1983
Pasadena, California

February 15, 1984

NASA
National Aeronautics and Space Administration
Jet Propulsion Laboratory
California Institute of Technology
Pasadena, California

JPL PUBLICATION 84-5

Satellite-Derived Sea Surface Temperature: Workshop-II

June 22-24, 1983
Pasadena, California

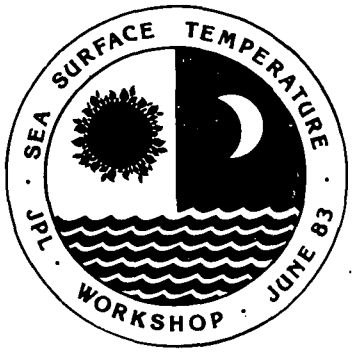

February 15, 1984

NASA
National Aeronautics and
Space Administration

Jet Propulsion Laboratory
California Institute of Technology
Pasadena, California

This publication was prepared by the Jet Propulsion Laboratory, California Institute of Technology, under a contract with the National Aeronautics and Space Administration.

ABSTRACT

Satellite-Derived Sea Surface Temperature Workshop-II is the second in a series of three workshops designed to evaluate global accuracies and error characteristics of presently orbiting satellite sensors. The workshops are intended to lead to a better understanding of present capabilities for sea surface temperature measurement and to improved measurement concepts for the future.

Workshop-II focused primarily on December 1981 data from the AVHRR and SMMR. Some November 1979 data from the HIRS and AVHRR were also examined. Comparisons of satellite data with ship and XBT measurements showed standard deviations in the range 0.5 to 1.3°C with biases of less than 0.4°C, depending on the sensor, ocean region, and spatial/temporal averaging. SST anomaly maps showed good agreement in some cases, but a number of sensor-related problems were identified. These will be further investigated by examining additional data in Workshop-III.

ACKNOWLEDGEMENTS

A number of individuals contributed to Workshop-II. SMMR data were provided by A. Milman, T. Wilheit, C. Prabhakara, and E. Njoku. AVHRR global-coverage data were obtained from NOAA/NESDIS and reviewed by P. McClain. R. Bernstein provided local area coverage AVHRR data. HIRS/MSU data were provided by J. Susskind and M. Chahine, and J. Bates discussed VAS data. Ship and buoy data were collected and analyzed by S. Pazan. Discussion sessions were led by T. Barnett, D. Chelton, D. Hagan, and E. Njoku. Intercomparison of global data sets and generation of analysis products were performed on the JPL Pilot Ocean Data System (PODS) by J. Hilland and the PODS staff. The first part of this report was compiled from written contributions submitted by the above participants. Symposium papers on satellite SST measurement were presented by several authors, and valuable contributions to the discussions were made by all participants. The workshop was chaired by E. Njoku. A complete list of the workshop attendees is provided in Appendix C.

The workshop was sponsored by the Oceanic Processes Program, Earth Science and Applications Division, of the National Aeronautics and Space Administration.

GLOSSARY

AVHRR	Advanced Very High Resolution Radiometer
ENSO	El Nino Southern Oscillation
FGGE	First GARP Global Experiment
FNOC	Fleet Numerical Oceanography Center
GARP	Global Atmospheric Research Program
GOSSTCOMP	Global Operational Sea Surface Temperature Computation
HIRS	High Resolution Infra-Red Sounder
ITCZ	Inter-Tropical Convergence Zone
JPL	Jet Propulsion Laboratory
MCSST	Multi-Channel Sea Surface Temperature
MSU	Microwave Sounding Unit
NESDIS	National Environmental Satellite, Data, and Information Service
NOAA	National Oceanic and Atmospheric Administration
PEG	Pacific Environmental Group
PODS	Pilot Ocean Data System
SIO	Scripps Institution of Oceanography
SMMR	Scanning Multichannel Microwave Radiometer
SST	Sea Surface Temperature
STD	Salinity, Temperature, Density, Measuring Instrument
TIROS	Television Infrared Observational Satellite
TOGA	Tropical Ocean Global Atmosphere
VAS	Visible Infrared Spin-Scan Radiometer Atmospheric Sounder
XBT	Expendable Bathythermograph

CONTENTS

PART I: GLOBAL DATA ANALYSIS

PART II: SYMPOSIUM PAPERS

CONTENTS (Continued)

PART I: GLOBAL DATA ANALYSIS

SECTION I
INTRODUCTION

I.1 Background

The role of satellites in monitoring conditions of the Earth's atmosphere and surface is an increasingly important one. Satellite measurements are particularly useful in the fields of oceanography and climate because vast areas of the ocean cannot be sampled adequately by other means. Ocean surface temperatures have been measured continuously from satellites since the early 1970s. Only recently, however, have the accuracies of these measurements approached levels where they become useful for scientific research and commercial applications (approximately $1^{o}C$ or less). At the same time, models of ocean currents and air-sea interaction have developed to the stage where satellite data can be effectively utilized in conjunction with data from existing networks of surface sensors (i.e. ships, aircraft, and buoys).

A series of workshops was initiated under NASA sponsorship to evaluate present accuracies of satellite-derived sea surface temperature measurements and to examine their utility for scientific and commercial applications. The satellite sensors studied in the workshops, all currently operating, are the Advanced Very High Resolution Radiometer (AVHRR), the High Resolution Infrared Sounder and Microwave Sounding Unit (HIRS/MSU), the Scanning Multichannel Microwave Radiometer (SMMR), and the Visible Infrared Spin-Scan Radiometer Atmospheric Sounder (VAS). These instruments employ different techniques for measuring SST, and each has unique advantages and limitations. Their estimated accuracies lie in the 0.5 to $1.5^{o}C$ range.

The workshop approach is to examine global data sets from each sensor for the same time periods and geographic locations, and to compare them against each other and against common in situ data using common analysis methods. The Pilot Ocean Data System (PODS) at the Jet Propulsion Laboratory has provided an appropriate mechanism for computer-based analysis of the different data sets. Four months of data were selected for study in the workshops: November 1979, December 1981, March 1982, and July 1982. Satellite-derived and in situ SSTs for these months were delivered to JPL, archived on PODS, and processed through specially developed software to provide comparison products for evaluation. The first workshop (Workshop-I) was held at the Jet Propulsion Laboratory, Pasadena, on January 27 and 28, 1983. A report of that workshop has been published (Ref. 1). A more detailed discussion of workshop background and rationale, and satellite sensor descriptions, can be found in the Workshop-I report.

I.2 Workshop-I Results

In Workshop-I, Nimbus-7 SMMR data were evaluated for November 1979, which also provided a test of the data analysis methods implemented on PODS. Three versions of SMMR sea surface temperatures were examined (produced with different algorithms), and were compared with ship SST data obtained from Fleet Numerical Oceanography Center (FNOC), and with climatology. SST measurements were compared point-to-point within specified time and space windows, and as monthly averages in $2^{o}x2^{o}$ latitude-longitude bins.

Analysis products included global maps of raw observation locations, contour maps of absolute SST, contour maps of SST anomaly (difference from climatology), histograms of SST in 20° latitude bands, and scatterplots of sensor SST versus climatology and of SST from one sensor versus another.

The results confirmed that FNOC ship data (engine intake and bucket temperatures) are noisy and must be carefully edited. Even after editing they are too noisy to be used for evaluating satellite SST accuracy in point comparisons. As binned monthly averages, however, they are useful for comparing SST anomalies and for evaluating bias drifts in the satellite data (i.e. although the ship data may have a bias of a few tenths °C, this bias tends to be fairly uniform in space and time).

Anomaly maps generated from ship and SMMR data in the north Pacific showed some similarities but the agreement was not satisfactory. One of the major areas of disagreement occurred as one proceeded north of 40°N where the SMMR showed an increasing warm bias. The rms difference between the binned SMMR and ship data in the north Pacific was approximately 1.3°C. The reader is referred to the Workshop-I report (Ref. 1) for more discussion of these results. Several recommendations were made concerning improvements to the methods of analysis and data displays. Most of these were implemented for Workshop-II and are discussed in the next section.

I.3 Workshop-II Data Sets and Processing

Table 1-1 lists the SST data sets available for Workshops I, II, and III. November 1979 data from SMMR and FNOC ships were examined in Workshop-I. For Workshop-II, December 1981 data from SMMR, AVHRR, FNOC ships, and TRANSPAC XBTs were evaluated. Also, some HIRS and AVHRR (GOSSTCOMP) data from November 1979 were studied. Approximately half the remaining data, primarily March and July 1982, are scheduled for processing and evaluation in Workshop-III (to be held in February 1984).

A major change in the processing approach was adopted for Workshop-II in that all sensor SSTs were evaluated as deviations from climatology. Removing the long-term mean geophysical signal in this manner permitted a better evaluation of sensor capabilities for detecting real signals of interest, i.e. deviations from the climatological average (which rarely exceed ±3°C). The climatology used was that produced by Reynolds (Refs. 2,3) on a 1° latitude-longitude grid. The climatology was interpolated linearly in space and time to the positions of each sensor SST measurement, and subtracted. These "raw anomalies" were maintained as separate files and were also averaged for the month into 2° latitude-longitude cells to form "binned anomalies". Raw anomalies with absolute values greater than 5.75°C were filtered out prior to binning. Monthly averaged "absolute" SSTs were obtained by adding the binned SST anomaly to the climatological value at the center of each bin.

The products generated for the workshop on the Pilot Ocean Data System were either "global" or "regional". Global refers to processing of all SST data received at JPL for the given month, whereas regional products were limited to three regions: N. Pacific, S. Pacific, and N. Atlantic. Tables 1-2 and 1-3 list the global and regional products. As shown in Table 1-1, the main data sets studied in Workshop-II were SMMR, AVHRR, FNOC ships, and XBTs

Table 1-1. Data Sets Available for Workshop Processing

	November 1979	December 1981	March 1982	July 1982
SMMR	1	2	3	3
AVHRR	2*	2	3	3
HIRS/MSU	2*	3	3	3
VAS	-	-	3	3
FNOC SHIP	1	2	3	3
FGGE BUOY	2*	-	-	-
TRANSPAC XBT	2*	2	3	3
OTHER+	-	-	3	3

NOTES: 1 = available for Workshop-I
2 = available for Workshop-II
3 = available for Workshop-III
* delayed processing
+ limited additional fixed buoys, research ships, etc.

for December 1981. Three SMMR SST versions were examined, produced using different algorithms by A. Milman/T. Wilheit, C. Prabhakara, and E. Njoku, respectively. Two versions of AVHRR SSTs were provided, one being the global MCSST data set generated operationally by NOAA/NESDIS, the other being a local-area, high-resolution data set provided by R. Bernstein. Not all the comparison products listed in Tables 1-2 and 1-3 were generated for each SST data set since some would have been inappropriate. (For example, the Bernstein AVHRR and Njoku SMMR data sets were provided for the Pacific only, hence no regional plots in the north Atlantic were made).

In addition to the December 1981 data, some results were available from the November 1979 HIRS MSU data provided by J. Susskind. Additional processing of this data set was performed subsequent to the workshop, and some results have been included in this report. Due to space limitations, only one set of results from each sensor are presented. These are the Wilheit/Milman SMMR, the NOAA/NESDIS AVHRR (MCSST), and the Susskind/Chahine HIRS. Descriptions of these sensors and retrieval algorithms can be found in Ref. 1. Summary papers describing updates to the sensor data products can be found in Part II of this report.

I.4 Workshop-II Format

The Workshop-II Agenda is provided in Appendix B. The program was divided into three parts: (a) Review of global SST data comparisons, (b) Symposium papers on satellite SST measurements and applications, and (c) Discussion sessions on major topics of interest.

Table 1-2. Global Comparison Products for Workshop-II

1. Global Distribution Maps of Raw SST Observation Locations
2. Histograms of Raw SST Anomalies; 55°S to 55°N, 0° to 360°E
3. Contour maps of Absolute SST
4. Gray Scale Maps of Binned SST Anomalies
5. Contour Maps of Binned SST Anomalies
6. Gray Scale Maps of Binned Data Density
7. Contour Maps of Binned Data Density
8. Scatter Plots of Binned SST Anomalies versus Climatology; 55°S to 55°N, 0° to 360°E
9. Scatter Plots of Binned SST Anomalies versus Climatology; 60°S to 60°N, 0° to 360°E, in 20° Latitude Bands
10. Tables of Correlations between Binned SST Anomalies; 55°S to 55°N, 0° to 360°E
11. Tables of Partitioned error in Binned SST Anomalies; 55°S to 55°N, 0° to 360°E

Table 1-3. Regional Comparison Products for Workshop-II

North Pacific: 0° to 55°N, 100°E to 290°E
South Pacific: 55°S to 0°, 100°E to 290°E
North Atlantic: 0° to 55°N, 290°E to 360°

1. Histograms of Raw SST Anomalies
2. Scatter Plots of Raw SST Anomalies, Sensor versus Sensor (Windows: 12 hr/100 km, 12 hr/20 km, 6 hr/100 km)
3. Gray Scale Maps of Binned SST Anomalies
4. Contour Maps of Binned SST Anomalies
5. Scatter Plots of Binned SST Anomalies, Sensor versus Sensor
6. Scatter Plots of Binned SST Anomalies versus Climatology
7. Tables of Correlations between Binned SST Anomalies
8. Tables of Partitioned Error in Binned SST Anomalies

The Symposium papers provided considerable insight into present applications and problems of satellite data from a user standpoint, and those for which written material was provided have been grouped together in Part II of the report.

SECTION II
IN SITU DATA

A review of in situ data compiled for the SST workshops can be found in Ref. 1. This discussion is intended to supplement and complement that review with information pertinent to the second workshop; detailed discussion of the Reynolds climatology and results of the first workshop will not be reproduced here.

II.1 Sources of Data and Processing Techniques

Ship Data

Ship injection temperature data for December 1981 were obtained by PODS from the Fleet Numerical Oceanography Center (FNOC). These reports were from ships and buoys reporting synoptically over the Global Telecommunications System. FNOC routinely archives the radioed marine weather reports and sends them to the Scripps Institution of Oceanography (SIO), where they were acquired for JPL/PODS by S. Pazan. These radio reports were edited and then summarized into 1^{o} lat-lon bins at JPL.

Fairly extensive editing procedures were applied to the ship data set after obtaining it from SIO. First, land data were edited from the file. The particular set of tapes obtained included land reports (as distinct from ship reports), and over half of the total reports were eliminated on the first pass (Table 2-1.)

The remaining ship reports were indexed by ship name and date/time, and the speed of each ship as calculated from the position and date/time of its last two reported positions was calculated. If the speed exceeded 35 knots the report was rejected. Next, ship reports without a sea surface temperature were rejected, and then sea surface temperatures less than $0^{o}C$ or more than $35^{o}C$ were also rejected. Following the gross edit an edit against climatology was applied. At a few points there was no climatology to edit against and those points were discarded.

Table 2-1. Data Editing Budget For FNOC Ship Reports

SHIP DATA EDIT BUDGET	NUMBER	PERCENT OF TOTAL
ORIGINAL FILE	304,715	100%
Land	166,318	55%
OCEAN FILE	138,397	100%
Ship Speed	~17,000	~2%
No SST Data	14,439	10%
Gross Edit	9,032	7%
Climatology Edit	45,632	33%
No Climatology	32	<<1%
O.K.	52,260	38%

The procedure for editing against climatology was developed by Roger Bauer of Compass Systems, Inc., and Doug McLain of the NOAA Pacific Environmental Group (PEG) at FNOC. The technique edits data that vary by more than a threshold value from the climatological mean. The threshold is determined from climatology as follows: For the December 1981 ship data set, the November, December and January climatological monthly means for each 2^{o} square are read from the PODS climatology file (derived from the original 1^{o} lat-lon Reynolds climatology (Ref.2)). Six differences are made from the climatological field: two north-south differences; two east-west differences; and two time differences, November from December and December from January. The maximum of these six differences is the "index of variability" for each 2^{o} square in the December climatology. A tolerance limit was set somewhat arbitrarily at 1.3 times this index of variability. If any of the first 10 observations in a month and 1^{o} square differed by more than the tolerance limit from the mean for that month and 1^{o} square, it was discarded. After 10 good observations had been obtained in this way, the edit was continued with respect to the mean of the observations in that month, rather than the climatological mean. This allows the signal of large, non-stationary events to come through.

XBT Data Summaries

A discussion of the XBT data acquisition can be found in Ref. 1. The TRANSPAC XBT data volume is adequate to produce bi-monthly anomaly fields on a 5^{o} grid on the major trade routes between Japan and the United States in the central North Pacific, around Hawaii, and in areas north of Tahiti and New Caledonia/Fiji. It is not adequate, however, to produce maps of monthly anomaly fields on a 2^{o} grid using the simple binning method of the Workshop. PODS has received and will continue to receive XBT cast data from the edited TRANSPAC file for the Workshop months.

II.2 Data Quality and Spatial/Temporal Coverage

Marine Weather Report Data from Ships

These temperatures are roughly accurate only to the nearest degree Celsius, and there are intake temperature biases of up to several tenths of a degree, generally positive, depending on season and ship position (Refs. 4 and 5). Bucket temperatures were the earliest sea surface temperature data to be systematically archived. Engine intake temperatures, however, form the greatest part of the weather report data set, particularly after World War II. Intake temperatures are biased up to perhaps $0.5^{o}C$ higher than bucket temperatures, as is apparent from comparing average temperatures from before 1930, when bucket temperatures predominated, with those after 1950 when intake temperatures predominated (Ref. 21). The difference has been ascribed to the effect of warm engine room temperatures on the intake thermistor, and evaporative effects on bucket temperatures.

XBT Accuracy

The companies that make XBTs have tested and rated them, claiming accuracies of about $0.1^{o}C$. It takes around 0.1 second for the XBT thermister to correctly read the water temperature after it penetrates the surface. Water

with an exponential temperature profile tends to force the equilibrium depth of the instrument to around 4 meters (Ref. 6). This may be an important effect in temperate and northern latitudes, particularly during wintertime cold air outbreaks. Where such a lag bias is a problem, some investigators believe that surface temperatures should be derived by extrapolation from the 4m level to the surface.

There have been some studies of this lag bias effect. During the POLE experiment in the Northern Pacific in February 1974, for example, intercomparison of XBT and STD temperatures showed "large error with respect to the STD data ... (which) indicate that XBT reads consistently high ..." (Ref. 7). Barnett et al (Ref. 7) assumed a positive bias of 0.38°C in all XBT temperatures when performing calculations with them. This bias brought XBT values to within $\pm$0.2°C of the STD temperatures. In another study in the Northeastern Pacific (Ref. 8) XBT surface temperatures had a bias of 0.16°C and RMS of 0.14°C.

Ship Data Coverage

Figure 2-1(a) is a scatterplot of the number of ship reports in December 1981. There were about 50,000 edited ship reports in this month. Most of the observations occur at the synoptic hours of 0000, 0600, 1200 and 1800 GMT.

XBT Data Coverage

Figure 2-1(b) is a scatterplot of the XBT drops for December 1981. Data are concentrated along ship tracks between North America, Japan, New Caledonia, Hawaii, Tahiti and the Panama Canal. A scattering of other points occurs wherever fishing vessels or military vessels have reported casts. Particular concentrations of casts may be noted off the west coast of North America, and Japan and the Japan Sea. For this month there were 604 drops utilized by PODS.

II.3 Characteristics of Binned and Contoured Data

Global Reynolds Climatology

Climatological SST for the Pacific (Figure 2-2(a)) and Atlantic and Indian Oceans (Figure 2-2(b)) are taken from Reynolds (Ref. 2). These December climatologies show such seasonal features as the cool temperatures in northern temperate latitudes, warm temperatures in southern temperate latitudes, warm temperatures off the coast of Peru, cool temperatures in the California coastal waters and off Western Africa, and warm temperatures off southwest Africa. In general, the features are those one would expect in northern hemisphere winter.

Global Binned Ship SST

The binned ship SST anomalies in the Pacific and Atlantic were computer-contoured for the month of December 1981 (Figure 2-3(a), (b)). Contouring was limited to the northern hemisphere because of the lack of data south of 20°N. There are three anomalies of 1°C/1000 km scales in both the Atlantic and Pacific. There are negative (cold) anomalies associated with the Kuroshio and Gulf Stream at 35-45°N and 25-35°N, respectively. These anomalies probably arise from a combination of the smeared resolution of the

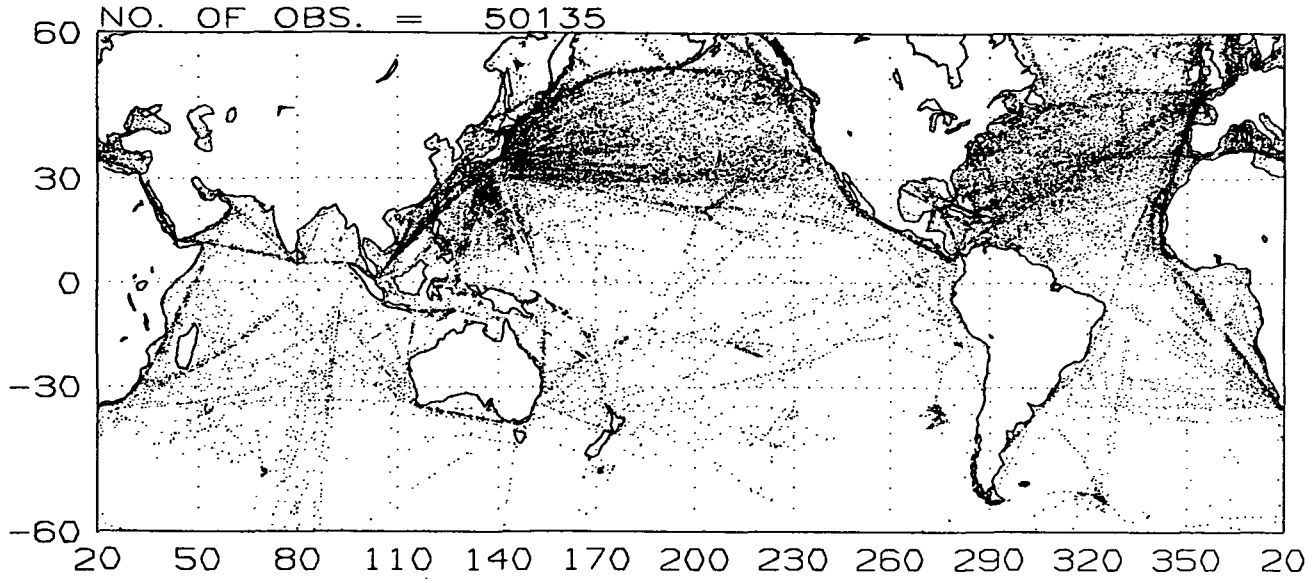

(a)

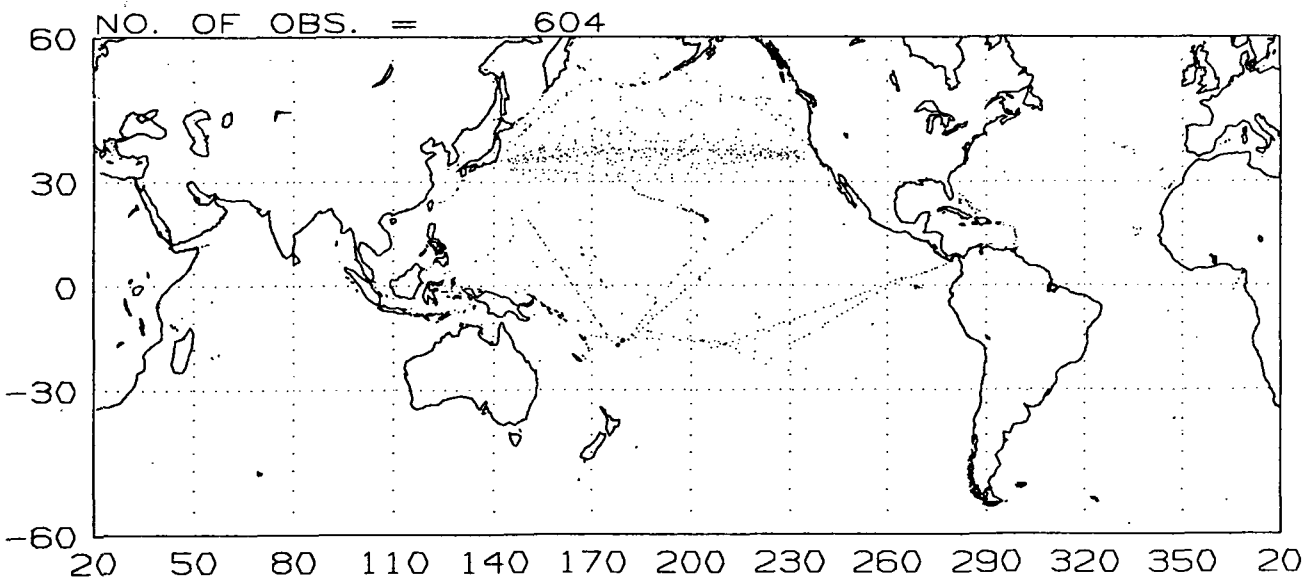

(b)

Figure 2-1. Distribution of global, in-situ SST measurements for December, 1981. (a) Ship reports. (b) TRANSPAC XBTs

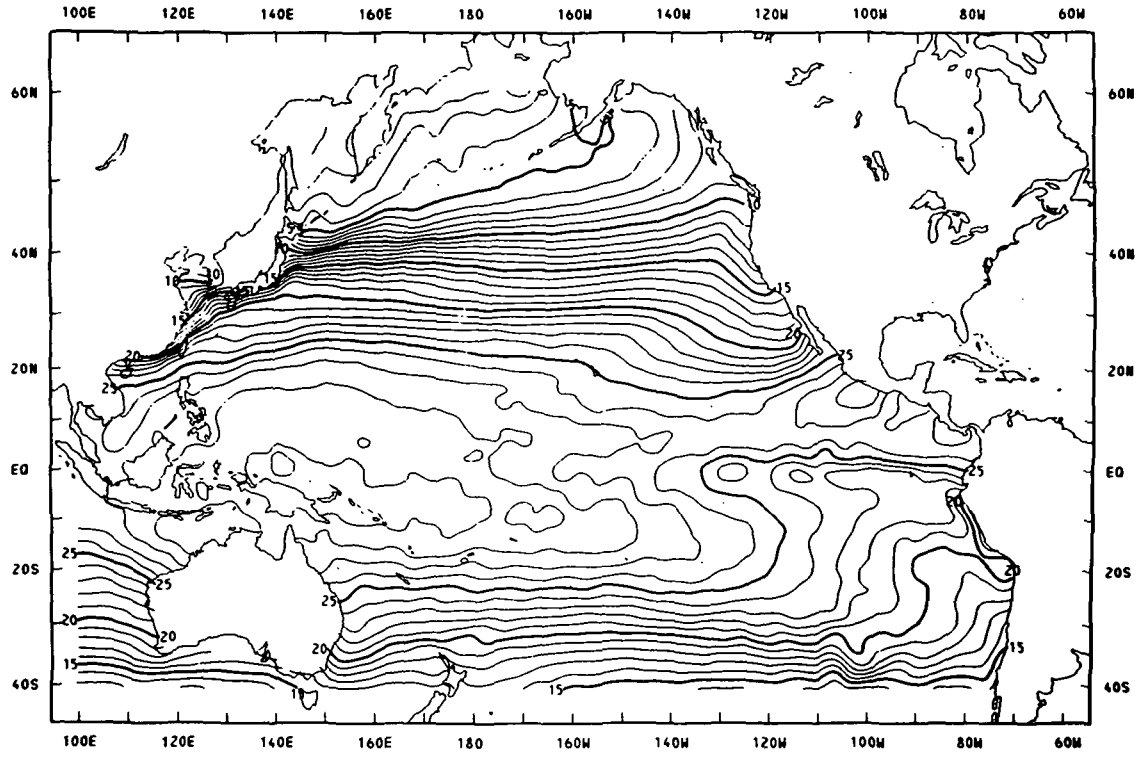

(a)

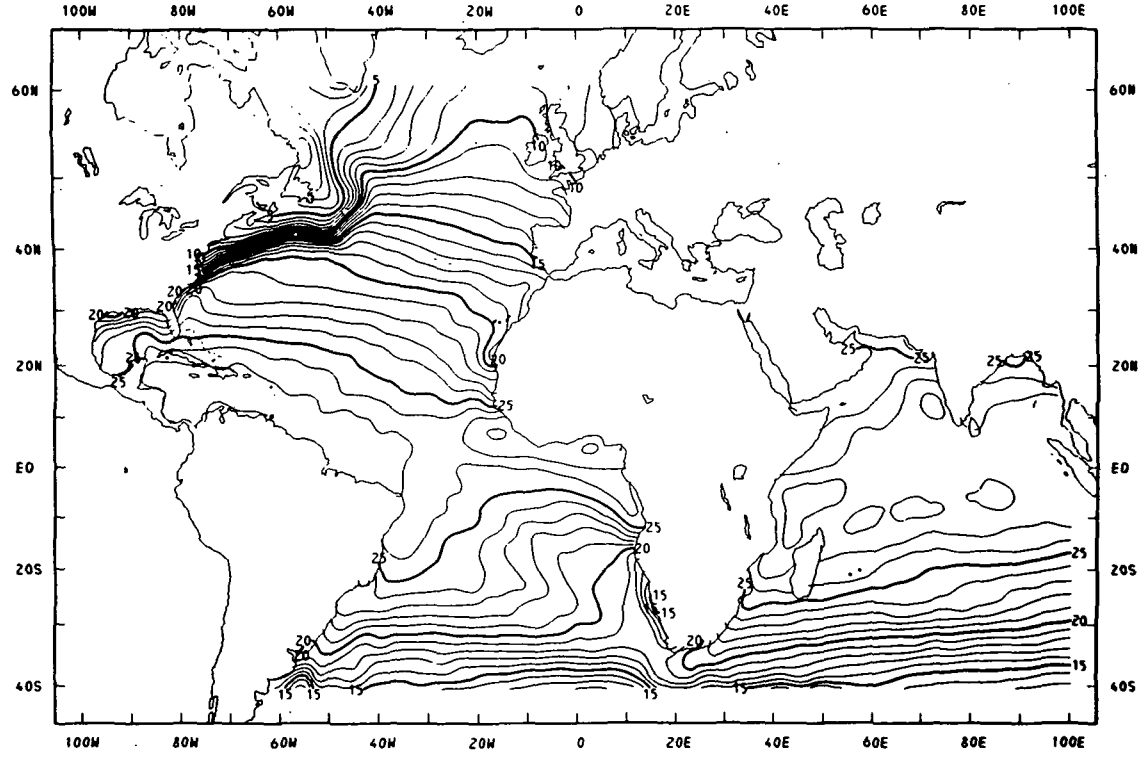

(b)

Figure 2-2. Monthly averaged climatology of SST for December. Countour interval is 1^{o} C. (a) Pacific Ocean. (b) Atlantic and Indian Oceans. (Source: Ref. 2)

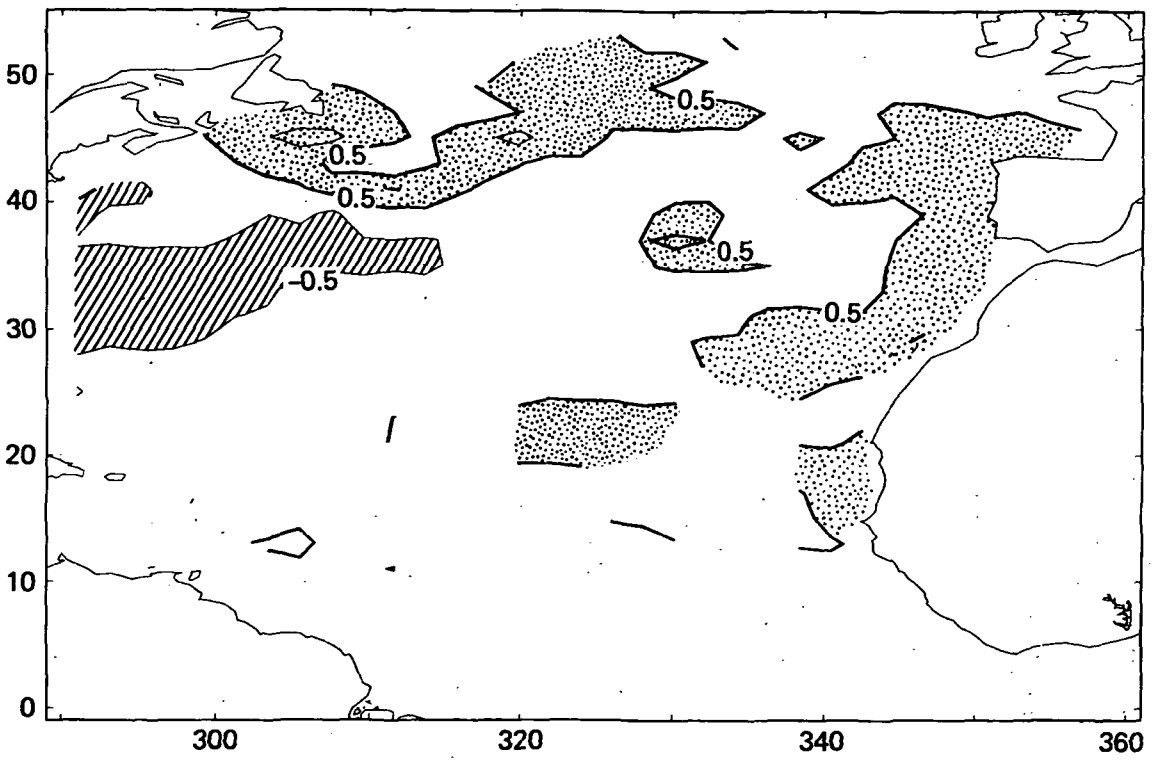

(a)

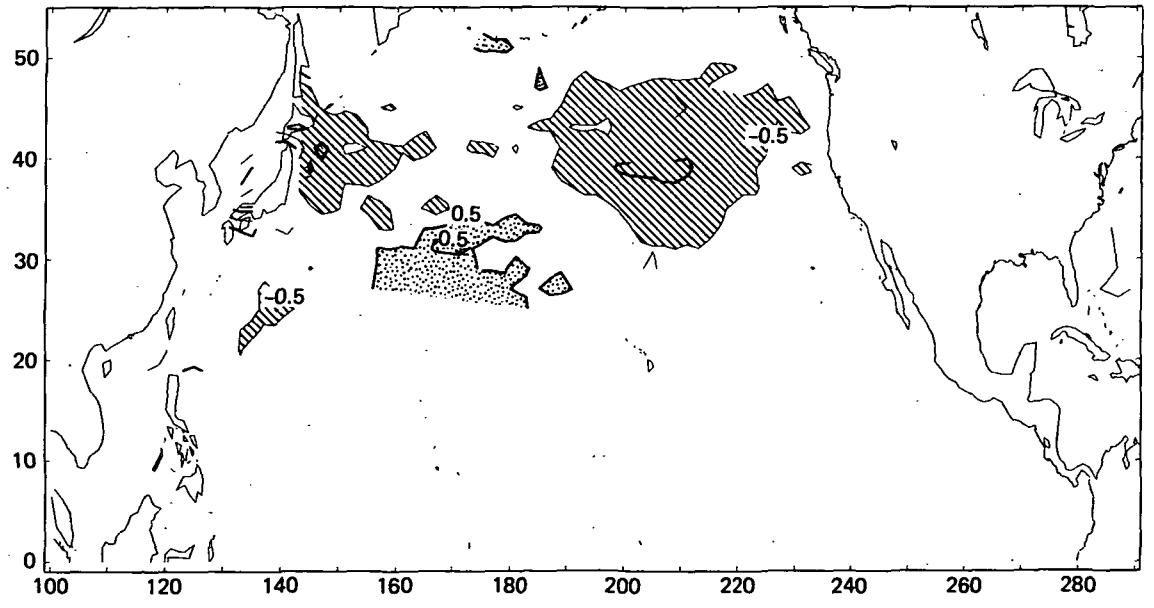

(b)

Figure 2-3. Countour map of SST anomalies from ship reports for December 1981. (a) North Atlantic Ocean. (b) North Pacific Ocean

western boundary currents in the climatology and from actual changes in the strength and position of these western boundary currents for this particular December. There is a $\geq 0.5^{o}C$ negative anomaly in the eastern North Pacific at 30-50°N and 190-220°E, reaching a maximum value of $-1^{o}C$ at about 40°N, 200°E. There is a positive (warm) anomaly in the North Pacific at about 25-35°N and 155-180°E. In the Atlantic, there is a positive $0.5^{o}C$ anomaly stretching east of Labrador and Nova Scotia to 330°E. Another positive anomaly stretches from the Bay of Biscay to West Africa, in the area bounded by roughly 25-45°N and 330-355°E. These six anomalies are of sufficient intensity and scale to be resolved by the contoured ship data. They should also be observable in the satellite-derived SST fields for this month (see Section III).

The histogram of raw ship SST anomalies in Figure 2-4(a) shows a somewhat asymmetric distribution, slightly biased to positive values, with fairly large outliers. The climatology was created in large part from bucket temperatures, which should be lower on average than the intake temperatures that make up the present day ship SST reports (see Section II.2). Also, the climatology was created from older reports, when the average sea temperature was lower over the entire globe. This factor may possibly account for the positive bias in the histogram. The outliers may be due in large part to large anomalies in the region of the western boundary currents.

The histogram of raw XBT anomalies in Figure 2-4(b) shows a small bias towards negative values, again implying that the ship temperatures may be biased high. This cannot be stated conclusively however since the XBT coverage is very limited with respect to that of the ships. A few large outliers are also observed in the XBT histogram.

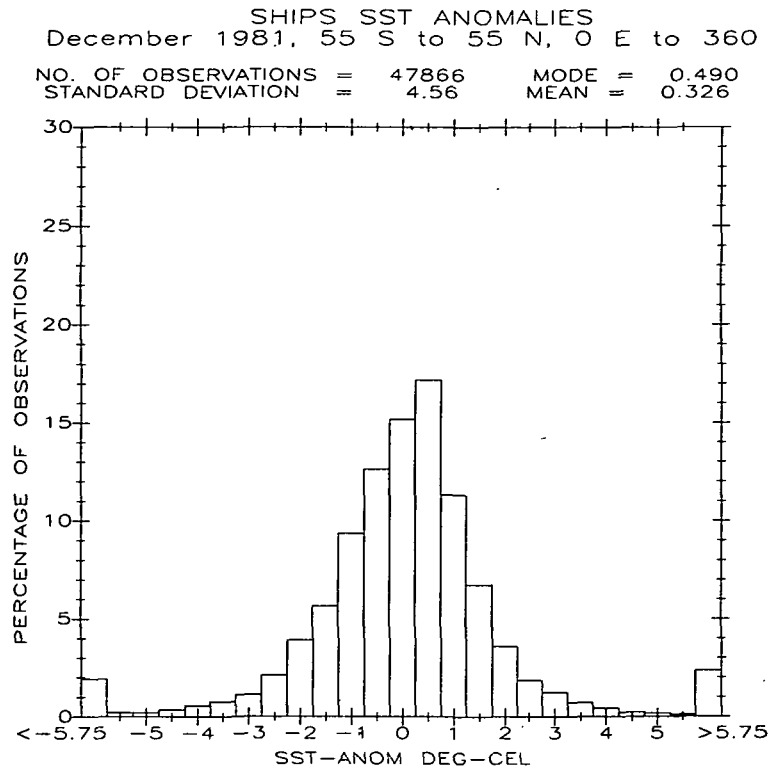

(a)

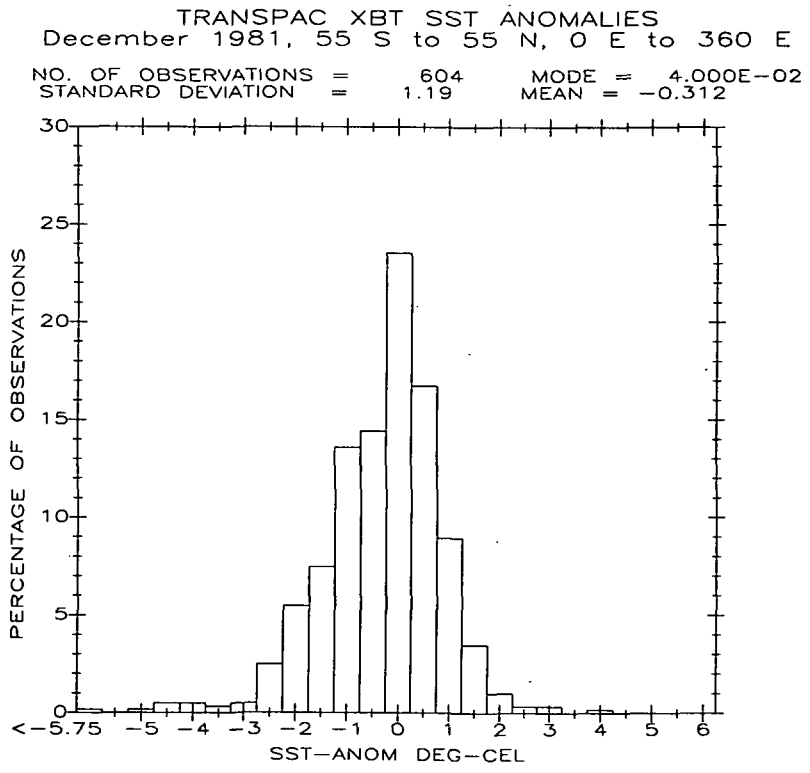

(b)

Figure 2-4. Raw SST anomaly histograms for global in-situ data. (a) Ship reports. (b) TRANSPAC XBTs

SECTION III
SATELLITE DATA

Of the three primary satellite data sets studied in the workshop, two were from December 1981 (AVHRR and SMMR), and the third (HIRS) was from November 1979. The HIRS data were compared retrospectively with other November 1979 satellite and in situ data sets examined in Workshop-I. Descriptions of the satellite sensors and retrieval algorithms were provided in the Workshop-I report (Ref. 1). Additional sensor information relevant to this workshop is provided in Part II of this report.

III.1 Data Coverage and Distribution

Due to different spatial resolutions, swath widths, and data editing requirements (cloud filtering, night only, etc.) global distributions of raw SST retrievals from the various sensors are quite different. The total number of raw SST observations obtained globally between latitudes $\pm 60^{o}$ for the months stated above were AVHRR: 804,885, SMMR: 16,652, and HIRS: 75,751. Figure 3-1 shows the number distributions of raw SST retrievals falling within each 2^{o} lat-lon bin. Note that to accommodate the wide disparities in sensor data density the gray-levels are scaled differently in each case.

The AVHRR global-area coverage data (Figure 3-1(a)) has a wide swath (~2500 km) and high sampling density (up to 25 km) in cloud-free areas. This leads to a high count of total SST observations in any given month, limited mainly by editing of cloud-contaminated data. Thus, in cloud-free areas, over 300 observations per month per 2^{o} lat-lon bin are common. In cloudy regions, especially along the convergence zones, the data count is much reduced, and in a few areas no observations at all may be possible for the whole month.

Figure 3-1(b) shows the HIRS coverage (swath width 2,240 km; sample spacing 125 km). HIRS SST retrievals can be obtained under partly cloudy conditions, hence the percentage reduction in data density along the ITCZ and other cloudy regions is not as marked as with the AVHRR.

The SMMR, for reasons discussed in Workshop-I, is limited for useful SST retrievals to night-only operation and center-swath cells (Ref. 1). In addition, the instrument is turned on only every other day. The reduced swath width (450 km) and sample spacing (150 km), plus the other factors just mentioned, result in a relatively low monthly data count for the SMMR. A 600 km coastal area is also deleted from the coverage because of probable data contamination from land radiation in the antenna sidelobes. Most of these sources of data reduction are due to poor instrument design, as opposed to problems inherent in the microwave technique, and are further discussed in Section V. Figure 3-1(c) shows the resulting SMMR coverage density. The overlapping night-time orbital pattern is clearly visible. The SMMR SST retrieval algorithms make no requirement for editing in cloudy regions unless rain is present (as determined by the SMMR rain-rate retrieval algorithm).

For comparison with the satellite data coverage maps, Figure 3-1(d) shows the ship SST data density (another way of presenting the same data as in Figure 2-1). The data coverage is limited by the frequency and location of

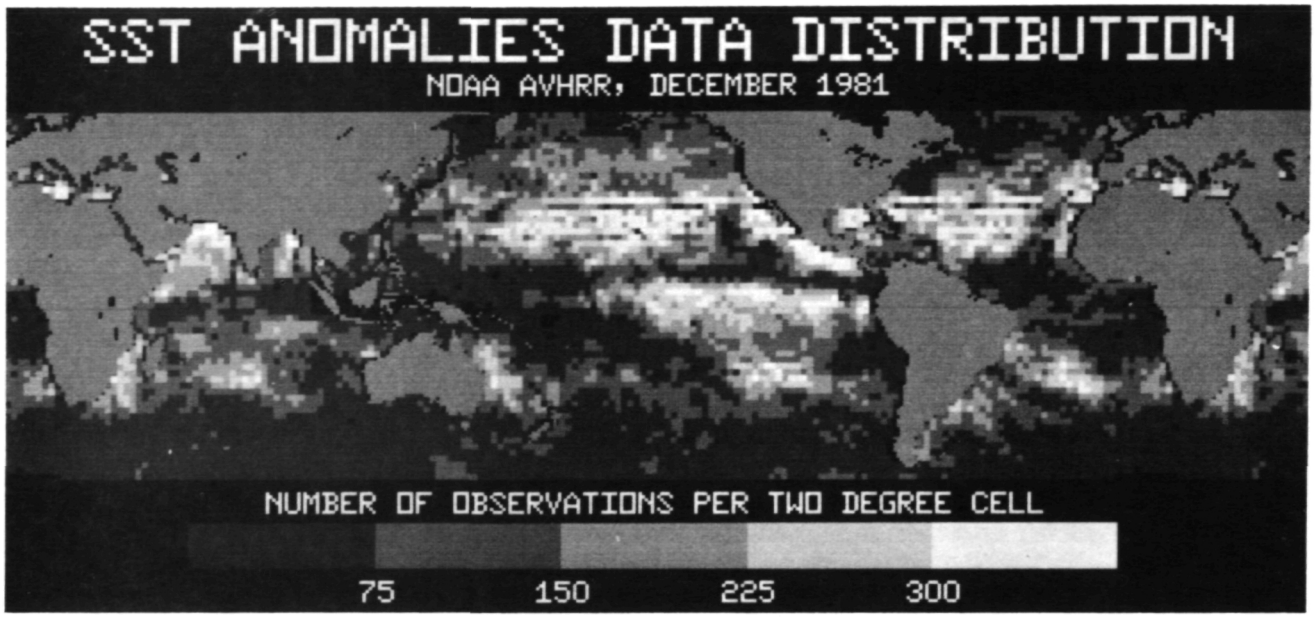

(a)

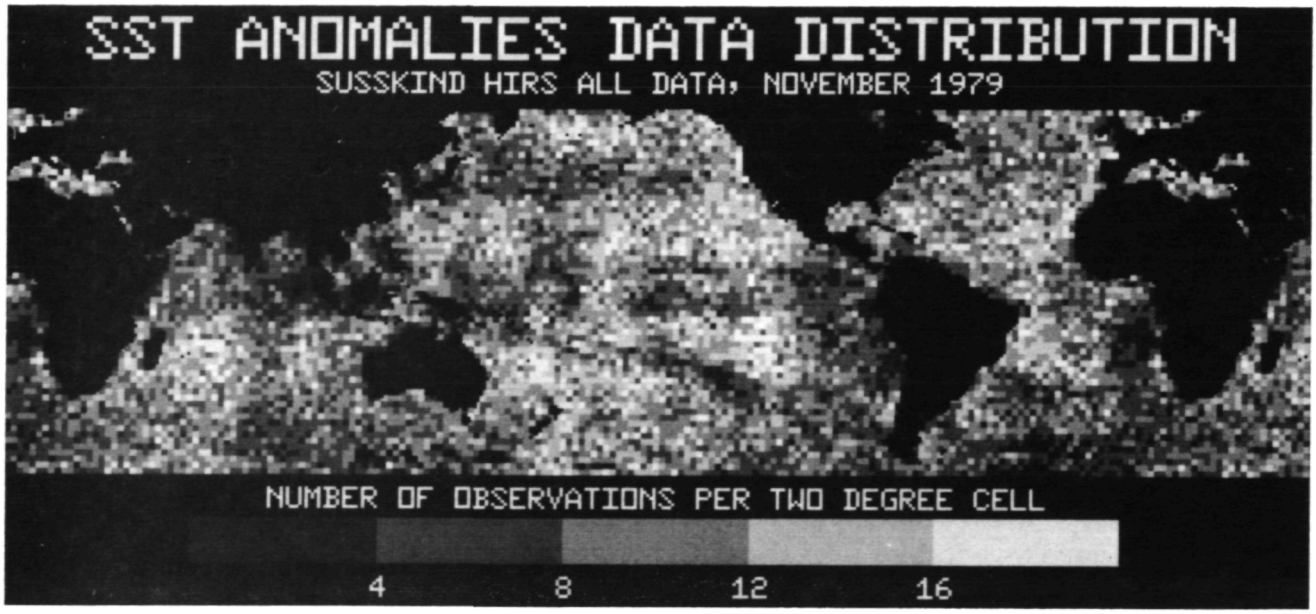

(b)

Figure 3-1. Number density of raw SST measurements falling within each 2^{o} latitude - longitude bin. (a) AVHRR: December, 1981. (b) HIRS; November, 1979. (c) SMMR: December, 1981. (d) Ship reports: December, 1981.

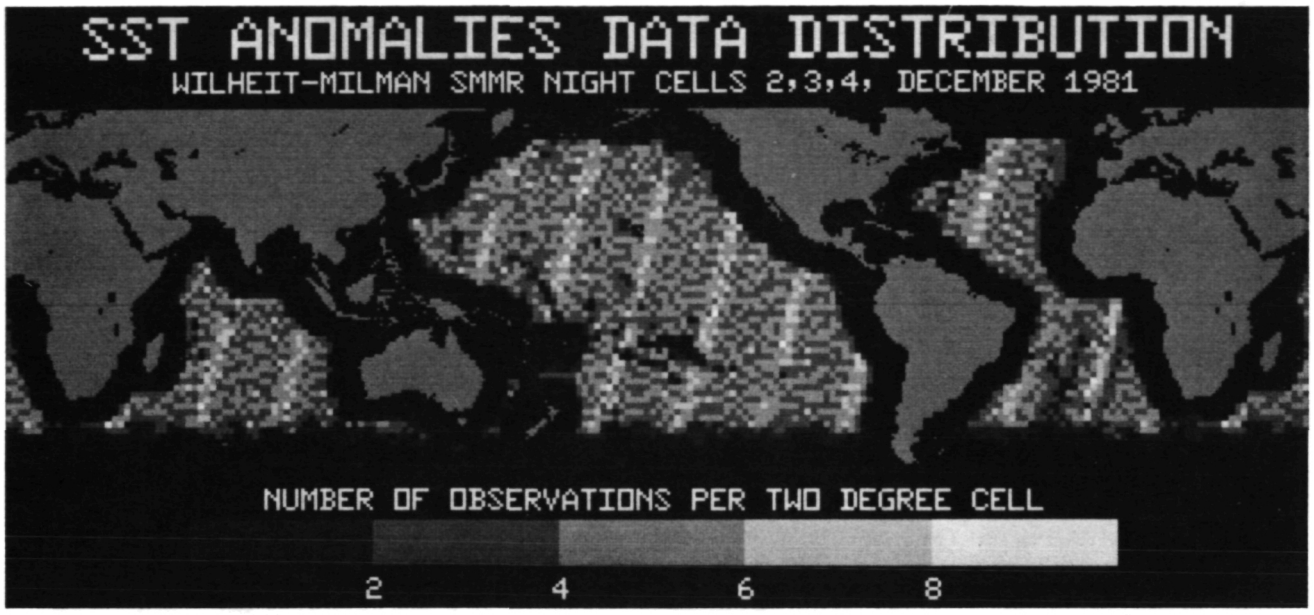

(c)

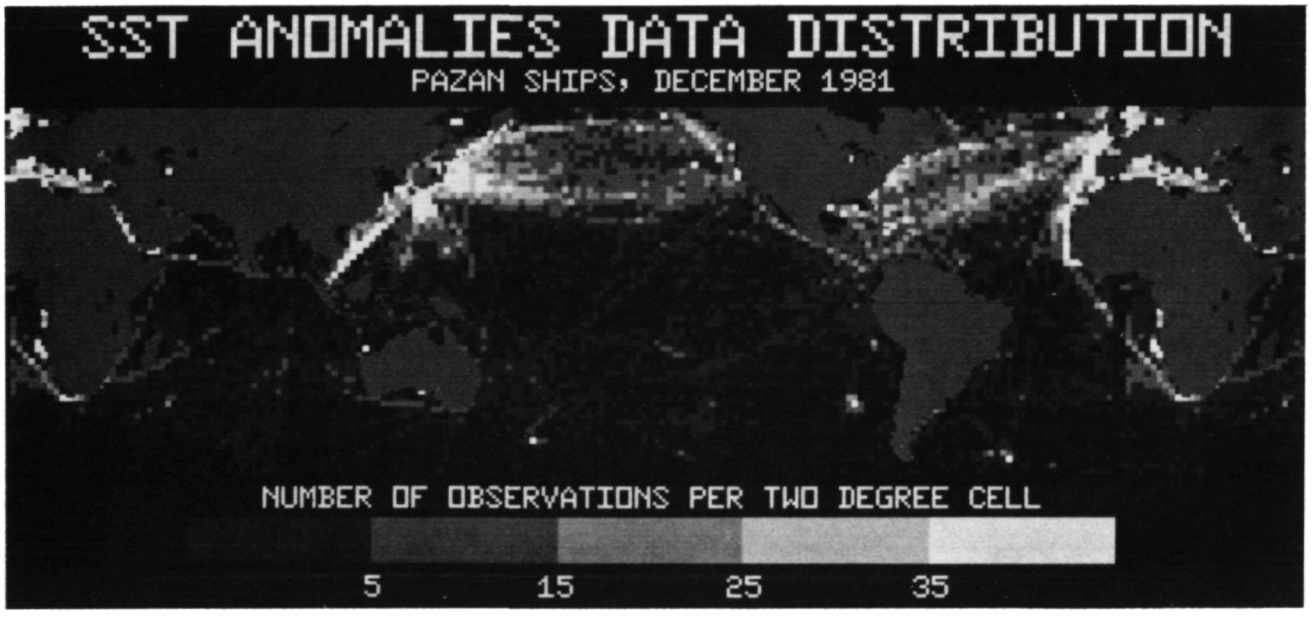

(d)

Figure 3-1. (Contd.) (See caption on facing page)

commercial shipping movements. Satellite sensors are clearly needed to fill the data voids in global ship coverage.

III.2 Raw SST Anomalies

Histograms of raw SST anomalies prior to binning are shown in Figure 3-2 for latitudes between $\pm 55^{o}$. Figure 3-2(a) shows the first 200,000 (out of 778,412) global AVHRR retrievals in this latitude range, corresponding approximately to the first week of December 1981. Figure 3-2(b) shows the entire month of December 1981 SMMR observations. Similarly, the HIRS observations (Figure 3-2(d)) are for the entire month of November 1979, whereas the AVHRR GOSSTCOMP are for approximately the first week only. These histograms give some idea of the scatter of the satellite data, as compared with the in situ data (Figure 2-4). The AVHRR MCSST has the narrowest histogram, thus giving rise to the smoothest anomaly fields (Figure 3-3). The AVHRR has the advantage of high sampling density in most areas enabling a significant reduction in the random component of error when the binned fields are produced.

III.3 SST ANOMALY FIELDS

Binned SST anomaly fields are shown in Figure 3-3 for December 1981, and Figure 3-4 for November 1979.

December 1981

Figure 3-3 shows three SST anomaly fields derived from December 1981 data: (a) NOAA-7 AVHRR, (b) Nimbus-7 SMMR, and (c) Ships. The AVHRR field appears the least noisy. In the northern hemisphere, where the ship data can form a continuous field, the agreement between AVHRR and ships is very encouraging. The relative patterns of negative and positive anomalies in the north Pacific and north Atlantic are virtually identical. The magnitudes of the anomalies show some discrepancies, however, as is seen upon closer examination of the contours in Section IV. (For example, the AVHRR anomaly in the N. E. Pacific is about $0.5^{o}C$ colder than the ship anomaly). Elsewhere on the globe, even where ship data are sparse, good agreement can be seen between AVHRR and ships e.g., warm off the coast of South Africa and Madagascar, warm and cold regions in the S. Atlantic and S. Indian oceans. One disturbing feature, however, is the extremely warm ($\sim 3^{o}C$) AVHRR anomaly off the coast of New Guinea. This anomaly is quite large in spatial extent and yet it occurs in an equatorial ocean region where anomalies greater than $1^{o}C$ are known to be extremely rare. Unfortunately, Figure 3-3(c) shows no ship data in this region for comparison. This feature is also located where the AVHRR observation density is very sparse due to persistent cloudiness (see Figure 3-1(a)). It has been speculated that high humidity and associated atmospheric conditions may be causing errors in the AVHRR data for that region. This would imply an over-correction for humidity, however, since inadequate corrections usually result in temperatures that are too low (i.e. negative anomalies).

The SMMR SST anomalies (Figure 3-3(b)) show similarities to those of the AVHRR in the S. Atlantic and Indian oceans. However, the N. Atlantic, and particularly the N. Pacific, look quite different. Large positive SMMR anomalies occur in the N.W. Pacific where AVHRR and ships indicate relatively

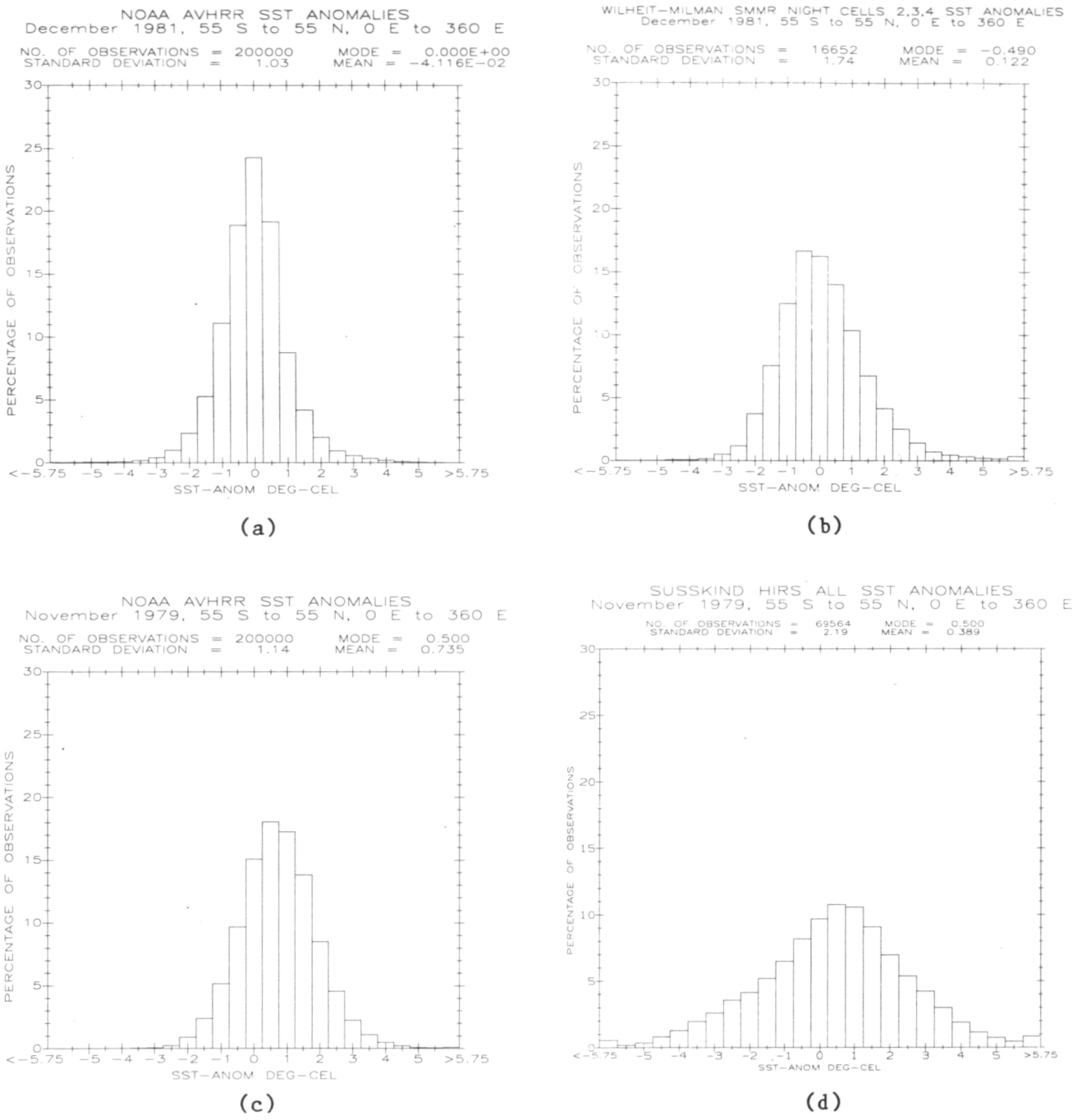

Figure 3-2. Raw SST anomaly histograms of global data sets. (a) AVHRR (MCSST): December, 1981. (b) SMMR: December, 1981. (c) AVHRR (GOSSTCOMP): November, 1979 (d) HIRS: November, 1979

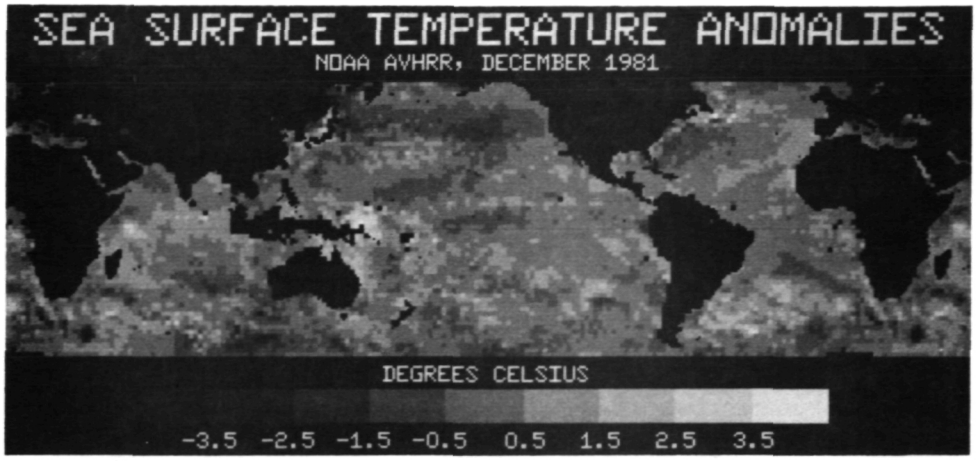

(a)

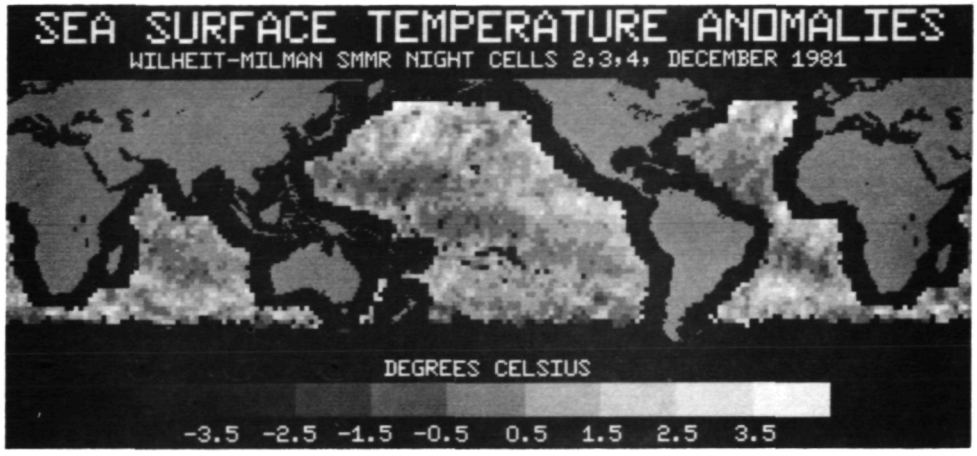

(b)

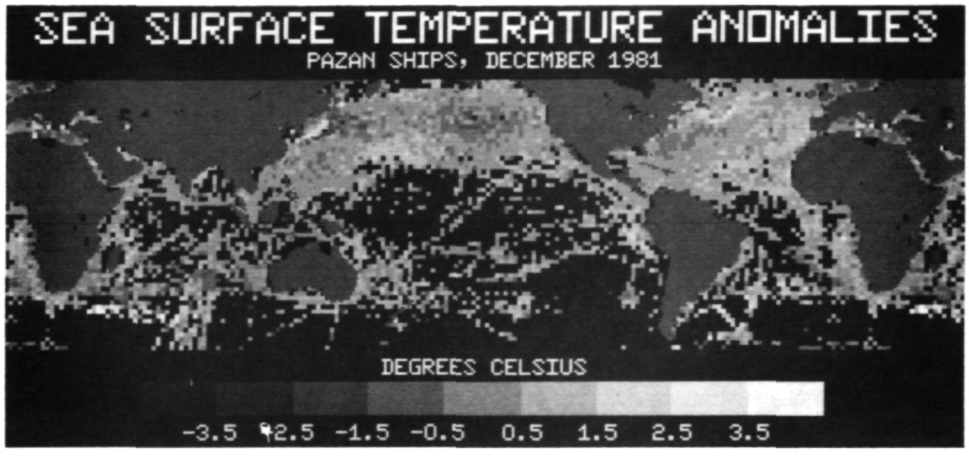

(c)

Figure 3-3. Gray-scale maps of binned SST anomalies for December, 1981. (a) AVHRR (MCSST). (b) SMMR. (c) Ship reports

cool water. Suggestions were made that these positive anomalies are possibly from SMMR errors caused by incomplete correction for high-wind effects on ocean microwave emissivity. It was also pointed out that a latitude-dependent temperature bias, if removed from the SMMR data, would align the SMMR (SST) field more closely with AVHRR and ships. There is some evidence for this in Figures 3-3(a) and (b) for the Pacific region as a whole. Latitude-related calibration errors are known to be a problem in the SMMR data (Ref. 1).

November 1979

Figure 3-4 shows four SST anomaly fields derived from November 1979 data: (a) NOAA-6 AVHRR (GOSSTCOMP) product, (b) TIROS-N HIRS, (c) Nimbus-7 SMMR, and (d) Ships. The GOSSTCOMP is the predecessor to the current NOAA-7 AVHRR MCSST and is expected to be somewhat less accurate (Refs. 9, 16). There are fairly large gaps in this product along the ITCZ because of the necessity for extensive cloud filtering. Two large negative anomaly regions dominate the picture, one each in the North and South Pacific. Compared with ships (Figure 3-4(d)), the AVHRR product shows excellent general agreement in both N. Pacific and N. Atlantic. This was discussed previously in Workshop-I (Ref. 1).

The HIRS SST anomalies (Figure 3-4(b)) are rather noisy, but they agree fairly well with the AVHRR and with ships in the N. Pacific and N. Atlantic. The HIRS SSTs appear too warm near certain coastlines, such as Southeast and West Africa, northwestern S. America, Australia, and Indonesia. This may be due to land effects contaminating retrievals in pixels adjacent to land. The negative anomalies visible in the HIRS for the Southern Oceans data are not seen in the AVHRR. Nor do the HIRS and AVHRR agree well in the tropical Pacific. As there is little ship data in these regions, one cannot say which sensor is the more correct. The SMMR data available for this month (Figure 3-4(c)) do not extend into the Atlantic or Indian Oceans. However, the large negative anomaly centered in the S. Pacific at approximately 30°S., 145°W. shows clearly for all sensors. The SMMR, as with December 1981, shows problems in the north Pacific, where the pattern of positive anomalies is quite different from that obtained from other sensors.

III.4 LATITUDINAL TRENDS

One way of comparing trends in the global data sets is to plot binned SST anomalies versus climatology. This is shown in Figure 3-5. Figures 3-5(a) and (b) are AVHRR and SMMR, respectively, for December 1981, while 3-5(c) and 4(d) are HIRS and AVHRR for November 1979. In all cases except (c) the mean global deviation from climatology is less than 0.1°C. The standard deviations of the monthly-averaged anomalies are on the order of 1°C or less for all sensors. Part of this standard deviation is real geophysical variation, the rest being due to instrument error, including bias variations. For example, there are differing trends in the plots of Figure 3-5 that may correspond to fictitious anomaly variations as functions of temperature or latitude. To examine this further, the data were divided into six 20° latitude bands from 60°S to 60°N, and mean anomalies were computed for each band. The results are shown in Figure 3-6. For both November 1979 and December 1981 the SMMR shows a trend of increasing mean zonal anomaly as one proceeds north, a feature

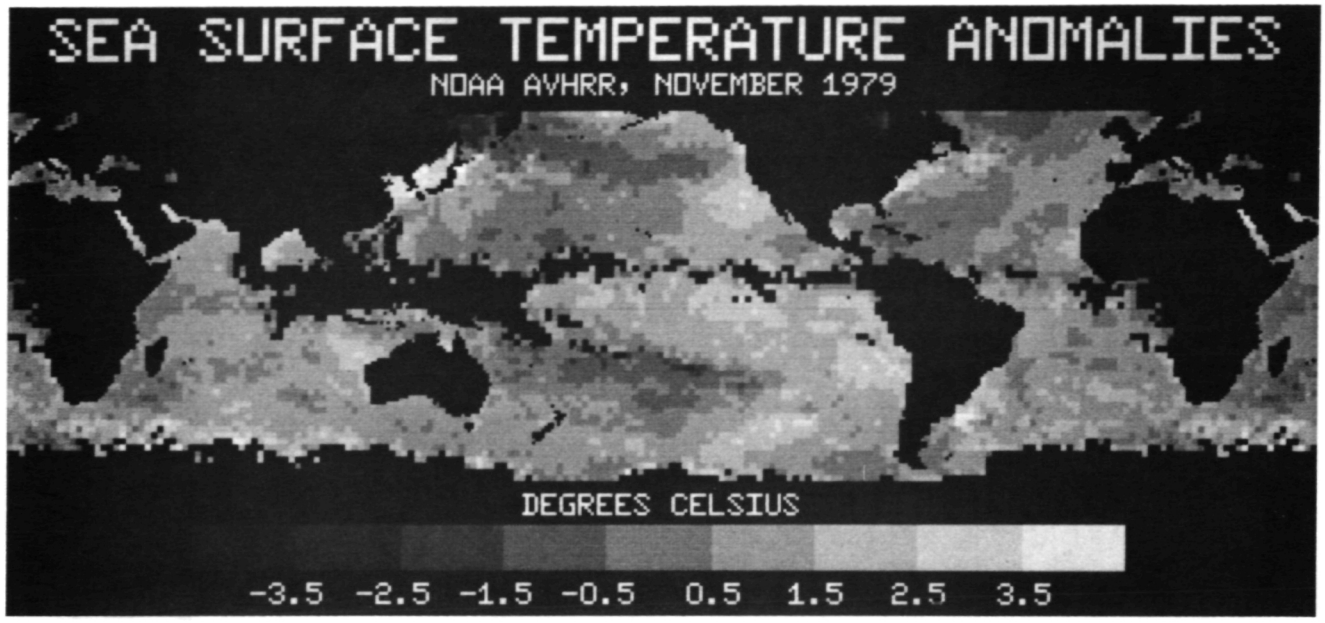

(a)

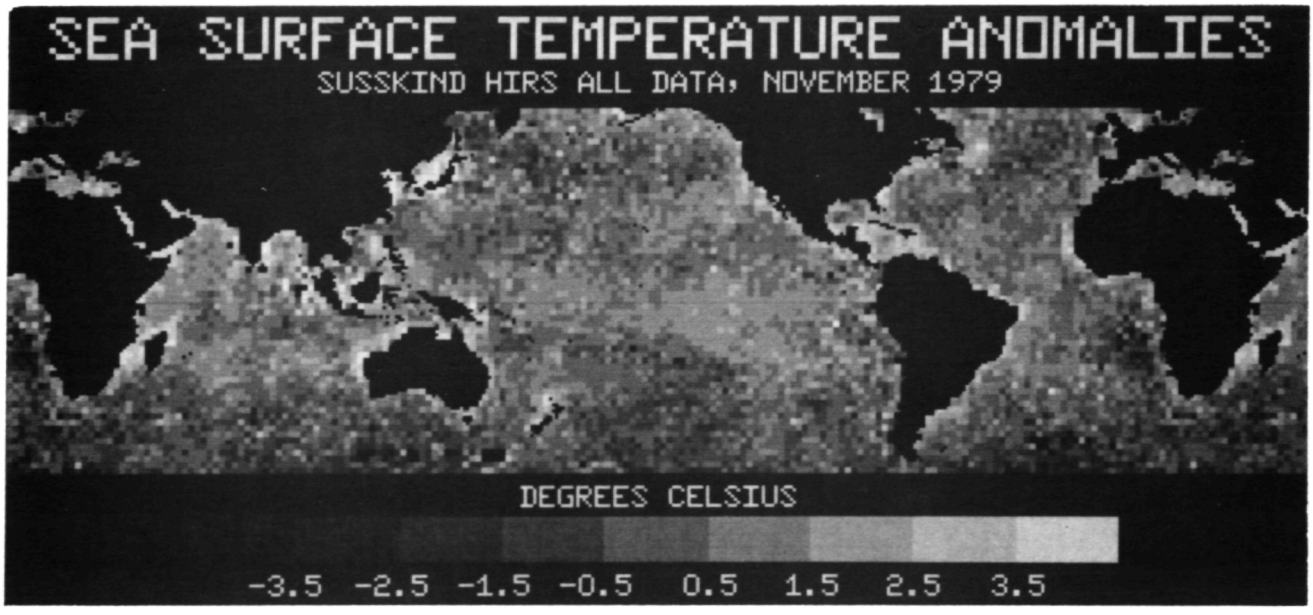

(b)

Figure 3-4. Gray-scale maps of binned SST anomalies for November, 1979. (a) AVHRR (GOSSTCOMP). (b) HIRS (c) SMMR. (d) Ship reports.

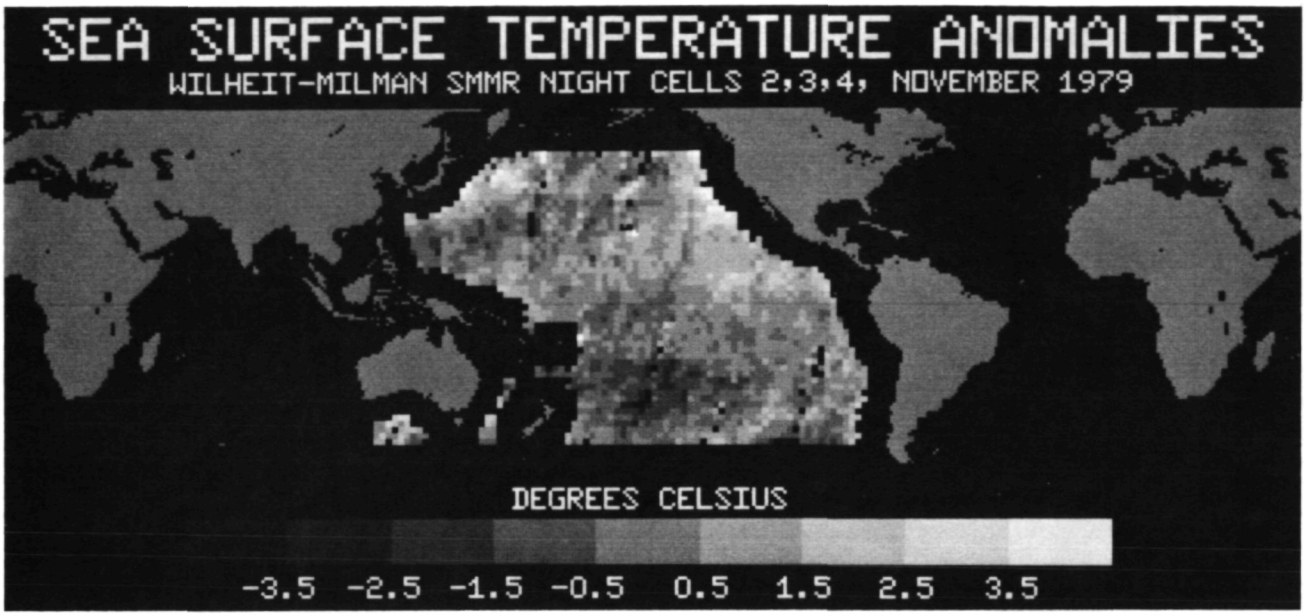

(c)

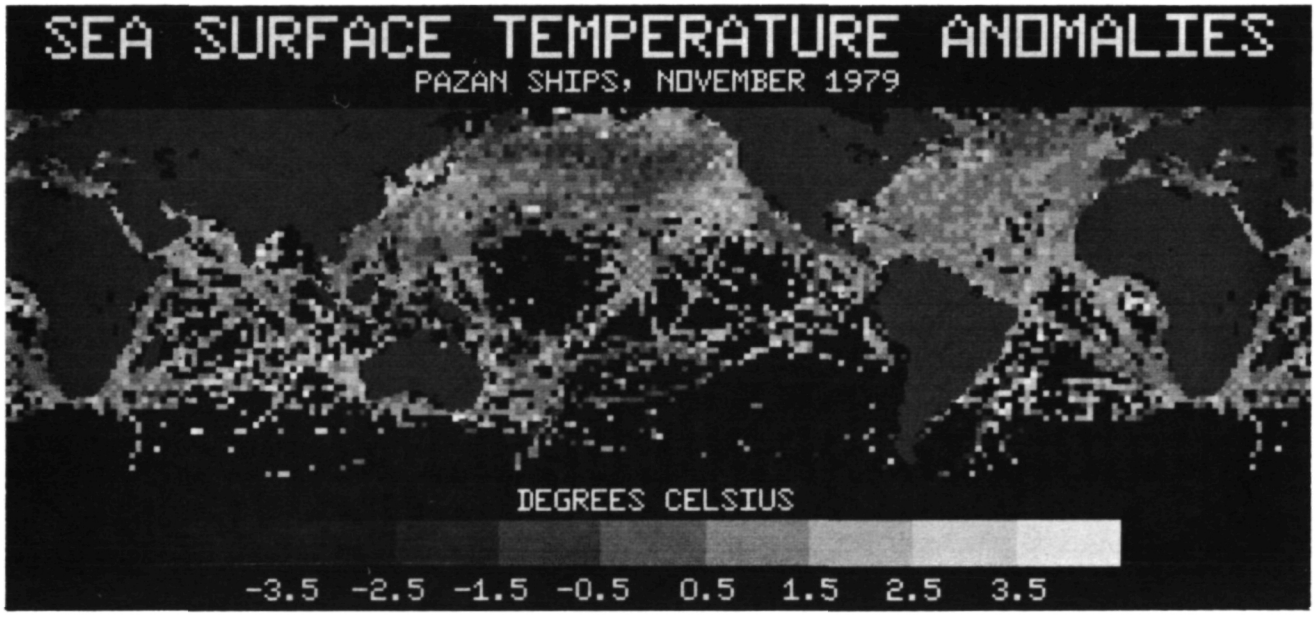

(d)

Figure 3-4. (contd.) (See caption on facing page)

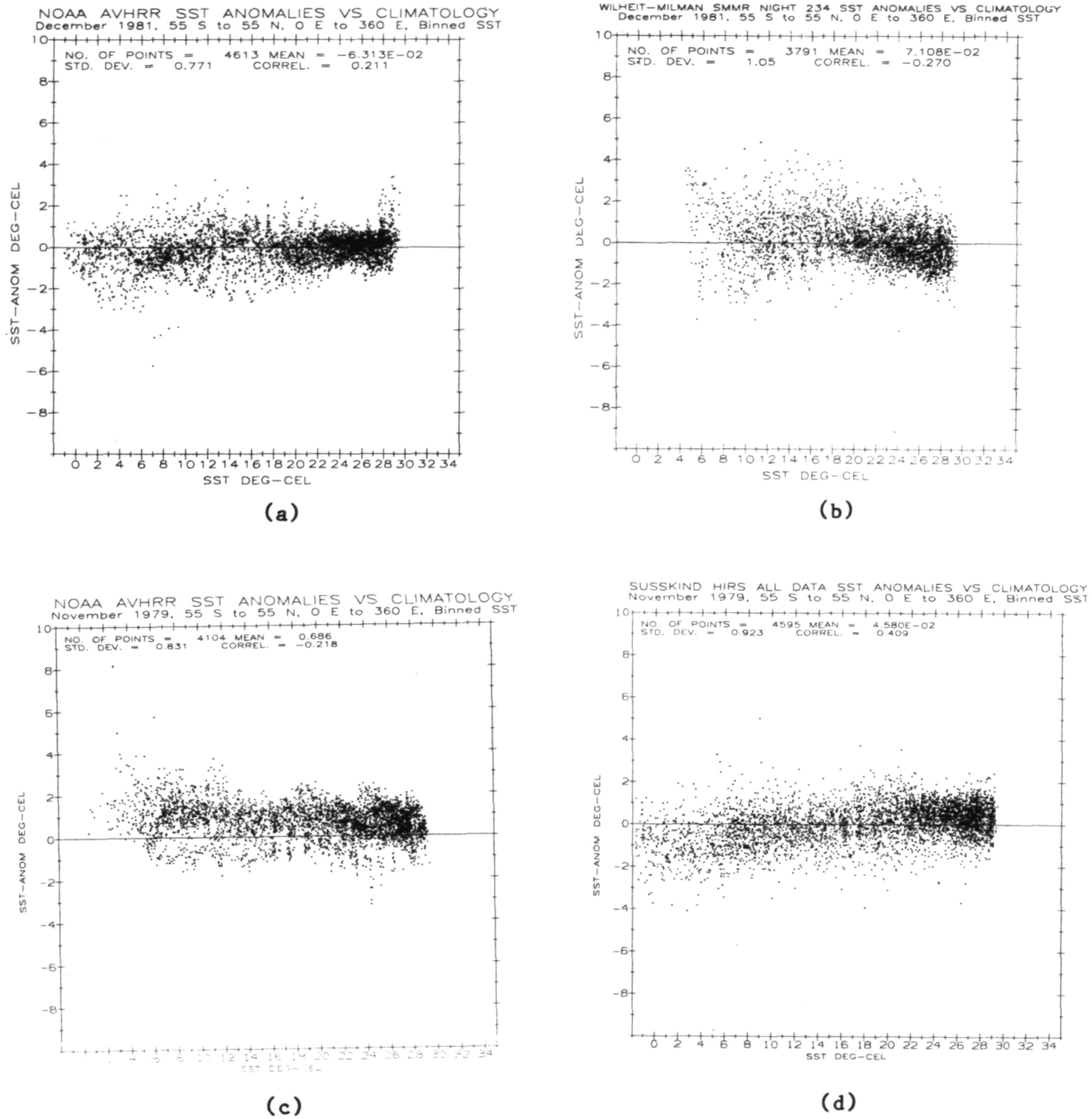

Figure 3-5. Scatterplots of binned SST anomaly (global) versus Climatology. (a) AVHRR (MCSST): December, 1981. (b) SMMR: December, 1981. (c) AVHRR (GOSSTCOMP): November, 1979. (d) HIRS: November, 1979.

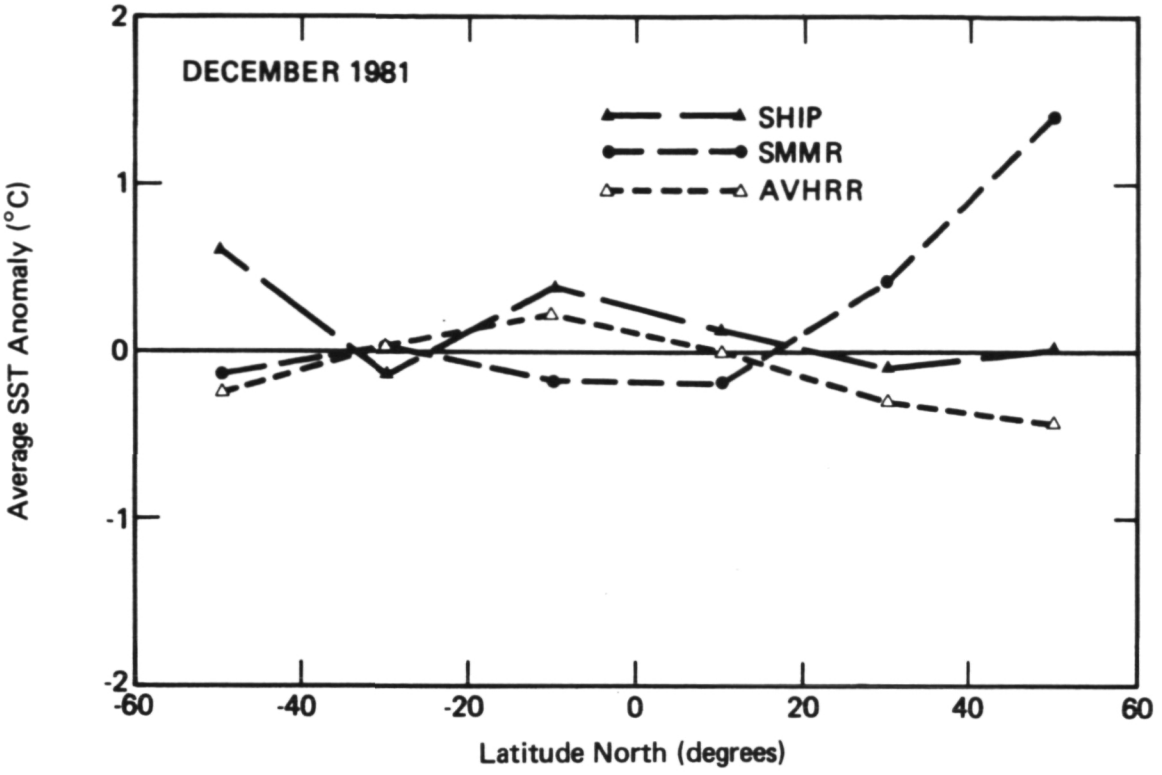

(a)

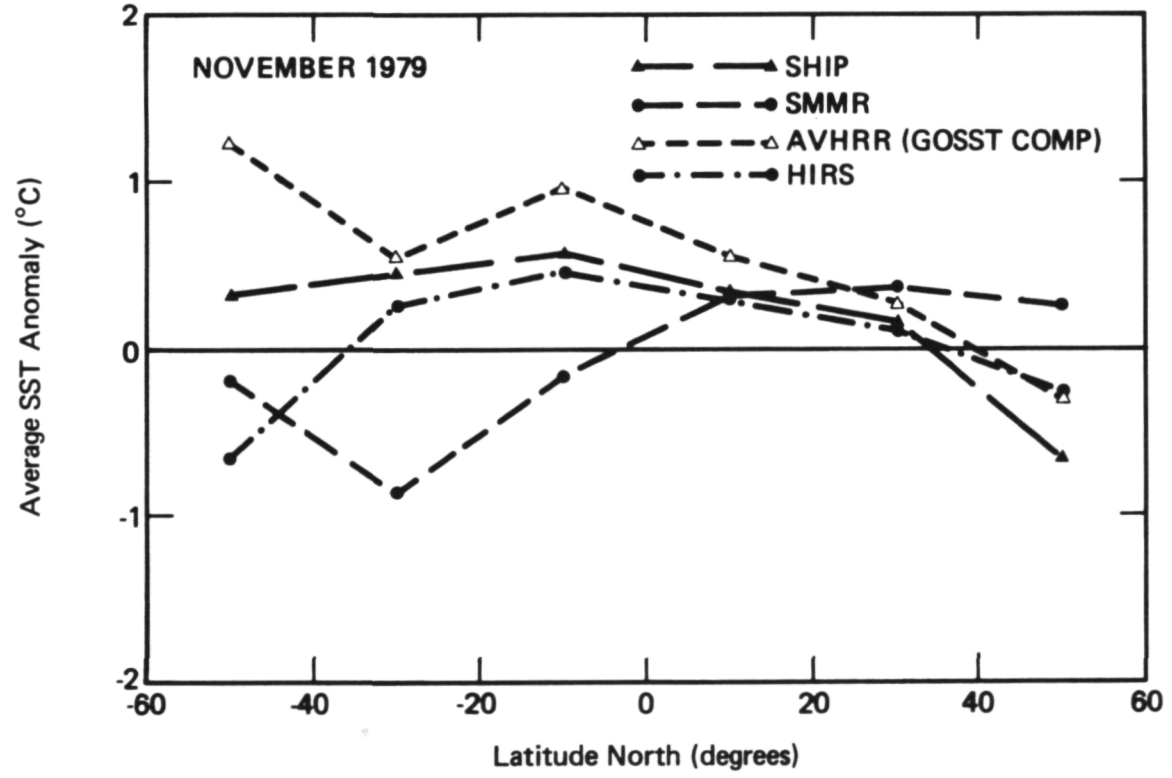

(b)

Figure 3-6. Zonal mean SST anomalies (averaged by 20° latitude band) versus latitude. (a) December, 1981. (b) November, 1979

that is not evident in the other data sets and thus may be due to calibration problems or to incomplete correction for geophysical effects (e.g. high winds, atmospheric water). The other data sets all show a positive peak in the 0 - 20°S region, tapering off to more negative anomalies at higher latitudes. When first observed in the AVHRR data, this phenomenon was suspected to be due to a residual temperature-dependent bias in the retrieval algorithm. The fact that the ship data show similar features, however, argues against this. The ship data cannot be relied on too heavily since the spatial distribution in the southern hemisphere is too sparse to form accurate zonal means. Similarly, the November 1979 SMMR data is for the Pacific only and thus is weighted differently than the other data sets.

SECTION IV
SATELLITE AND IN SITU SST COMPARISONS

Two types of data set intercomparisons were performed for the workshop: (1) match-ups of individual observations close in space and time; and (2) monthly data, binned into 2° latitude-longitude squares, with the binned averages of different data sets compared statistically as well as by visual inspection of the resulting global and regional maps. The TRANSPAC XBT data, because of its limited coverage, does not lend iteslf well to binned averages, yet individual observations are good to about 0.2°C. The routine ship data are far more abundant than XBT data, but are of far poorer quality, with individual observations accurate only to about 1°C rms (Ref. 10). It was therefore decided to examine the routine ship data only after it had been binned, and only for monthly bins containing five or more observations. This generally restricted the data to the mid-latitude North Atlantic and North Pacific between 20°N and 60°N. Figure 4.1 illustrates the noise level of the routine ship data by cross-plotting all pairs of such observations taken within six hours and 100 km of each other. The standard deviations of the temperature differences are 1.49 and 1.17°C for the North Pacific and North Atlantic, respectively. Weighting the variance by the number of observations in each of the two oceans, and dividing by two to eliminate the doubling of noise variance created by the differencing process, yields a one-sigma noise level for the routine ship observations of 0.98°C, in good agreement with Saur (Ref. 10).

IV. 1 Point Comparisons

The individual NOAA AVHRR observations are derived from instantaneous spatial average radiances over 8 km squares, whereas the HIRS and SMMR observations are from 125 km and 150 km squares, respectively. The small AVHRR footprint makes it appropriate to compare point observations from ships and buoys with the AVHRR data. This is not the case with the HIRS and SMMR, where it is important to first bin separately the ship and satellite data in order to compare the larger area average differences.

For the NOAA AVHRR one can thus make two types of intercomparisons with in situ data: (1) individual matchups with XBTs, and (2) comparison of binned AVHRR with binned routine ship data. Figure 4-2 provides the match-up results in the north Pacific. For 68 AVHRR-XBT pairs of observations taken within 12 hours and 20 km of each other the AVHRR has a standard deviation of 0.81°C about a mean of 0.19°C (AVHRR colder than XBT). These values are similar to, but slightly larger than those reported by McClain in comparisons to moored and drifting buoys.

IV.2 Binned Comparisons

December 1981

For binned comparisons, we restrict attention to the relatively well-travelled North Atlantic and North Pacific north of 20°N. Here, as before, we depict the monthly mean departure (anomaly) of sea surface temperature from climatology. Note the excellent correspondence between the ship and AVHRR anomaly patterns in the North Atlantic (Figure 4.3(a), (b)). This is a more detailed view of the gray-scale images shown in Figure 3-3. A negative tongue extends eastward into the western North Atlantic at about 35°N, while a positive anomaly is seen extending eastward from Newfoundland. A

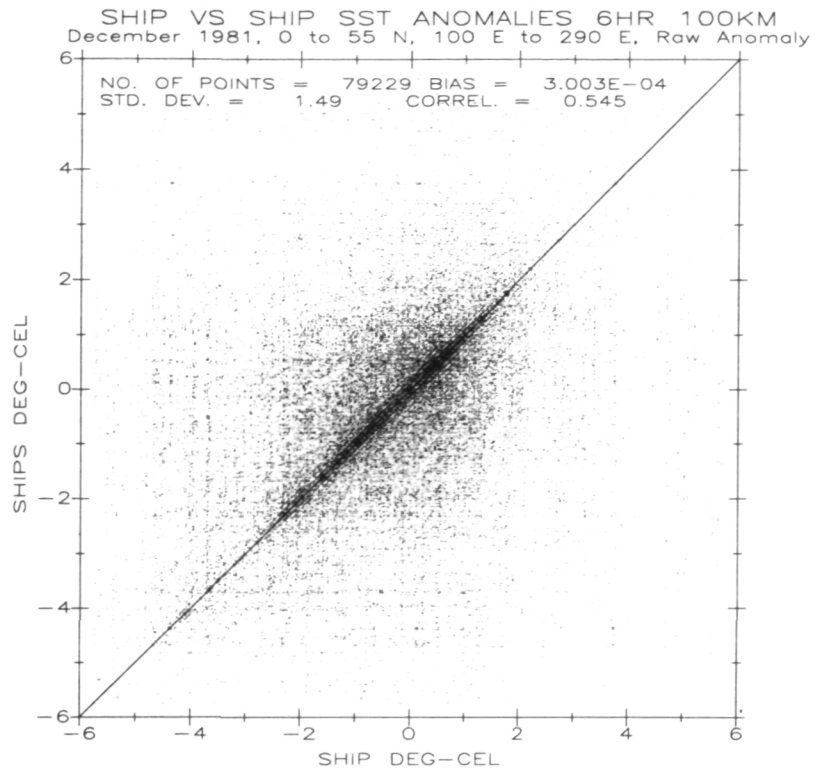

(a)

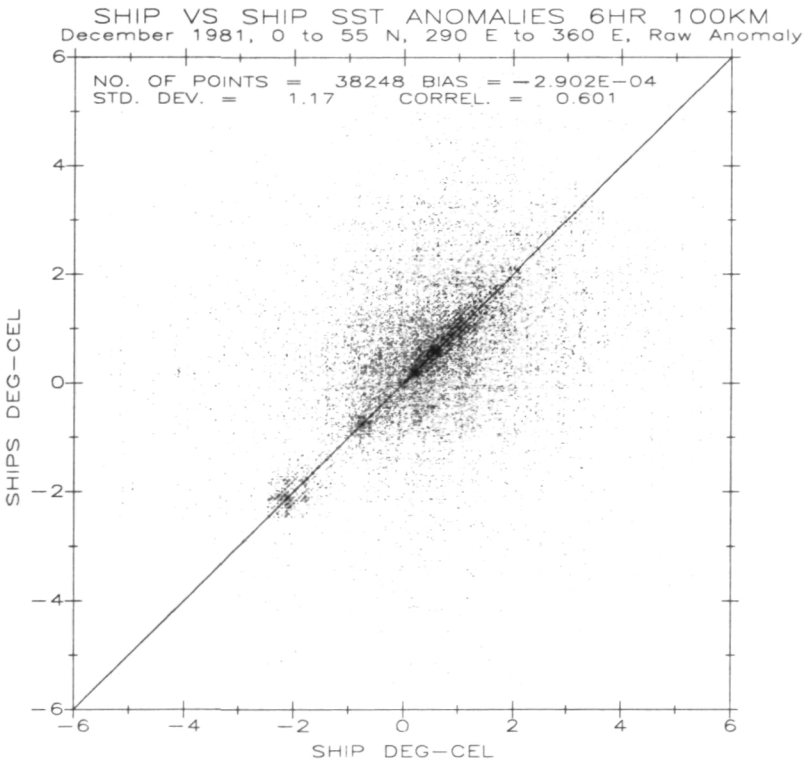

(b)

Figure 4-1. Scatterplot of all pairs of raw Ship SST observations taken within 6 hours and 100 km of each other during December, 1981. (a) North Pacific Ocean. (b) North Atlantic Ocean.

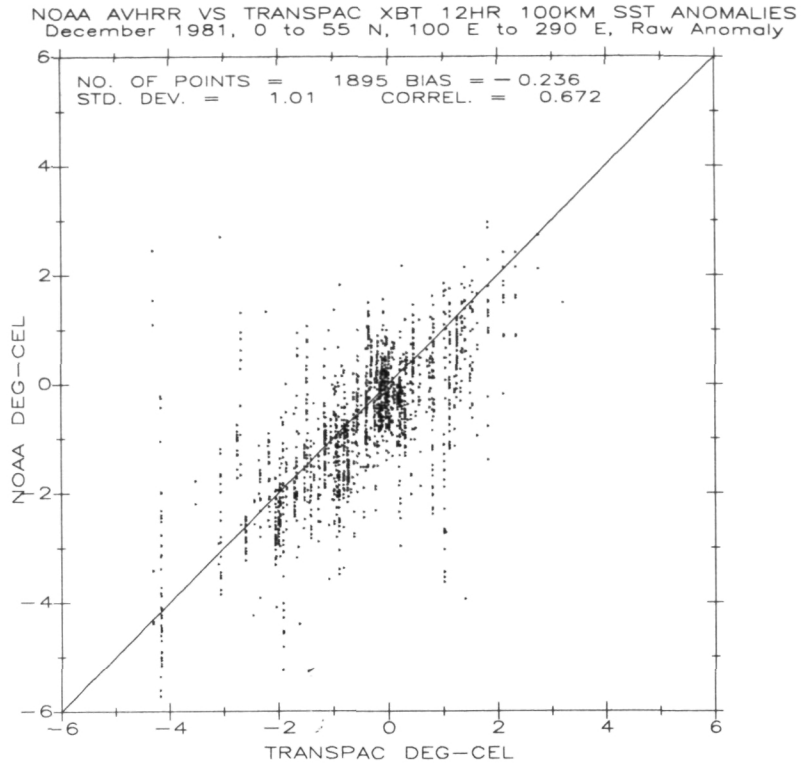

(a)

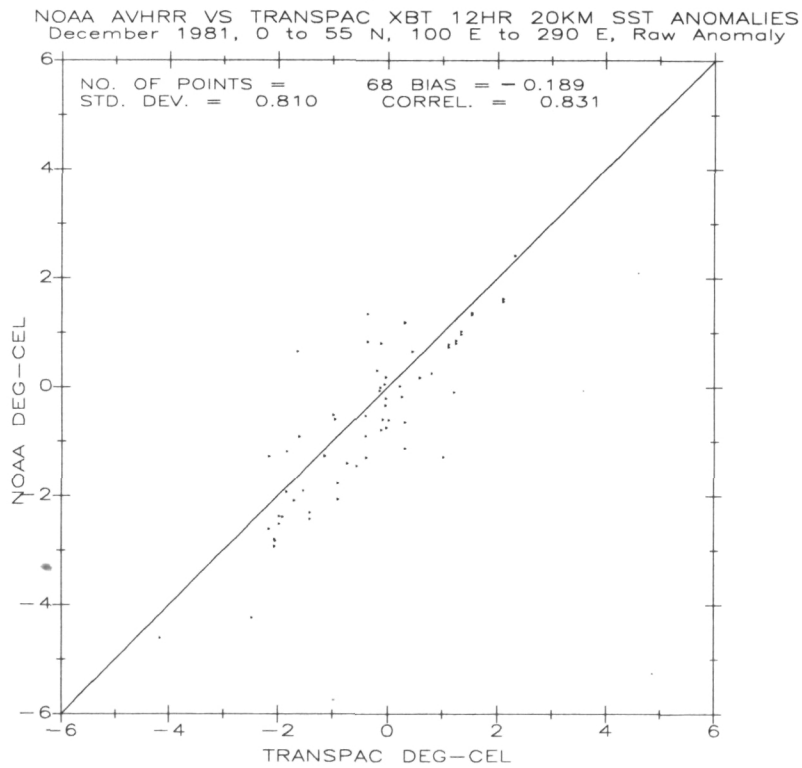

(b)

Figure 4-2. Scatterplot of all pairs of raw AVHRR and TRANSPAC XBT sea surface temperatures taken within 12 hours and (a) 100 km, (b) 20 km, of each other. North Pacific Ocean, December 1981.

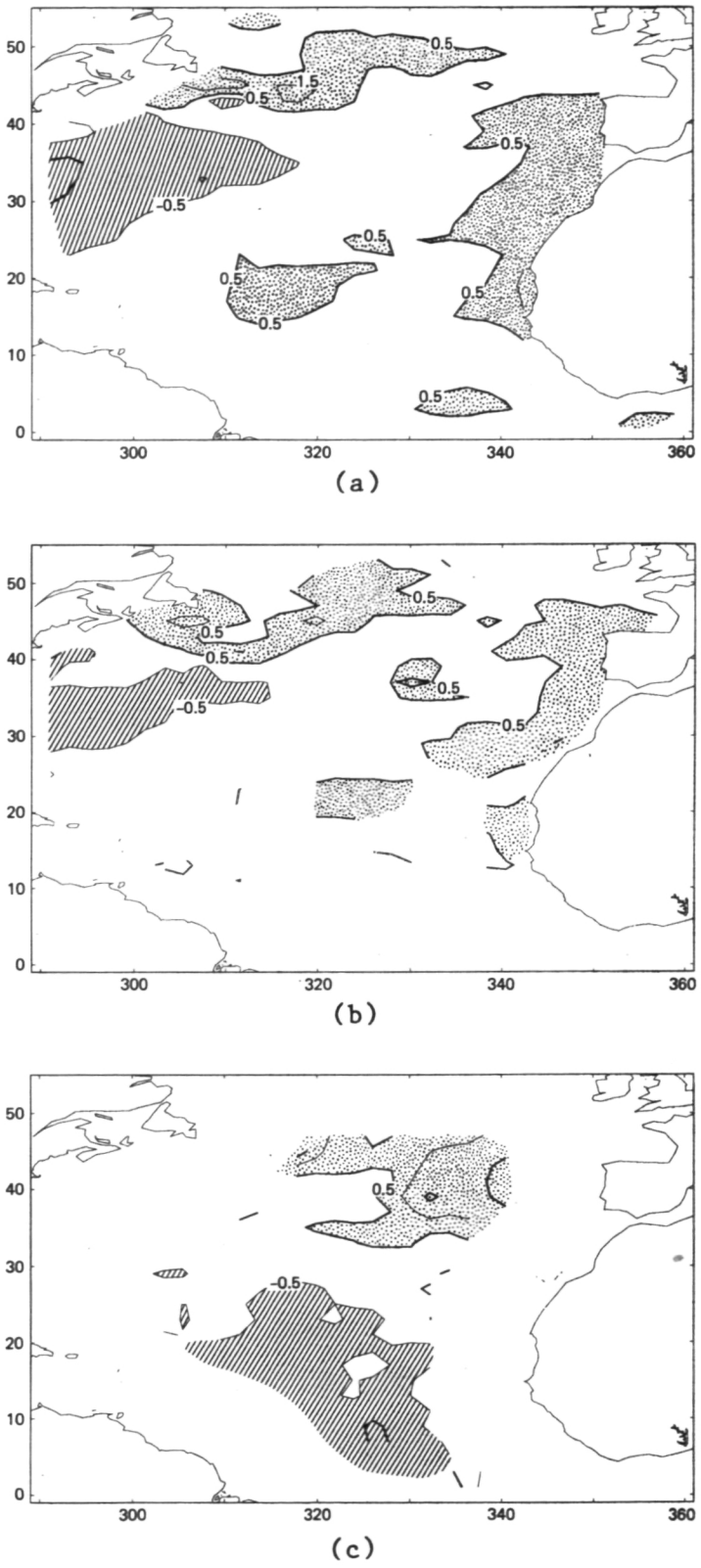

Figure 4-3. Contour map of SST anomalies in North Atlantic Ocean, December, 1981. (a) AVHRR. (b) Ship reports. (c) SMMR

positive anomaly occupies the coastal region of Spain and North Africa. When cross-plotted bin by bin (Figure 4.4(a)), we see the AVHRR-ship temperature difference exhibits a standard deviation of 0.56°C about a mean of 0.11°C (AVHRR colder than ships).

In the North Pacific (Figure 4.5(a), (b)) note that the ship and AVHRR anomaly patterns correspond, but with a bias of about 0.5°C (AVHRR colder). Thus, the two negative anomaly features defined by the -0.5°C contours in the ship map, and located along 40°N at 150°E and 200°E, also appear in the AVHRR map, now defined approximately by the -1°C level. However, the region around 30°N, 170°E where the ship map indicates a 0.5°C feature, the same 0.5°C levels are found in the AVHRR map. When cross-plotted by bin (Figure 4.4(a)), we see that the AVHRR - ship temperature difference has a standard deviation of 0.70°C about a mean of 0.35°C (AVHRR colder than ships). The tendency for MCSST to be colder than ship data was in fact noted by McClain, and operationally corrected in September 1982 (Ref. 13). This tendency appears more visible here in the N. Pacific than in the N. Atlantic.

The SMMR data may be compared in similar fashion with ship data over the North Atlantic and North Pacific. Unlike the MCSST, it is impossible to visually identify any correspondence in the anomaly patterns between ship and SMMR over either the North Atlantic (Figure 4.3(c)) or North Pacific (Figure 4.5(c)). This is also reflected in Figure 4.6(a), (b) where no trend is apparent in cross-plotted ship and SMMR anomalies. In both the Atlantic and Pacific, the SMMR is biased warm relative to ship, by 0.38 and 0.94°C, respectively, with standard deviations of about 1.2°C.

November 1979

There is general agreement between the AVHRR (GOSSTCOMP) and ship anomaly patterns in the North Atlantic (Figure 4-7), showing the positive anomaly off Newfoundland, and warm water patches in the central and northeast regions. A scatterplot comparison of the binned data (Figure 4-9(a)) shows a standard deviation of 0.75°C about a mean of 0.33°C (AVHRR warmer than ships). This performance is somewhat poorer than for December 1981 (AVHRR MCSST) as expected.

The HIRS data in the North Atlantic show similar features to the AVHRR and ships except for the negative HIRS anomaly in the region around 42°N, 330°E. This anomaly does not appear in the AVHRR and ship maps. The scatterplot of HIRS versus ship binned data (Figure 4-9(b)) exhibits a standard deviation of 1.24°C about a mean of 0.25°C (HIRS warmer than ships).

The similarity between AVHRR (GOSSTCOMP) and ship SSTs is again evident in the North Pacific (Figure 4-8), showing the band of cold water between 40° and 50°N, and the warm water off the coasts of Japan and the western USA. The scatterplot of AVHRR versus ships (Figure 4-9(c)) shows a standard deviation of 0.85°C about a mean of 0.28°C; values very similar to those found in the North Atlantic.

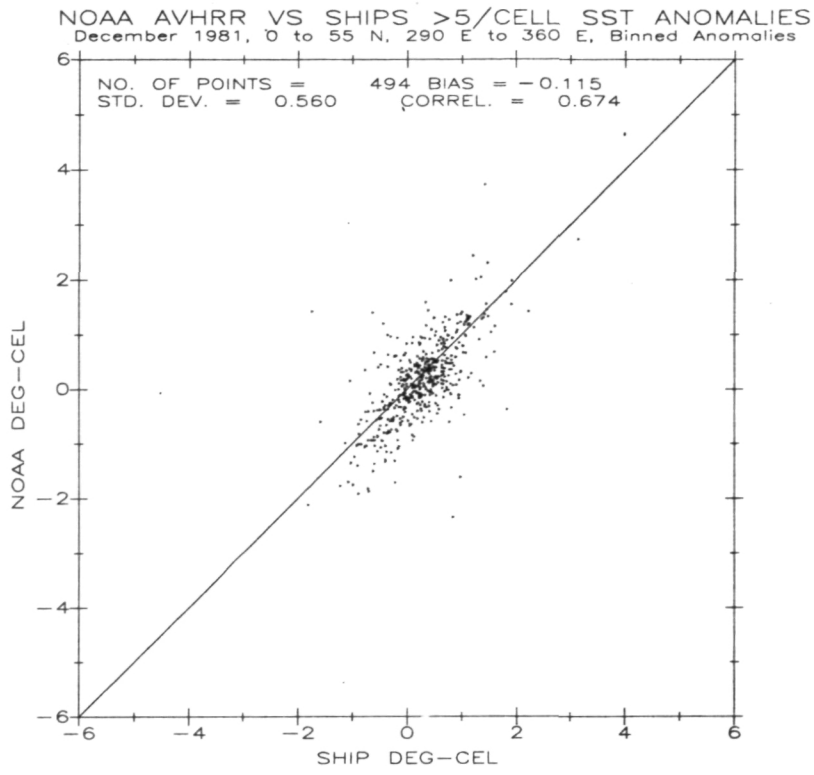

(a)

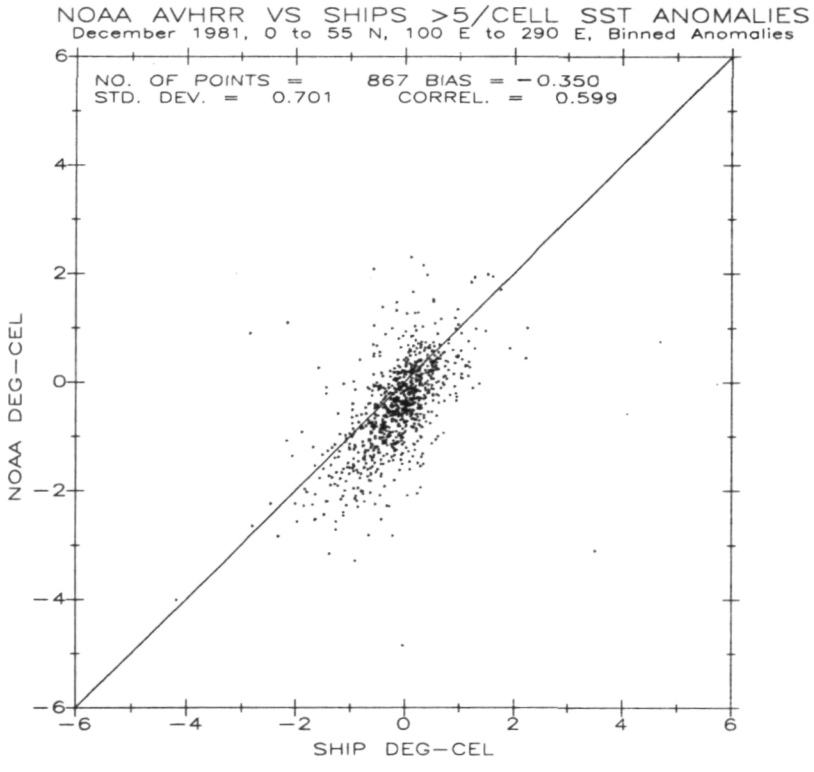

(b)

Figure 4-4. Scatterplot of binned SST anomalies, AVHRR versus Ship reports, December 1981. (a) North Atlantic Ocean. (b) North Pacific Ocean

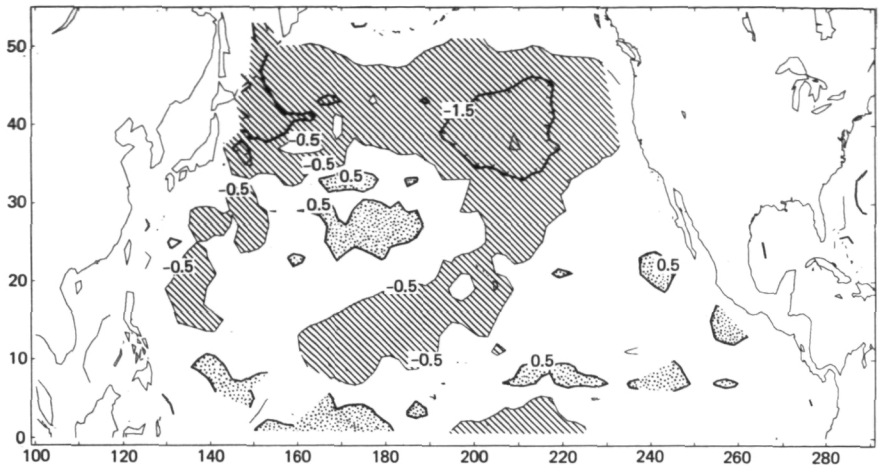

(a)

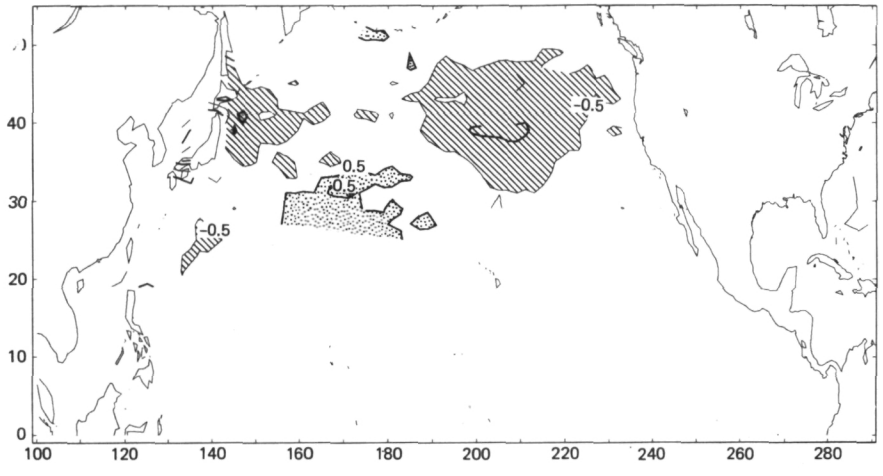

(b)

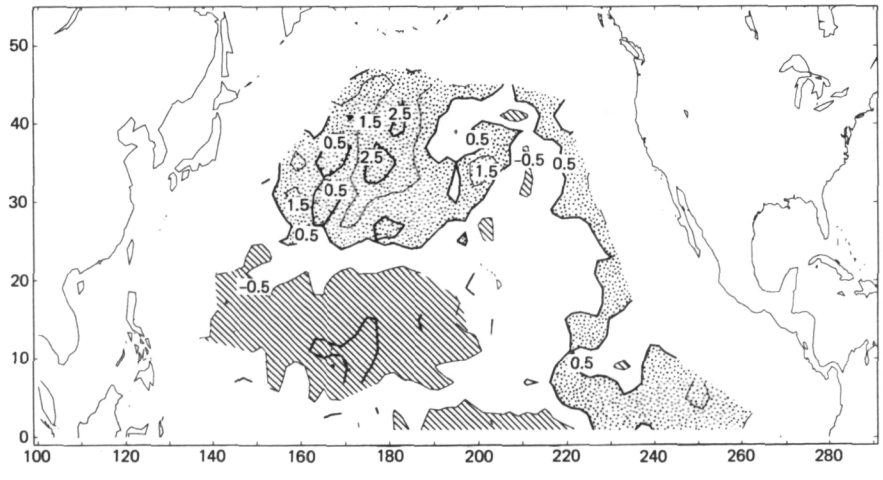

(c)

Figure 4-5. Contour map of SST anomalies in North Pacific Ocean, December, 1981. (a) AVHRR. (b) Ship reports. (c) SMMR

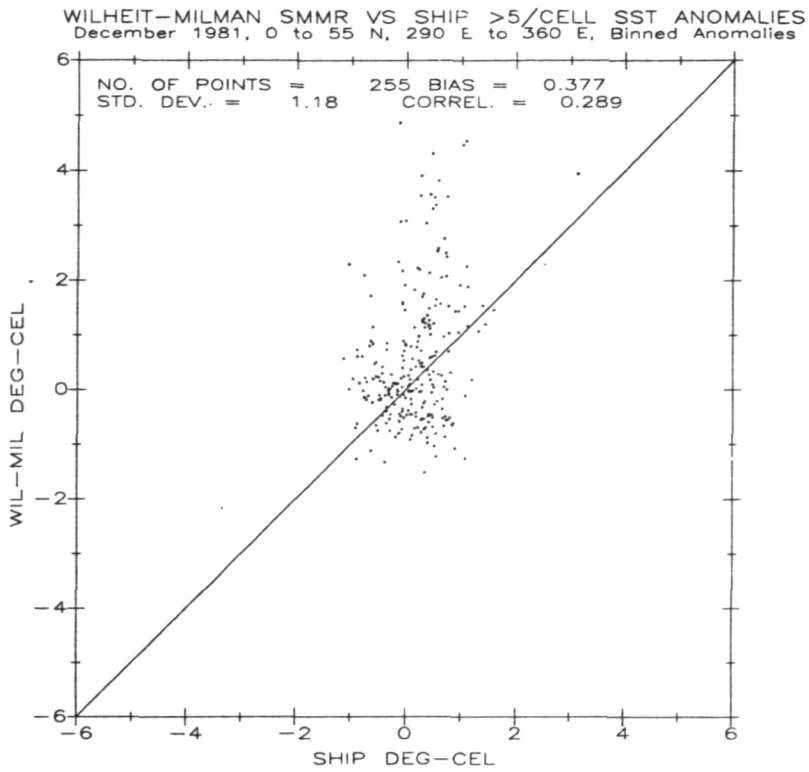

(a)

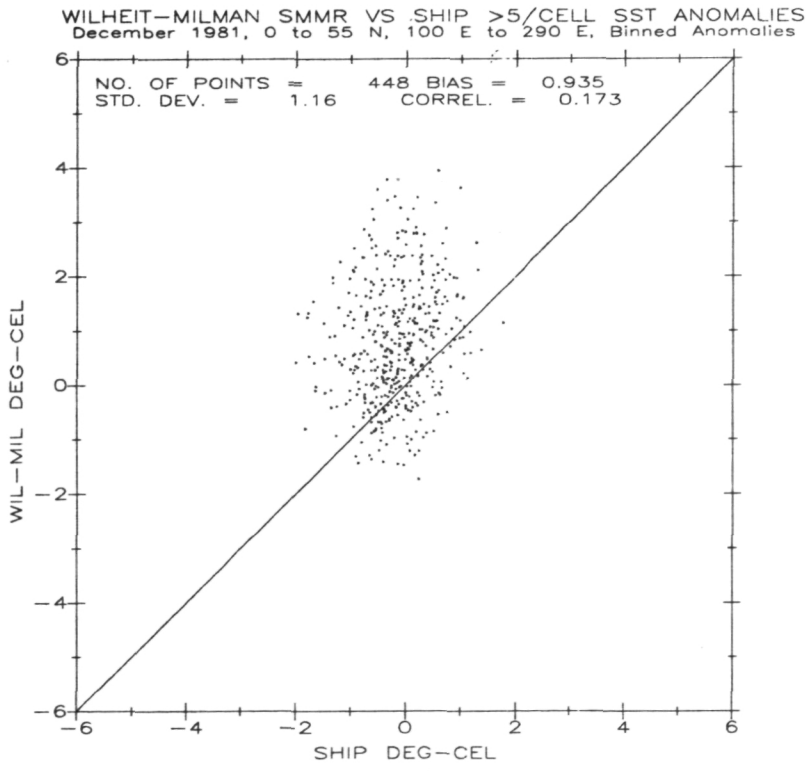

(b)

Figure 4-6. Scatterplot of binned SST anomolies, SMMR versus Ship reports, December 1981, (a) North Atlantic Ocean. (b) North Pacific Ocean.

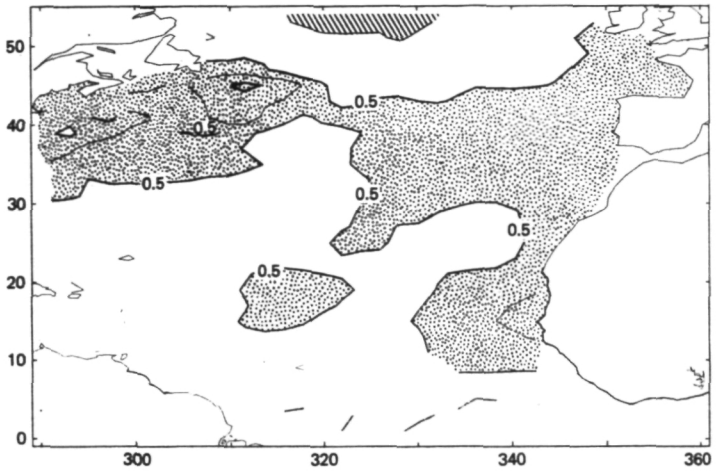

(a)

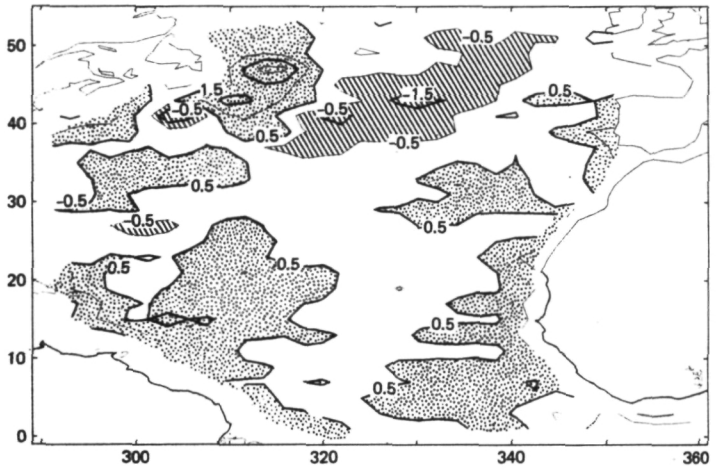

(b)

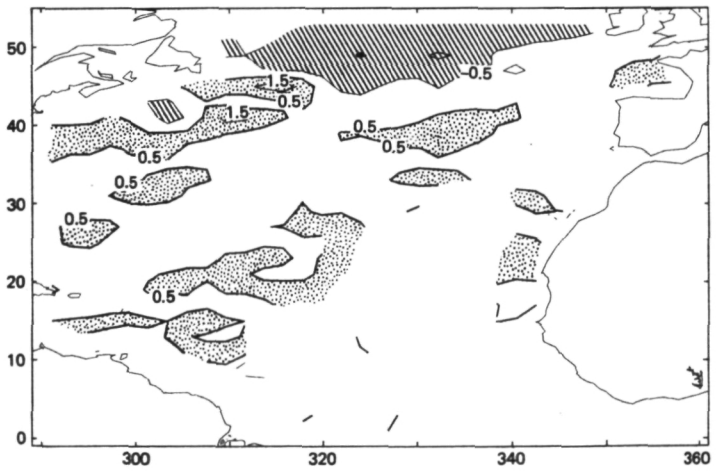

(c)

Figure 4-7. Contour maps of SST anomalies in North Atlantic, November 1979. (a) AVHRR (GOSSTCOMP). (b) HIRS. (c) Ships.

The North Pacific HIRS data (Figure 4-8(b)) agree quite well with both AVHRR and ships, although HIRS appears much noisier. This is evident in the scatterplot of HIRS versus ship (Figure 4-9(d)), which shows a standard deviation of 1.25°C about a mean of 0.36°C, again very similar to the comparison in the North Atlantic.

SMMR data for November 1979 were discussed in some detail in Workshop-I (Ref. 1), hence the results will not be repeated here.

IV.3 Correlation Tables

Another way to compare the binned data from different sensors is to examine their correlations. Tables 4-1(a) and (b) show data correlations for December 1981 and November 1979 respectively. The upper triangle in each table shows correlations between sensor pairs in the North Atlantic, while the lower triangle is for the North Pacific. In parentheses are the numbers of common grid points for each sensor pair used in computing the correlations. These numbers may vary significantly; for example, ship data are included only for those 2° lat-lon bins with more than five observations per month.

It is significant that the highest correlations (≥ 0.6) are found between AVHRR and ships, while the SMMR shows very little correlation with ships (≤ 0.3), and the HIRS is somewhere inbetween (0.2-0.4). Low correlations are indications of low signal-to-noise ratios. Thus, the low correlations in the North Atlantic for November 1979 are partly a consequence of the relatively small SST anomaly signal present there at that time.

IV.4 Error Partitioning

The standard deviations shown in Figures 4.4 and 4.6 are not true estimates of sensor rms error because they combine errors of both sensors. An attempt to apportion error between sensors can be made using sensor triad combinations in the error partitioning technique described in Ref. 1 (Appendix G) and elaborated further in this report (Appendix A). As discussed later, this technique assumes that sensor errors are uncorrelated, which may not be a valid assumption. This approach was used on the November 1979 and December 1981 2° - binned data sets.

Table 4-2 shows an example of error partitioning between AVHRR and the other four data sets for November 1979. The data sets are listed 1 to 5 as: AVHRR, SMMR, HIRS, Ship, and Climatology. Since the data sets are all expressed as anomalies, Climatology is a data set consisting entirely of zeros, and represents a hypothetical sensor that assumes SST to be equal to Climatology everywhere. For each of the five sensors there are six possible triplet (triad) combinations with the other four. The error partitioning algorithm allocates an rms error to each sensor in the triad, and a table such as Table 4-2 is generated for each sensor. The case illustrated is for the AVHRR. For example, row 2, column 3 has a value of 0.75, which is the rms error allocated to the AVHRR (sensor 1) in combination with sensors 2 and 3 (SMMR and HIRS). Ideally, the AVHRR should end up with the same rms error in every triplet combination; but instead the errors range from 0.45 to 0.9. This is partly because of the different ocean coverage of each sensor (e.g., SMMR: Pacific only, Ship: mostly Northern Hemisphere). Nevertheless, comparing the average overall rms error partitioned to each sensor can be instructive. This has been done in Table 4-3. It will be noticed that Climatology has the lowest

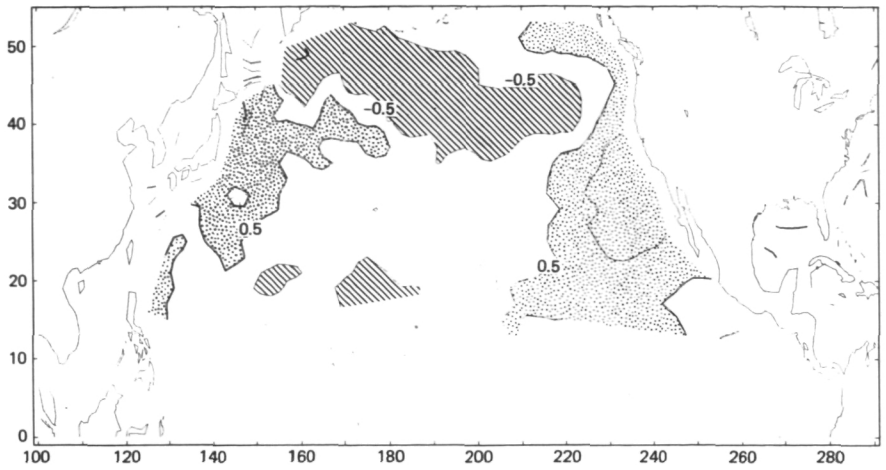

(a)

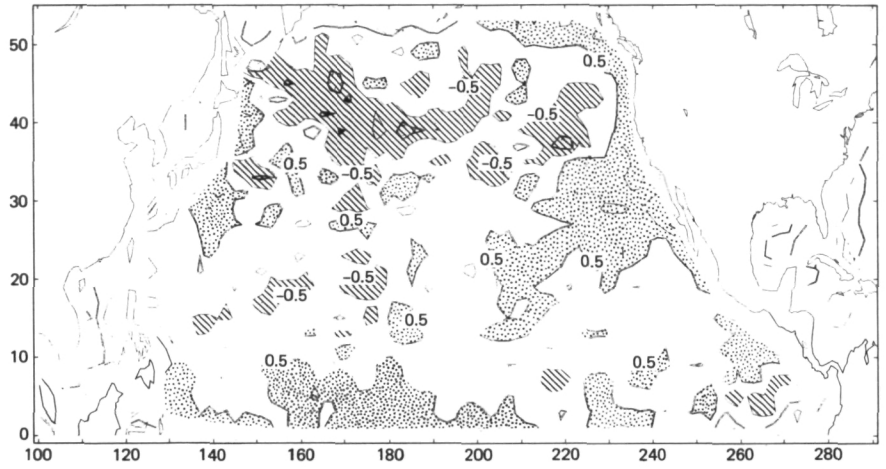

(b)

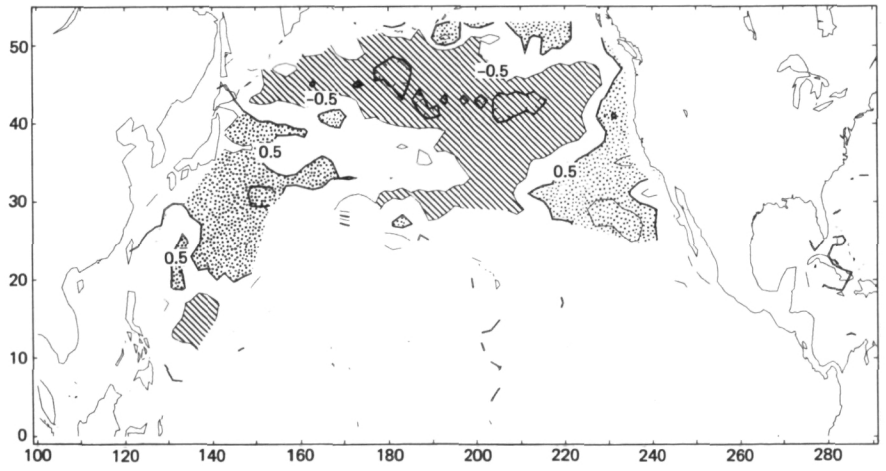

(c)

Figure 4-8. Contour maps of SST anomalies in North Pacific, November 1979. (a) AVHRR (GOSSTCOMP). (b) HIRS. (c) Ships.

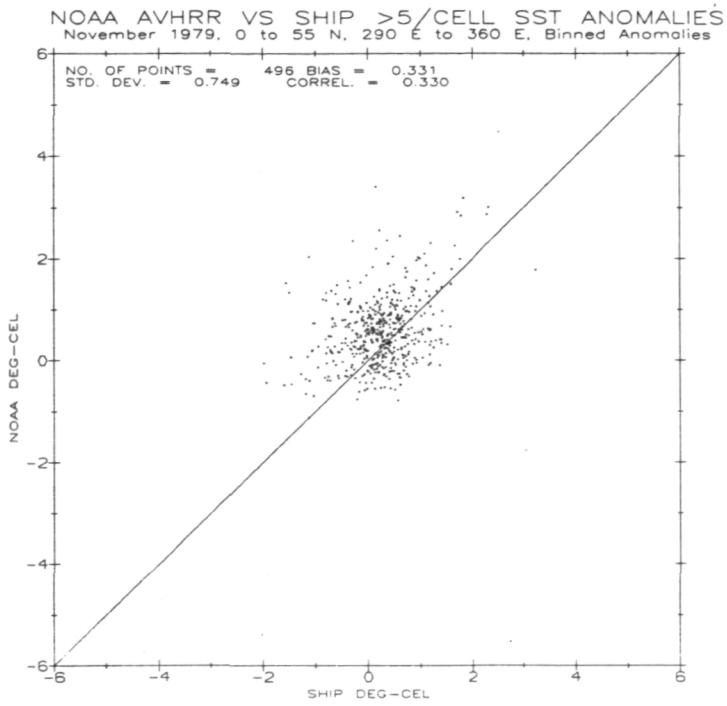

(a)

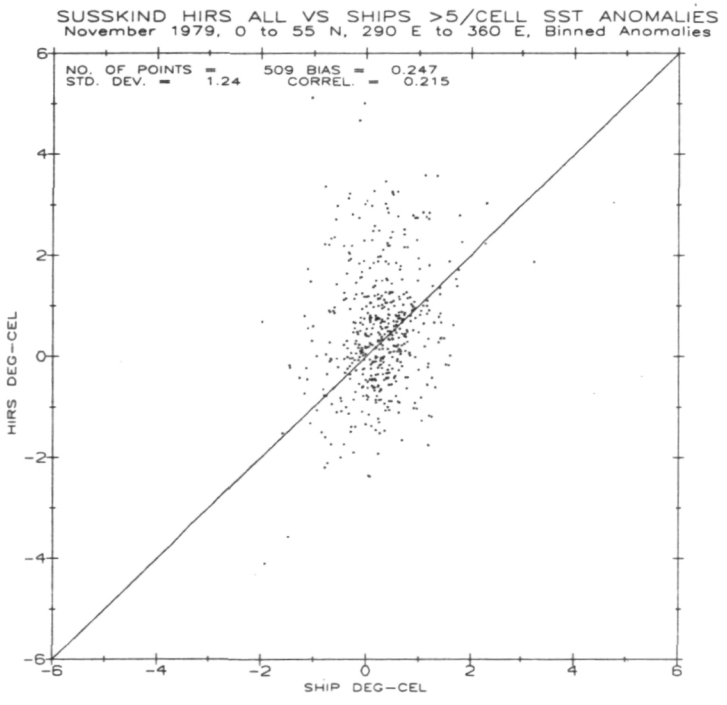

(b)

Figure 4-9. Scatterplots of binned satellite SST anomalies versus ship SST anomalies, November 1979. (a) AVHRR (GOSSTCOMP), North Atlantic. (b) HIRS, North Atlantic. (c) AVHRR (GOSSTCOMP), North Pacific. (d) HIRS North Pacific.

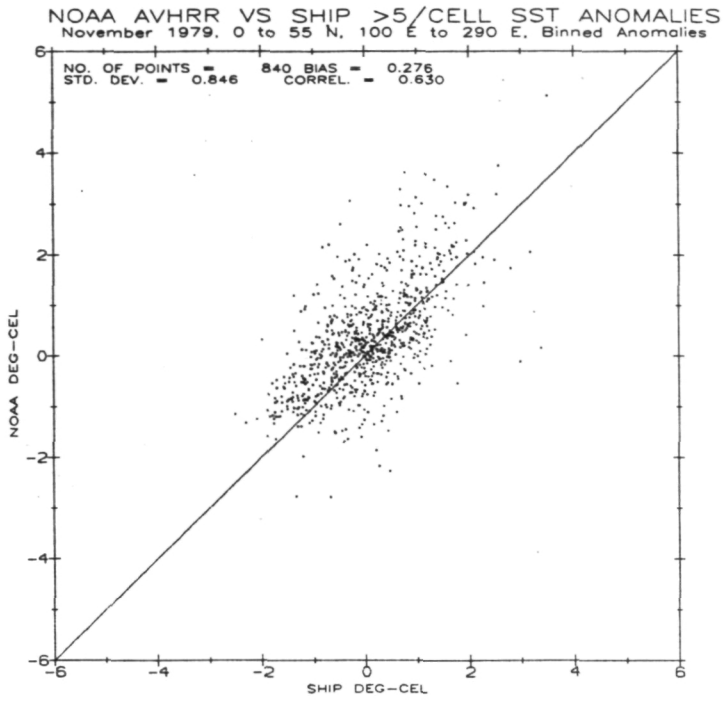

(c)

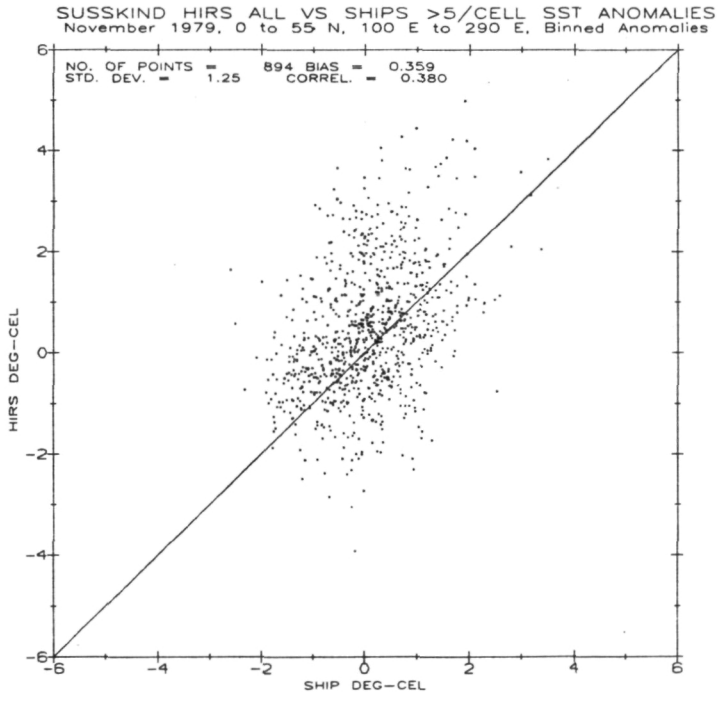

(d)

Figure 4-9. (Continued)

Table 4-1. Two-Degree Average SST Anomaly Cross-Correlations
(a) December 1981. (b) November 1979.

(a)	AVHRR	SMMR	Ship	
AVHRR		0.26 (386)	0.67 (494)	A t l a n t i c
SMMR	0.07 (1165)		0.29 (255)	
Ship	0.60 (867)	0.17 (448)		
	Pacific			

(b)	AVHRR	HIRS	SMMR	Ship	
AVHRR		0.25 (768)	*	0.33 (496)	A t l a n t i c
HIRS	0.45 (1675)		*	0.22 (509)	
SMMR	0.44 (958)	0.17 (1110)			
Ship	0.63 (840)	0.38 (894	0.34 (397)		
	Pacific				

Table 4-2. Rms Error Partitioning Table for AVHRR, November 1979

	1	2	3	4	5
1	-	-	-	-	-
2	-	-	0.75	0.45	0.88
3	-	2155	-	0.54	0.90
4	-	1011	3970	-	0.70
5	-	2156	7062	4011	-

Notes: (1) Upper right triangle of table contains rms error (^{o}C) in triad. Lower left triangle contains number of common grid points in triad. Row and column number define second and third data sets in triad.

(2)

Row/Column	Description
1	AVHRR
2	SMMR
3	HIRS
4	Ship
5	Climatology

(3) Average overall rms error partitioned to AVHRR = 0.70^{o}C

Table 4-3. Summary of Partitioned Average RMS Errors (^{o}C)

	November, 1979	December, 1981
AVHRR	0.70	0.62
SMMR	1.05	1.09
HIRS	0.93	-
SHIP	0.93	0.59
CLIMATOLOGY	0.62	0.42

rms "error". Ideally, the Climatology "error" is the real global, monthly-averaged rms SST anomaly. The fact that the Climatology rms error is less than for any other sensor implies that, averaged spatially over the entire globe, the rms SST anomalies are of the order of 0.5°C, which is less than the precision of the satellite sensors. However, in local areas where anomalies of greater than 1 or 2°C occur, the satellite sensors will clearly provide a better estimate of SST than Climatology.

From Table 4-3 it would appear that December 1981 was closer to climatology than November 1979. The reduction in ship error is probably due to the improved editing performed on the 1981 ship data. The improvement in AVHRR is probably due to the improved MCSST retrieval approach implemented in December 1981.

The error-partitioning procedure is based on the previously-stated assumption that errors in the sensor data sets are uncorrelated. Clearly, this is unlikely to be true. Errors from instrument noise are undoubtedly uncorrelated, but errors from instrument calibration drifts (e.g. sensor temperature variations due to sun effects) or geophysical effects (e.g. insufficient cloud filtering, SST-dependent biases, etc.) may be highly correlated in some regions. Thus, the error-partitioning approach can be used as a guide, but not as a quantitative method, for deducing sensor error. The fact is that there is no error-free standard or "truth" for comparing global SSTs and methods which infer sensor accuracies indirectly are necessary.

SECTION V
DISCUSSION SESSION SUMMARIES

In addition to evaluations of global data sets, discussion sessions were held during the workshop to focus on three issues: (1) Needs and applications for SST, (2) Atmospheric corrections to infrared SST measurements, and (3) New sensors and techniques. The discussion sessions are summarized below.

V.1 SST Applications and Requirements

Potential Uses of SST Products

Three general classes of SST product users are delineated in this section. The first group is interested in problems of climate dynamics. Potential uses here include diagnostic and prognostic studies of climate variation, as well as initialization for general circulation models. Spatial scales of interest are of order 500 kilometers or larger with associated time scales of weeks to months or longer. The second general class of user is termed simply "oceanography". The associated studies here include investigation of boundary currents, mesoscale eddies, fronts/plumes, the coastal boundary layer equatorial currents and upwelling phenomena. The appropriate spatial scales are from less than one kilometer to the order of 1000 kilometers and associated daily to weekly or longer time scales. The third general class of users are with fisheries or biological oceanography. Here the emphasis is on mean daily temperatures and frontal positions in the coastal regions, as well as water color. The time and space scales of interest are, respectively, daily and 1 to 100 km.

Climate: Studies of climate using satellite-derived sea surface temperatures are in their infancy. There are at least three major problems that confront users in this area. Problems of instrumental bias with respect to conventional climatology can introduce apparent anomalies in the data sets. The Workshop gave ample evidence that the bias problem is under attack by those producing satellite SST data sets.

Two more severe problems are associated with calibration drifts of the satellite-borne instrumentation over time and the dependence of the error in sensing sea surface temperature on other atmospheric variables. These last two problems are of first order importance and do not seem to have been adequately considered in the past. However, AVHRR MCSST operational products are monitored daily by matchups with ships in 20^{o} latitude belts and monthly with respect to fixed and drifting buoys.

Contrary to some popular opinion, climate users will be largly interested in regional SST variability. For some purposes, satellites may be effective now in providing some of the information they need. For instance, off the coast of South America anomalies of order $6^{o}C$ have been observed in the last year. Nearly all of the satellite products discussed at Workshop II appear capable of detecting changes of this amplitude. By contrast, in the North Atlantic Ocean away from the western boundary, the RMS variability is of order $0.3^{o}C$. It appears from this Workshop that none of the satellite products alone can presently provide that level of accuracy.

Finally, it should be noted that the absolute value of sea surface temperature produced by satellite methods, not just the anomalies, is also of importance. A good example here is the sensitivity of the water vapor pressure to absolute value of temperature. In the western equatorial Pacific, errors in the SST products of order 0.5°C can cause serious problems in establishing boundary conditions for atmospheric models. Similar errors in the high-latitude oceans will not be nearly as important. Thus the sensitivity and the accuracy required by climate users on a regional basis will be a strong function of both space and time.

It is of utmost importance to determine the space/time structure of the error field associated with satellite SST products. As noted above, dependence of these errors on atmospheric variability can be fatal for climate studies. It is also vital to determine the magnitude of expected error relative to the climate signal that is being studied. It appears that Workshop II was on the verge of developing the type of error data needed by the climate community, but longer time series of satellite products will need to be investigated to complete the picture.

In summary, one can pose the question: Are satellite SST data presently useful for climate research? The answer for now must be "unknown". Verification of satellite products in the tropical regions where the future ENSO and TOGA programs will be concentrated is still a problem, although the situation has improved over the last few years.

Physical Oceanography: The study of western boundary currents, eddy fields, and fronts appears virtually impossible without the use of satellite products. The discussions presented by Vastano, Brown et al, Hagan, and others at Workshop II amply demonstrated that the rich spatial structure of these features will be virtually impossible to measure effectively with conventional oceanographic instrumentation.

Some of the presentations at Workshop II gave hope that the strictly "gee whiz" days of satellite oceanography have come to a conclusion. Thus investigators are now beginning to put quantitative pictures of the ocean forward, as opposed to simply showing an IR image of an eddy and expressing their amazement at its complexity. It is perfectly clear, however, that in many cases the satellite products require surface truth to either tie down the satellite product to actual ocean conditions or to verify that satellite algorithms are performing adequately.

Problems in the coastal boundary layer, such as upwelling, appear to have many of the complex properties associated with the other ocean features noted above. They are event-like, spatially complex, etc. Unfortunately, many of the coastal zones are often cloud-covered, and that presents problems for the infrared sensors, the best developed and highest resolution of the current SST sensing devices.

In summary, it appears that satellite-derived SST products are now useful for studying ocean variability. It is desirable to go from the qualitative description of satellite products to a more quantitative assessment of their usefulness. Some surface truth will continue to be necessary.

Fisheries: In many of the coastal regions it is known that fish tend to congregate along frontal zones, i.e. strong horizontal gradients in temperature. The satellite again offers several ways to detect and monitor the behavior of such frontal zones. In addition fishermen require information on the mean temperature (not as critical) and also on water color. All of these variables, for instance, have been successfully used by National Marine Fisheries Service to vector fishermen into areas of high tuna concentrations off the west coast of the United States.

The problems associated with fisheries are somewhat different from those noted above. As indicated, the mean temperature is not as critical as knowing where the gradient is. Other problems that have come up, unfortunately, are the effect of cloud cover on remote sensing in the infrared. Fishermen need to follow the fronts and the fish on a day-to-day basis and the AVHRR cannot provide this information continuously because of cloud cover. This opens the possibility for microwave devices (SMMR) which at least can see through most clouds, the data processing problem presumably being soluble as it would be with AVHRR. Unfortunately the SMMR experiences sidelobe contamination in the coastal regions, just where most of the fishing information is desired, and where better spatial resolution is needed. Thus its eventual application to the fisheries problem is uncertain. The HIRS/MSU system discussed briefly at Workshop II may be able to use the best of infrared and microwave technique to provide the necessary information, but this has so far not been demonstrated.

Concerns

In trying to synthesize the results of the conference from a users standpoint, three major areas of concern arose. These are listed below and briefly discussed. A set of recommendations aimed at resolving these concerns is presented in the final section.

Technique: The theoretical basis for infrared emission by the surface and transmission through the atmosphere is quite well understood although some problem areas remain (see discussion in Section V.2). The AVHRR MCSST equations were initially derived by regression using theoretically computed radiances. When applied operationally to satellite data these equations produced SSTs that compared well with high-quality in situ measurements although subsequent tuning of the equation coefficients was performed to remove a small temperature-dependent bias (Ref. 20). Other investigators have derived equation coefficients by direct regression of the satellite radiances against in situ measurements (e.g., Ref. 14). It was shown in the Workshop that regression coefficients derived under one set of regional environmental condtions can result in large SST errors when applied to satellite data in other regions. The operational MCSST equations, although tuned using globally and seasonally representative in situ data, are still vulnerable to error under anomalous atmospheric conditions. More work is needed for a full understanding of these effects.

The situation with SMMR is less advanced than with the AVHRR. This is perhaps as it should be as SMMR is a much newer instrument. The current algorithms are again based on theory with regression coefficients tuned for better accuracy. Indeed, the regression is tied to climatology which is

distressing for studies of climate variability. Further, Workshop II presented examples of large variations in SMMR derived SSTs that could not be explained physically. It appears there is much work to be done in understanding this measurement technique before it can be applied practically.

Highly encourgaging results from the HIRS/MSU system were presented during Workshop II. It is desirable to factor this system more fully into the SST intercomparisons for Workshop III and to understand its performance versus AVHRR and SMMR.

As a final note, Workshop II occasionally took on the appearance of a competition between SMMR and AVHRR. The casual observer might note that infrared instruments and techniques for analyzing their output have been around for at least 15 years, while the microwave approach is really in its first generation, both mechanically and with regard to interpretation. From a user's point of view SMMR potentially offers more than AVHRR because of the number of variables to which it is sensitive. Thus, further development of this instrument is something that an interested user might want to follow, although it will continue to suffer from relatively coarse spatial resolution. It appears premature to use SMMR products on most current scientific problems.

Intercomparison: It is common to compare sea surface temperatures derived from satellites with those from ships. The bias and standard deviation between the two sets seem to be the standard measures of correctness of the satellite product. It is suggested that this approach has perhaps outlived its practicality for a variety of reasons. For instance, we know that the ship sets are "lousy". We also know that two different analyses of the same set of raw ship data can exhibit differences that are nearly as large as many of those between satellite products and ships discussed during Workshop II. This raises the question of what the RMS error estimates really mean. Further, the question of their statistical significance needs to be addressed.

It also appears that those involved in remote sensing have been more concerned with "correctness" tests than with "usefulness" tests. The former tests might take the very best ocean data available in an attempt to verify to one or two decimal places the accuracy of the satellite derived SSTs. These tests have tended to be limited to rather special (highly favorable) areas. "Usefulness" tests, on the other hand, are just beginning to be conducted by the remote sensing community and others. These tests take the satellite product and attempt to ask if it can be used to solve the problems of the researcher. It is clear that the outcome of such tests will depend on the problem being considered, e.g., the results of Workshop II indicate that whereas the SST products are perhaps marginal for climate studies, they are being used successfully right now for investigation of western boundary current features. Many other examples of oceanographic applications of AVHRR data have been reported in the open literature.

Reliability: A factor not sufficiently considered by the developers of satellite SST products is that of reliability. A potential user in many cases has no indication of where a product is apt to be good or where it is apt to be bad. For some products there is no indication of where climatology has been factored into the analysis because of the lack of observations. The discussion presented by D. Halpern in Workshop II was an example of the

problems that a user is apt to encounter in trying to use satellite or blended products without some type of reliability index. If the satellite SST people expect to develop a strong and faithful following of users of their product, then it will be incumbent upon the remote sensing community, in cooperation with oceanographers and meteorologists to develop ways of indicating the reliability of their product.

Many users seem to feel that the attempt to derive satellite-only SST products is valuable, but to solve research problems a combination of satellite, ship, buoy, ... data is required. The remote sensing community might do well to keep this idea of blending data sets in mind. The National Meteorological Center is one group actively attempting to develop such an overall blended product.

Recommendations/Needs

The usefulness and reliability of satellite-derived SST products could be greatly enhanced if the remote sensing community were to address the problems noted below. These recommendations were developed in open forum at the end of Workshop II.

The need to understand the basic physics of remote sensing: The AVHRR MCSST is the only operational satellite SST product available and has been shown to be useful for a number of applications. However the algorithms do not work under all cloud-free conditions and the reasons for this are unclear. It is recommended that situations where the MCSST product gives erroneous results be examined more closely to determine the atmospheric and/or surface conditions giving rise to these errors. Similarly, the need for temperature-dependent bias corrections should be understood on a physical basis. These recommendations apply equally to SST products from the SMMR and HIRS which are currently still in the research (i.e. non-operational) mode.

Meaningful intercomparisons: It was a concensus of the users at the Workshop that meaningful comparisons of the satellite products and ship data could be carried out and that many of these might be available for Workshop III. Specific recommendations included:

(a) That the difference between satellite products, ship products, etc., be expressed as a function of averaging time and spatial averaging domain. Thus some of the satellite-ship intercomparisons discussed during the workshop might be ascribed to point versus point comparisons. More interesting for climate studies, on the other hand, would be intercomparisons over an averaging distance of 1000 km and time scales of order a month. Such a space-time distribution of error should make it possible to determine, for each research application, a critical scale in both space and time above which the SST products might be useful (assuming the random component of error is reduced by space/time averaging).

(b) It seems vital to intercompare ship-derived SST products in the same way that satellite SST products are compared with ship products. This will give a threshold of difference against which the satellite products could be measured. Certainly if they are doing as well as the ships now, that should be noted. Indeed the limited AVHRR and HIRS/MSU intercomparisons with ship products were highly favorable to the satellite systems.

(c) It is crucial to determine the dependence of the errors in satellite derived SST on geographic region. The dependence of the error on phase of the annual cycle and even the phase of the daily cycle are also important to potential users.

(d) A number of detailed aspects of the intercomparison error analysis were discussed. For instance, what is the effect of the 600 km mask now applied to SMMR data on the intercomparisons. It was also noted that the errors are apt to be biggest in areas of strong spatial SST gradients. Therefore it was suggested that the dependence of product differences be evaluated in terms of these gradients, the latter being easily obtained from existing climatology.

It was also suggested that the subgrid variability associated with the SST products be investigated in much the same way that the subgrid variability in cloud composites is now being estimated. Along with ths subgrid study would go an investigation of the dependence of SST product errors on the actual number of observations in a given averaging area. This might lead the way to the reliability index called for earlier.

Blended SST products

It seemed the consensus of many at the Workshop that some thought should be given to developing a blended product, i.e., one using all available SST information. Such a product might eliminate bias problems in satellite SST estimates by using research ships and buoys to "tie down" the mean field, allowing the higher resolution "adjusted" satellite data to be used in filling in the sometimes large areas between surface observations. Something along these lines is now being done at the National Meteorological Center. While this activity does not seem appropriate to Workshop III, it is a larger problem for the remote sensing/user community that might represent a logical follow up to the current workshops series.

V.2 Atmospheric Corrections for Infrared SST Measurements

Introduction

The global SST evaluations were paralleled by discussions addressing the atmospheric correction problem for regional and global ocean surface radiances sampled by the AVHRR. The discussions were motivated by awareness that differences in AVHRR-retreived SSTs may be due to variations in algorithm design and application, as well as to geophysical sampling variability. The session talks focused mainly on multichannel methods for atmospheric correction and possible error sources in the derived SSTs. It was hoped that these talks

would improve understanding of algorithm suitability and limitations in specific observing programs. The following paragraphs highlight the discussion topics, and these are summarized at the end of the section with recommendations by the discussion participants.

Background

Determination of the exact surface temperature from AVHRR radiance measurements requires elimination of cloud effects and correction for the atmospheric contribution, in particular that from water vapor. The formalism of the multichannel approach for retrieving atmosphere-corrected surface temperatures can be obtained from Refs. 11, 12. In effect, the method proceeds on the basis that, for a given cloud-free field of view, radiance differences between two or more selected IR wavebands are related primarily to appreciable variation in water vapor absorption properties in these spectral regions. The IR channels used on the AVHRR correspond to the broad spectral wavenumber bands of approximately 2450-2900 cm-1 and 840-1000 cm-1, which are considered high transmission windows. Absorption and emission by near-surface tropospheric water vapor affects the outgoing surface radiant flux, especially for the longer wavelengths. The most comprehensive AVHRR correction procedures to date involve IR transmittance simulations and statistical regressions of the calculated temperatures against measured in situ temperatures, the end result being linearized approximations relating SST to sampled brightness temperatures in two or more channels.

An examination of regression relations for the NOAA/NESDIS operational global SST products (Ref. 13) and similar relations developed for NOAA-6 (Ref. 14) and for NOAA-7 (Ref. 15) led to one conclusion: empirical factors that influence the development and testing of these relations can be a major error consideration when assessing relative accuracies for regional applications. i.e., although the model predictions are limited by inexact knowledge of the water vapor continuum and aerosol interactions, the effectiveness of a given method depends also on a combination of parameters such as geographical selection, instrument viewing geometry, cloud detection and filtering techniques, and pixel array size. Further, AVHRR multichannel procedures are empirical to a varying degree. For multi-spectral methods in development at Rutherford Appleton Laboratory (RAL), the empiricism relates strictly to atmospheric experimental and laboratory observations and standard radiosonde measurements to parameterize the transmittance model and perform the statistical regressions. The SST procedure of McClain, et al. (Ref. 13) incorporates bias corrections to relations derived in a manner similar to that used by RAL (discussed below), whereas the method of Bernstein (Ref. 14) relies on the theory of differential water vapor absorption but is based on multiple regression of quasi-syntoptic in situ and satellite radiance difference values to obtain the predictive SST relation. Each of the above methods has reported RMS accuracies very near 0.5°C and effectively no bias. The accuracies are determined through comparisons of spatially-averaged satellite-derived SST and in situ point measurements where the single point observation is assumed representative of an ensemble mean value over the spatial dimensions characterizing one or more pixels.

According to McClain (Ref. 13), the MCSST (Multi-channel SST) method has improved the RMS accuracy of the recent NOAA/NESDIS global SST products over the previous GOSSTCOMP products by at least $1^{o}C$. Unfortunately, there are no regional case studies in the literature that demonstrate that the bias present in the early GOSSTCOMP products, such as the 1^{o} to $4^{o}C$ tropical bias reported by Barnett, et al. (Ref. 16) and Pathak et al. (Ref. 17), have been resolved by use of the two or three channel multi-spectral approach. A recent comparison of MCSST and a multi-window SST derived by independent but similar procedure (Ref. 15) shows close values for satellite-minus-research ship statistics ($0.29 \pm 0.68^{o}C$; $0.1 \pm 0.53^{o}C$) and indicates consistency in the multichannel approach.

Discussion

Although there was general agreement that bias corrections might be necessary for adapting present global relations to regional applications, questions were raised as to what may be considered appropriate and significant corrections. As a case in point, recent temperature-dependent bias corrections applied to the NOAA/NESDIS global SST relations were discussed. Opinions varied regarding statistical assumptions on the drift buoy data used for this purpose, but it was considered that in future regional studies, data sets used for tuning and subsequent testing should be, at least, statistically independent and should lead to measurable improvement in the SST accuracy. To assess the local bias would thus require development of standard data sets that are representative of the local field variance. Mechanisms for such an effort were not explored, although prototype data sets could conceivably be incorporated into present data networks.

Possible error sources contributing to AVHRR SST retrievals and verification by in situ measurements were a major focus of the session. Error estimation for the procedures cited has essentially been determined through comparisons of ship or buoy observations and satellite measurements, where emphasis has been placed on minimizing discrepancies between the in situ/satellite match-ups. Saunders et al. (Ref. 15) have demonstrated the low RMS achievable ($<0.2^{o}C$) in numerical/statistical modelling efforts. In practice, the predicted SST is subject to error. Causes for the increased error from observations (0.5 to $1^{o}C$) were speculated on at length. Partitioning of error is the crux of the problem. As present AVHRR correction methods rely on regression, and assumptions are made that certain variables are fixed, a careful separation of the various error contributions to derived SST has not been realized. Spatial inhomogeneity of aerosols and surface emissivity variations were put forward as possible error sources. The general procedure has been to assume a constant emissivity value in the IR wavelength range of interest. Slight emissivity variations related to surface roughness conditions could introduce a non-systematic error. More discussion, however, was oriented to the unknown error from scattering effects due to aerosols. The correction process should account for variability in local aerosol concentration and behavior near the air/sea interface and seasonal variability of hygroscopic aerosols in relation to the large-scale, latitudinal gradient of tropospheric water vapor. In terms of stratospheric aerosols, contamination from the eruption of El Chichon was reviewed as a serious hindrance to AVHRR surface sensing and, in particular, to the detection and monitoring of anomalous SST fields in the eastern and south equatorial Pacific during the 1982-1983 El Nino event. Steps have been taken by NOAA/NESDIS investigators to correct for the

volcanic effects by development of a new formulation of the triple-window equation that is significantly less sensitive to the El Chichon type of aerosol.

A stumbling block to continuing improvement and practical application of the AVHRR multichannel method for real-time analyses is related to electrical interference problems from contamination of uncoated terminals and leads of the indium antimonide detector of the 3.7 μm channel. This is apparently caused by inadequate outgassing procedures immediately after launch. For at least 6 months to one year past launch, the noise levels in this channel of the NOAA-6 and NOAA-7 spacecraft were low and could be mitigated adequately by application of Fourier filtering techniques or simple averaging schemes. For the NOAA-8 instrument, launched in March, 1983, the noise problem has been so serious as to preclude any useful application of data from the 3.7 μm channel in multichannel correction methods. Attempts to reduce the noise in this channel by repeating the outgassing procedure for a 7-day period were quite successful. However, there was subsequently an indication of a gradual increase in noise level, so the outgassing may need to be repeated once or twice a year. NASA engineers are continuing to investigate solutions to this problem. Multichannel correction methods are restricted to NOAA-7 channels 4 and 5 during this period. As the 3.5 to 4 μm wavelength range is less sensitive to water vapor, making the Planck relation more sensitive to thermal variations and theoretically permitting more accurate surface measurement than in the 10.3 to 12.5 μm region (Ref. 18), the lack of the shorter wavelength channel for the correction appears a serious disadvantage, especially for tropical measurements. This channel is also important for cloud filtering.

Two other methods for obtaining SST from satellite measurements were briefly discussed. These are the direct inversion method of Chahine (Ref. 18) and optical depth correction methods based on multiple viewing angles (Ref. 19). Regardless of the approach taken, many methods and instruments will be applied to the SST problem in the future. A regular system of cross-checks between derived SST products would be highly desirable in order to improve data consistency and reliability for studies in regional ocean/atmosphere dynamics.

Recommendations

The following general recommendations arose out of this discussion session:

(1) Atmospheric radiative transfer modeling for passive infrared and microwave sensing techniques should be continued.

(2) Experimental and theoretical investigations of aerosol effects on passive visible and infrared observing methods should be continued.

(3) Programs should be developed to provide long-term verification data sets for satellite observations. These should include: (a) Systematic air-sea interaction studies to focus on effects such as skin-bulk temperature differences, emissivity variations due to roughness, etc, and (b) specific experiments to address calibration of absolute satellite-derived SST on large scales in various oceanic and atmospheric conditions.

SECTION VI
CONCLUSIONS AND RECOMMENDATIONS

The series of SST workshops, of which this is the second, will eventually cover four months of global SST data from four satellite sensors. Conclusions derived here are thus only interim, as data from the Spring and Summer months (March and July 1982) have not been examined yet. Discussion at the workshop covered several topics, some in great detail. Several recommendations arose out of the discussion sessions, and these were listed in Section V. In this section we repeat some of those recommendations and add others to provide a more balanced conclusion to the workshop.

1. AVHRR (MCSST)

By far the majority of satellite SST applications have been performed using the AVHRR. Based on data studies so far in the workshop, the AVHRR provides the least noisy and apparently most accurate SSTs in a global analysis. The data distribution is sparse in cloudy regions because of the necessity for cloud filtering. The AVHRR SST measurements may be susceptible to error in regions of high humidity due to the regression approach used in the operational retrieval algorithms. More case studies should be performed in the tropics to validate the AVHRR accuracy in these conditions. Aerosols are a source of error if not adequately detected and filtered out (as is routinely done with clouds). Further investigation of this issue will be made at the next workshop, when effects of aerosol contamination from the eruption of El Chichon will be studied.

Both point-to-point XBT and monthly-averaged (2^{o} lat-lon bins) ship comparisons indicate rms SST accuracy of ~0.6 to $0.8^{o}C$, with biases of a few tenths of a degree, for the operational MCSST product. The pattern of the biases, however, is not clearly understood, e.g., the difference between North Pacific and North Atlantic biases with respect to ships in December 1981 and the positive anomaly in the western equatorial Pacific in the same month.

2. SMMR

The two months of SMMR data studied so far (November 1979 and December 1981) both show positive bias problems in the Northern Hemisphere winter. It is postulated that this may be associated with inadequate decoupling of high-wind effects, which cause significant variations in ocean emissivity. Attempts to remove these effects have so far not been successful.

Other bias errors in the SMMR SST data predominantly appear to be connected with instrument problems. These problems are listed below:

(a) Poor calibration of the instrument prior to launch.

(b) On-off operation on alternate days mandated by satellite power limitations, leading to large thermal transients in the instrument.

(c) Scan-dependent polarization rotation from shared radiometers and poor antenna system design (the latter mandated by the restricted location of the instrument on the satellite).

(d) Low beam-efficiency antenna pattern and poor spatial resolution (again due to antenna design deficiencies).

(e) Spacecraft attitude uncertainties leading to geophysical algorithm error.

These instrument problems stem directly from the fact that the SMMR is a first-generation microwave SST sensor, unlike present infrared instruments, which have gone through several iterations since the first developmental satellite sensors. Explicit solutions to the problems listed above, if implemented in a future microwave system, would remove many of the apparent SMMR problems. These solutions are:

(a) Thorough pre-launch calibration (design and execution).

(b) Full time, continuous operation on the spacecraft.

(c) Separate radiometers for all channels, and scanning of the online antenna system.

(d) Bigger antenna with reduced aperture blockage.

(e) Better spacecraft attitude knowledge (star tracker).

3. HIRS and VAS

HIRS and VAS data have not been studied sufficiently so far (in Workshops I and II) to draw adequate conclusions or to make specific recommendations. This will be deferred until Workshop III.

4. Comparisons

Differences between satellite and in situ SST measurements should be studied, for completeness, as functions of averaging time and spatial averaging domain. Some of this work may be beyond the scope of the present workshop. However the following suggestions were made:

(a) In addition to the existing Workshop comparisons, data sets should be stratified by day-night, boundary current-open ocean, and tropics-extratropics. This would allow more detailed examination of the error structures.

(b) Comparison of independently-derived ship products should be performed as a baseline for errors to be expected from ship products alone. If satellites approach this level they will have shown their usefulness.

(c) Because of many factors (such as skin versus bulk temperature, point versus areal average, etc.), satellites and in situ SST comparisons may never improve beyond the approximately $0.5^{o}C$ level. At this stage satellite data should be evaluated according to the "usefulness" criterion by application in models, forecasts, etc.

5. Algorithms

Retrieval algorithms should be based, where possible, on solid understanding of the physical processes involved. This understanding needs to be improved in the areas of:

(a) Atmospheric continuum absorption and radiative transfer modeling in the infrared and microwave regions of the spectrum.

(b) Investigation of aerosol effects on visible and infrared radiation.

(c) Ocean emissivity variations due to roughness (wind).

Retrieval algorithm error should be determinable by simulation of contributing error sources. Comparisons between algorithms should be performed and the physical reasons for their differences determined.

6. Products

The user of SST data desires an SST "product" which combines the best attributes of the various data sets available, including satellite sensors, ships, buoys, and climatology (the latter only if unavoidable). Steps should be taken towards providing such a merged product, with the proviso that the end user must know the expected reliability of the product at all times and locations, i.e., a "reliability" map should be provided with the SST map.

7. Operational Validation

To ensure the long-term validity of SST data sets, especially for use in climate studies, dedicated verification sites are needed. These would be specially-instrumented sites in selected ocean regions whose main purpose would be to monitor long-term drifts in satellite data and regional satellite SST biases.

REFERENCES

1. Jet Propulsion Laboratory, "Satellite-Derived Sea Surface Temperature: Workshop-I," JPL Publication 83-34, Jet Propulsion Laboratory, Pasadena, CA, 1983.

2. Reynolds, R., "A Monthly Averaged Climatology of Sea Surface Temperature," NOAA Tech. Report NWS 31, Silver Springs, MD, 1982.

3. Reynolds, R., "A Comparison of Sea Surface Temperature Climatologies," J. Clim. Appl. Meteor., Vol. 22, pp. 447-459, 1983.

4. U.S. Navy, "U.S. Navy Marine Atlas of the World," IX, NAVAIR 50-1C-65, Washington, D.C., 1981.

5. Tabata, S., "An Evaluation of the Quality of Sea Surface Temperatures at Ocean Station P and NOAA Buoy Stations and Those Made by Merchant Ships Travelling in Their Vicinities in the Northeast Pacific Ocean," J. Appl. Meteorol., Vol. 17, pp. 374-385, 1982.

6. Wannamaker, B., "XBT Measurements Near the Sea Surface - Considerations for Satellite IR Comparisons and Data Bases," SACLANTCEN Memorandum SM-132, NATO SACLANT ASW Research Center, I-19026 San Bartolomeo (SP), Italy, 1980.

7. Barnett, T.P., R.A., Knox, and R.A. Weller, "Space/Time Structure of the Near-Surface Temperature Field During the NORPAX POLE Experiment," J. Phys. Oceanog., Vol. 1, pp. 572-579, 1977.

8. Wood, W., "Practical Accuracy of Sippican T-7 XBTs," Pacific Marine Science Report, Institute of Ocean Sciences, Victoria, B.C., Canada, 1976.

9. Walton, C.C., "Deriving Sea Surface Temperatures from TIROS-N Data," In: Remote Sensing of Atmospheres and Oceans, (A. Deepak, Ed.), Academic Press, New York, N.Y., 1980.

10. Saur, J.F.T., "A Study of the Quality of Sea Water Temperatures Reported in `Logs of Ships` Weather Observations," J. Appl. Meteorol., Vol. 2, pp. 417-427, 1963.

11. Prakhakara, C., G. Dalu, and V.G. Kunde, "Estimation of Sea Surface Temperature from Remote Sensing in the 11 to 13 μm Window Region," J. Geophys. Res., Vol. 79, pp. 5039-5044, 1974.

12. McMillin, L.M., "Estimation of Sea Surface Temperatures from Two Infrared Window Measurements with Different Absorption," J. Geophys. Res., Vol. 80, pp. 5113-5117, 1975.

13. McClain, E.P., "NOAA Satellite-Derived Operational Sea Surface Temperature Products," In: Satellite-Derived Sea Surface Temperature: Workshop-I, (E. Njoku, ed.), JPL Publication 83-34, Jet Propulsion Laboratory, Pasadena, CA, 1983.

14. Bernstein, R.L., "Sea Surface Temperature Estimation Using the NOAA-6 Satellite Advanced Very High Resolution Radiometer," J. Geophys. Res., Vol. 87, pp. 9455-9465, 9182.

15. Saunders, R.W., P.J. Minnett, A.M. Zavody, and D.T. Llewellyn-Jones, "Multichannel Infrared Measurements of Sea Surface Temperature from Space Using AVHRR/2," Quart. J. Roy. Met. Soc., (submitted), 1983.

16. Barnett, T.P., W.C., Patzert, S.C. Webb, and B.R. Bean, "Climatological Usefulness of Satellite Determined Sea Surface Temperatures in the Tropical Pacific," Bull. Am. Met. Soc., Vol. 60, pp. 197-205, 1979.

17. Pathak, P.N., "Comparison of Sea Surface Temperature Observations from TIROS-N and Ships in the North Indian Ocean During MONEX," Rem. Sens. Envir., Vol. 12, pp. 363-370, 1982.

18. Chahine, M.T., "Remote Sensing of Sea Surface Temperatures in the 3.7 m CO_2 Band," In: Oceanography from Space, (J.F.R. Gower, Ed.), Plenum Press, New York, N.Y., 1980.

19. Llewellyn-Jones, D.T., P.J. Minnett, and A.M. Zavody, "Infrared Measurements of SST: Ship-Satellite Comparisons in the North Atlantic, and Future Developments," (This Report, Part II), 1984.

20. Strong, A.E. and E.P. McClain, "Improved Ocean Surface Temperatures From Space - Comparisons With Drifting Buoys," Bull. Am. Met. Soc., Vol. 15, 1984 (in press).

21. Barnett, T.P., "Long Term Trends in Surface Temperature Over the Oceans," Mon. Wea. Rev., (in press), 1984.

PART II: SYMPOSIUM PAPERS

Multi-channel Sea Surface Temperatures from the AVHRR on NOAA-7

E. Paul McClain
NOAA/NESDIS

The general background of multi-channel sea surface temperatures (MCSST), and some of the details on the multiple-atmospheric window corrections of the measured brightness temperatures for atmospheric attenuation, are given in Appendix C to the report on the first workshop (NASA/JPL, 1983) and in McClain et al. (1983). In this report some details of the cloud-filtering procedures that are used in the automated operational processing of MCSSTs are described. Highlights of the comparison of global monthly mean MCSSTs for December 1981 (the first full month this NESDIS operational product was produced) with the in situ SST measurements used in the workshop are summarized.

Daytime MCSSTs. The first daytime cloud test, the Gross Cloud Test, is applied to the Target Arrays (11x11 arrays of 4-km scan spots centered about every 25 km) to eliminate areas that are totally or mostly covered by continuous cloud layers (see Table 1 for details of this and subsequent daytime cloud tests). Unit Arrays (2x2) within each Target Array passing this first test are subject to each of the following tests, in sequence, with only the surviving Unit Arrays passing on to the next test in the sequence: High-Resolution Land/Sea Tag Test (optional); Visible Uniformity Test; and Visible Cloud Threshold Test. Provisions for adding two nighttime infrared (IR) cloud tests in the daytime has been made recently in order to capture glittercontaminated but cloud-free Unit Arrays, and thus increase the total number of daytime MCSSTs. For those Unit Arrays passing all tests, the 11 and 12μm brightness temperatures in °K are averaged and used as input to the following equation to obtain the MCSST in °C:

$$MCSST_{(4/5D)} = 1.021\ T_{11} + 2.544\ (T_{11}-T_{12}) - 279.23 \qquad (1)$$

The Unreasonable SST Test (see Table 1) is the final daytime test and is applied to the atmospherically-corrected MCSSTs obtained from Eq.(1). Table 2 gives representative statistics for the total number (global) of Unit Arrays available and the number remaining after application of each of the tests. The High Resolution Land/Sea Tags (10 km) were not in effect on this day.

Nighttime MCSSTs. The nighttime cloud tests cannot use the visual channels of the AVHRR, of course, but do take advantage of the differing optical properties of, and sensitivities to, clouds of the several infrared window channels. Again, as in the daytime, a Gross Cloud Test is applied to the 11x11 Target Arrays (see Table 3 for details of this and subsequent nighttime cloud tests). That Unit Array of each Target Array passing this first test that contains the warmest scan spot in the Target Array must then pass, in

Table 1. DAYTIME MCSST CLOUD TESTS - BRIEF DESCRIPTION

1. GROSS CLOUD TEST - reflectance in Ch. 2 (0.725-1.1μm)<20% for >20 spots in 11x11 target array.

2. VISIBLE UNIFORMITY TEST - reflectance in Ch. 2 varies <0.2% among spots in 2x2 unit array.

3. VISIBLE CLOUD THRESHOLD TEST - reflectance in Ch. 2 <1.7% or a value specified as function of solar zenith angle, satellite zenith angle, and azimuth of viewed spot (varies from 1.2 to 4.0%).

4. UNREASONABLE SST TEST: SST not <-2C or >35C.

Table 2. DAYTIME CLOUD TESTS - GLOBAL MCSST REPRESENTATIVE STATISTICS (4/23/82)

Total unit arrays available after application of low-resolution land/sea tags but before tests below: 1,464,715

Test	Number surviving after each successive test	Fraction of remainder failing this test
1. GROSS CLOUD	1,116,879	23.7%
2. HI-RES. L/S TAG	1,116,879	0.0%
3. VIS UNIFORMITY	239,982	78.5%
4. VIS CLOUD THRESHOLD	25,355	89.4%
5. UNREASONABLE SST	22,179	12.5%

Remaining unit arrays with SST after application of all tests: 22,179 (1.5%)

sequence, the following tests: High-Resolution Land/Sea Tag Test (optional) IR Uniformity Test, IR Cloud Test, and Uniform Low Stratus Test.

For those Unit Arrays passing all tests, the 3.7, 11, and 12 μm brightness temperatures are averaged and used as input to the dual-window, split-window, and triple-window equations below:

$$MCSST_{(3/4)} = 1.021\ T_{11} + 1.519\ (T_{3.7}-T_{11}) - 276.75 \qquad (2)$$

$$MCSST_{(4/5N)} = 1.053\ T_{11} + 2.624\ (T_{11}-T_{12}) - 288.28 \qquad (3)$$

$$MCSST_{(3/4/5)} = 1.031\ T_{11} + 0.982\ (T_{3.7}-T_{12}) - 280.43 \qquad (4)$$

The final screening of the nighttime MCSSTs comprises two tests (see Table 3): SST Intercomparison Test and Climatology Test. The atmospherically-corrected MCSST from the triple-window equation, Eq. (4), is used for the final temperature. The Uniform Low Stratus Test is necessary because when this type of cloud condition is present the other IR cloud tests are often passed. Table 4 gives representative statistics for the total number (global) of Target Arrays available and the number remaining after application of all tests.

Global MCSST Fields. All the daytime and nighttime MCSST retrievals are composited onto weekly 100-km global and 50-km regional grids. Although each MCSST is representative of an 8x8-km area (unit array size), one or more daytime MCSST and one nighttime MCSST, cloud conditions permitting, are obtained per target array, target arrays are being centered about 25 km apart. The search distance for each 100-km grid point is an inverse function of the SST gradient, the maximum being 200 km. Each MCSST within the the search area is weighted, the maximum weight being applied for those located within 33.3 km of the grid point, and the weight decreasing with the square of the distance from there. The distance-weighted average MCSSTs for each grid point each day are composited into a weighted-average for the week by further weighting as an inverse function of the age of the observations. The final weekly global field is contoured at 1C intervals with the isotherms being dashed where the grid-point MCSST has not been updated in the past 7 days. Figure 1 gives an example in the form of the North Atlantic portion of a 100-km global MCSST chart.

Workshop-II Comparisons

This section draws on the extensive charts and statistical tables on sensor comparisons that were distributed to the participants in Workshop-II. Table 5 collects the statistics with reference to the monthly mean MCSSTs (NOAA AVHRR) for December 1981 and relative to the screened SST data set from ships that was used as a common basis of comparison for all the sensors represented (Section IV, NASA/JPL, 1983). All anomalies were likewise computed with respect to a common climatology, the so-called Reynolds climatology (Reynolds, 1982). The NOAA/AVHRR SSTs are characterized by

Table 3. NIGHTTIME MCSST CLOUD TESTS - BRIEF DESCRIPTION

1. GROSS CLOUD TEST - Ch. 3 (3.55-3.93μm) brightness temperature >270.16K for >30 spots in target array.

2. IR UNIFORMITY TEST - brightness temperature in Ch. 3(3.55-3.93μm), Ch. 4 (10.3-11.3μm), or Ch. 5 (11.5-12.5μm) varies <0.2K among spots in 2x2 array.

3. IR CLOUD TEST - $|(1.0916\ T_{11} - 25.09) - T_{3.7}| < 3.0C$

   $- |(1.0439\ T_{12} - 11.49) - T_{11}| < 1.0C$

4. UNIFORM LOW STRATUS TEST - $(T_{11} - T_{3.7}) < 0.7C$

5. SST INTERCOMPARISON TEST - calculated values of SST from the three atmospheric correction algorithms vary <1.0C.

6. CLIMATOLOGY TEST - SST calculated from triple-window equation departs from climatological SST at nearest 1° lat/long location by less than a value that is a function of the horizontal SST gradient (varies from 4 to 7C).

Table 4. NIGHTTIME CLOUD TESTS - GLOBAL MCSST REPRESENTATIVE STATISTICS (4/3/82)

Total target arrays available after application of low-resolution land/sea tags but before tests below: 185,401

Test	Number surviving after each successive test	Fraction of remainder failing this test
1. GROSS CLOUD	111,812	39.7%
2. HI-RES. L/S/TAG	111,812	0.0%
3. IR UNIFORMITY	28,999	74.1%
4. IR CLOUD TEST	23,991	17.3%
5. UNIFORM LOW ST.	21,396	10.8%
6. SST INTERCOMPAR.	18,010	15.8%
7. CLIMATOLOGY	17,944	0.4%

Remaining target arrays with SST after application of all tests (one SST/target): 17,944 (9.7%)

Table 5. COMPARISON OF MONTHLY MEAN MCSSTs WITH SCREENED SHIP SSTs (Dec. 1981)

Cross Correlation	0.47	0.52	0.24	0.61
Bias	0.19	0.29	0.14	0.11
St. Dev. about Bias	0.83	0.76	0.89	0.56
Number	4,103	1,457	732	725
Latitude range	55N-55S	0-55N	0-55S	0-55N
Longitude range	0-360E	70W-100E	70W-100E	0-70W

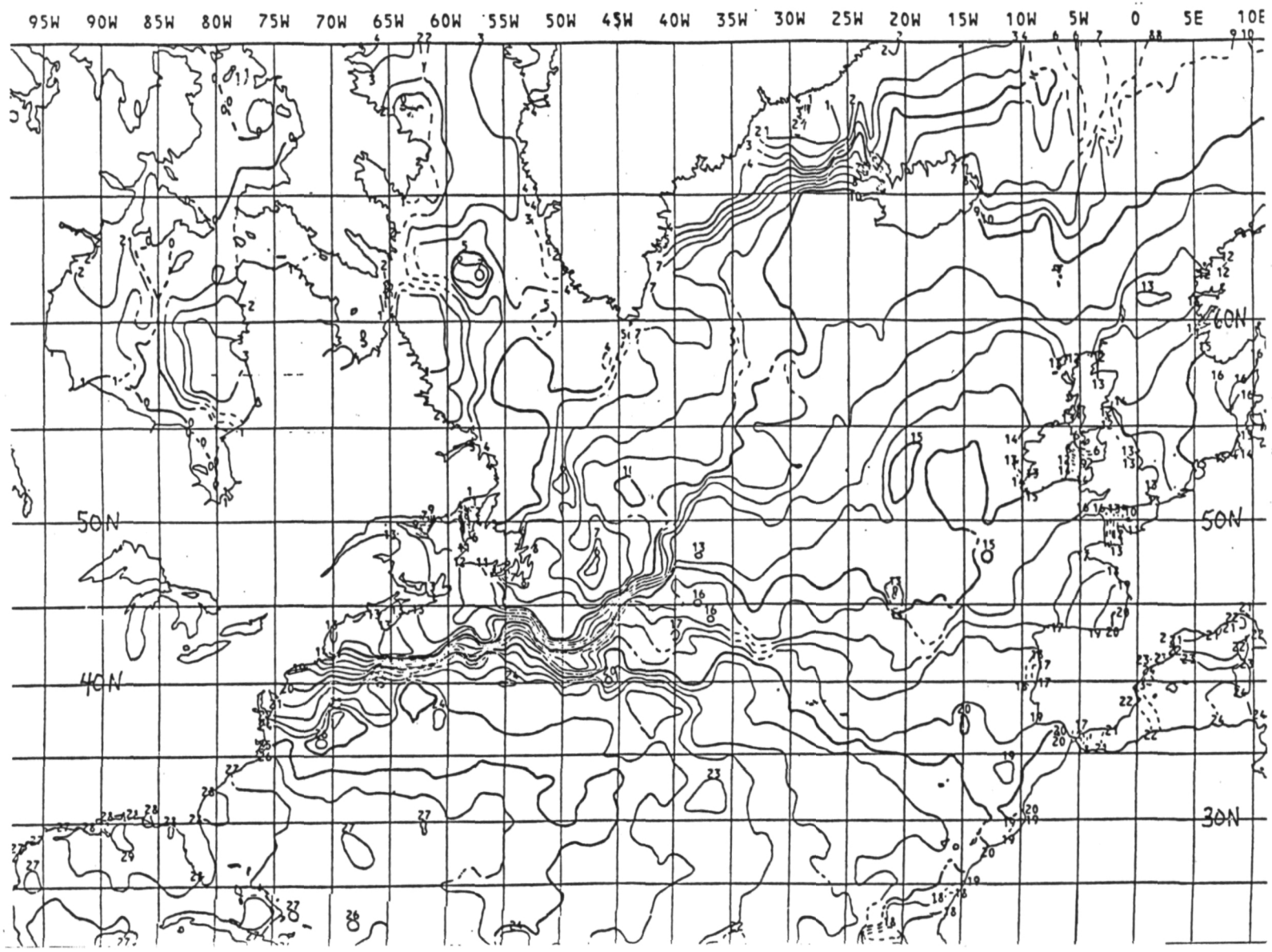
95W 90W 85W 80W 75W 70W 65W 60W 55W 50W 45W 40W 35W 30W 25W 20W 15W 10W 5W 0 5E 10E
60N
50N
40N
30N

Figure 1

significantly higher cross-correlations and substantially lower biases and standard deviations relative to the ship SSTs than any of the SMMR-based SSTs in the comparison (HIRS/MSU statistics were not available in time for the workshop, however).

Comparison of the NOAA/AVHRR SST anomaly patterns with those derived from the ship data set were not as satisfactory, although they were more so than those from the other sensors represented. The comparisons could not be made globally for lack of sufficient ship data nearly everywhere south of about 25N. The anomaly patterns in both the North Atlantic and the North Pacific were reasonably similar between the NOAA and the ship analyses, but the magnitude of the NOAA anomaly appear exaggerated in the Pacific.

Finally, it could be remarked that the NOAA/AVHRR SSTs had both a (sampling) and a coverage advantage over the SMMR-based SSTs because of the former's high spatial resolution and the latter's required exclusion of a 600-km wide zone around land masses.

References

NASA/JPL, 1983: Satellite-Derived Sea Surface Temperature: Workshop I. JPL PUblication 83-34, NASA Jet Propulsion Laboratory, Pasadena, CA, 160 pp.

McClain, E.P., Pichel, W.G., Walton, C.C., Ahmad, Z., and Sutton, J., 1983: "Multi-channel Improvements to Satellite-Derived Global Sea Surface Temperatures," Advances in Space Research, Vol. 2, No. 6, pp. 43-47.

Reynolds, R., 1982: A Monthly Averaged Climatology of Sea Surface Temperature, NOAA Tech. Rep. NWS 31, Silver Spring, MD, 35 pp.

SATELLITE SEA SURFACE TEMPERATURE ESTIMATION IN THE EASTERN TROPICAL PACIFIC OCEAN

R. L. Bernstein
SeaSpace, San Diego, CA

P. Pullen
NOAA/Pacific Marine Environmental Laboratory
Seattle, WA

Abstract

NOAA-6 and NOAA-7 AVHRR 1 km resolution daytime data was acquired for June and December 1981 over the eastern tropical Pacific. The data was processed using procedures described in Bernstein (1982), to extract estimates of sea surface temperature (SST). The estimates were gridded at 20 km resolution, and superimposed on 3.7 μm (AVHRR channel 3) infrared brightness temperature images of the same passes of data. Long (∿1000 km) wave structure is strikingly apparent in both the images and SST contours, where the cold equatorial upwelled water meets warmer water a few degrees of latitude away from the equator. Some of the waves were previously noted by Legeckis (1983) using GOES data. In addition, the gridded SST data were compared with ship data (R/V Oceanographer) and drifter data collected as part of the EPOCS (Equatorial Pacific Ocean Climate Study) Project. When the satellite and ship observations are nearly coincident in space and time, agreement is at the 0.5 C level.

References

Bernstein, R.L., 1982, Sea surface temperature estimation using the NOAA-6 satellite Advanced Very High Resolution Radiometer, J. Geophys. Res., 87, 9455-9465.

Legeckis, R., W. Pichel, and G. Nesterczuk, 1983, Equatorial long waves in geostationary satellite observations and in a multichannel sea surface temperature analysis, Bull. Am. Meteorol. Soc., 64, 133-139.

ACCURACY OF NOAA-7 OBSERVED SST IN THE NORTHEAST PACIFIC OCEAN

S. Tabata
Institute of Ocean Sciences
P.O. Box 6000
Sidney, B.C., V8L 4B2
Canada

Abstract

Five sets of sea surface temperature (SST) data obtained from NOAA-7 spacecraft and seaborne measurements during May through December 1982 have been utilized to provide a comparison between the satellite-derived and seaborne data. A linear regression curve fitted to each set of data indicated that the satellite is capable of providing SST to within ±0.5°C, as has been the case for other previous satellites. The slope obtained from the regression curve (average-0.39) is close to that indicated for the radiometer calibration data (-0.43). For most practical purposes the slope of the latter can be used to fit the data. The implication is that only a few sets of very good quality "sea-truth" data are necessary for field-calibration. However, frequent calibrations are recommended when changes in air masses over the area are suspected.

Introduction

In a previous study (Tabata and Gower, 1980; Tabata, 1981) the accuracy of satellite-observed sea surface temperatures (SST) for the various U.S. space-crafts (NOAA-3, NOAA-4, NOAA-5, NOAA-6, and Tiros-N) has been examined. It showed that the satellite-derived data can provide estimates of SST to within ±0.5°C if reliable sea-borne data are used to field-calibrate the satellite data. The present study is an update of the former study and concerns only the results obtained from NOAA-7.

Data

Five sets of data from May through December 1982 were utilized. The satellite data are the SST measured by the Advanced Very High Resolution Radiometer (AVHRR) of NOAA-7. They are based on the original Band 4 records and were processed at the Arctic Weather Centre of the Atmospheric Environment Service (Canada) at Edmonton, Alberta. The data were averaged to give mean SST over an area of approximately 2 km x 2 km. The radiometer calibration data were provided by the National Environmental Satellite Data and Information Service (NOAA).

The oceanographic data comprise SST observed continuously from research ships from a depth of 3-4 m at an area within 200 km of the Pacific coast of Canada and shore-based SST measured from a depth of one meter at the numerous coastal stations (mostly lighthouses). The accuracy of the above data are, respectively, ±0.1 and ±0.2°C.

Results

The plots of shipborne-shorebased SST against satellite-derived data for the dates in 1982: 8 May, 17 September, 28 September, 22 November and 10 December, are shown in Figure 1a, 1b, 1c, 1d and 1e, respectively. Details and statistics associated with the above data are shown in Table 1. It is evident from the results presented that the field-calibrations for the data for all periods, except 17 September, are basically similar, (Fig. 1a, 1c, 1d and 1e). The only difference with the 17 September data is that the curve is shifted 1-2° downward (Fig. 1b).

The scatter represented by the standard error of estimate is usually smaller for the comparison using shipborne data alone. It ranges from ±0.3°C for the 8 May data to ±1.1°C for the 17 September data. The corresponding values for those using shore-based data are, respectively, ±1.0 and ±1.2°C, and is as large as ±1.4°C (28 September), as indicated in Table 1.

Although the use of shipborne data for the comparison results in yielding a smaller value for the standard error of estimate it has the tendency to give an unrealistically low value for the slope (-0.12) due mainly to the narrow range of SST (2°C) available. (Table 1). The use of combined shipborne and shore-based SST for comparison with satellite data does result in increasing the magnitude of the standard error of estimate (than if only shipborne data were used) but, on the other hand, this appears to provide a more meaningful value (-0.39 average) for the slope.

Discussion and Conclusions

As was the case for observations from previous satellites (NOAA-3, NOAA-4, NOAA-5, NOAA-6 and Tiros-N) the satellite-derived data of NOAA-7, upon field-calibration with shipborne data yielded SST with an accuracy generally within ±0.5°C. Shore-based SST are characterized by relatively high level of "noise" due to local changes from diurnal heating and cooling to movement of water. The use of such data does, indeed, introduce more scatter about the regression line relating seaborne and satellite-derived SST. However, shore-based data frequently has a larger temperature range than those taken by a research ship cruising over a limited area. Their inclusion in the comparison is essential in that more realistic values for the slope can be obtained.

From the radiometer calibration data supplied by NOAA it is estimated that the slope of temperature versus count number is -0.43. At a count number of 100 the temperature is 12.9°C. The unweighted mean slope and the mean temperature at count number of 100, based on the present study (Table 1) is, respectively -0.39 and 13.97°C. The two curves resulting from the two sets of data are shown in Figure 2. Since there is only a 10% difference between the slope of radiometer calibration data and that utilizing observed SST, these slopes can be considered as similar. A curve with a slope of -0.43 drawn through the 100 count intercept of 13.97°C (one degree larger than that for radiometer calibration) would result in a calibration curve that would give estimated SST almost as good as that using the mean slope of -0.39 and 100 count intercept of 13.97°C. The implication of this is that a "practical" calibration curve for the satellite data can be obtained from only a few sets of very good quality "sea-truth" data. The source of such data can be SST taken by research or other vessels at about the time of the satellite overpass or they can be SST taken regularly from moored buoys. However, it would be necessary to field-calibrate regularly as the calibration may not apply from one day to another, due to changes in the atmospheric attenuation that may occur. An example of this can be cited from the comparison of the 17 and 28 September data.

It will be recalled that the field-calibration for 17 September (Fig. 1b) is slightly different from others, and particularly to that of 28 September (Fig. 1c). The reason for this appears to be due to a change in atmospheric attenuation. According to D. Faulkner of the Atmospheric Environment Service (private communication) the atmospheric condition in the area of the study on 17 September was featured by a presence of a well-defined easterly outflow from the continent, bringing very dry air over water and aloft. Both radiosonde and "surface observations" from coastal land stations indicated that the air was much dryer than normal. However, by 28 September conditions had evidently returned to normal when moist northwesterly airflow occurred over the area. It is likely that the presence of an uncommon air mass over the water on 17 September resulted in the reduction of atmospheric attenuation for that day. The need for frequent field-calibration during periods of changing air masses over the area is obvious.

Acknowledgements

I would like to thank the following for their assistance: E. Daghir of National Environmental Satellite Data and Information Service (NOAA) for providing the radiometer calibration data; G. Schram of Arctic Weather Centre and D. Faulkner of Pacific Weather Centre, both of the Atmospheric Environment Service for providing the original satellite data and weather information on dates of satellite overpass, respectively; L.F. Giovando for providing shore-station data; D. Ramsden for processing shipborne data; D. Truax for computer-processing of satellite data; P.M. Kimber for assisting in the analysis and making illustrations and A.L. Mathias for typing.

References

Tabata, S. and J.F.R. Gower, A comparison of ship and satellite measurements of sea surface temperatures off the Pacific coast of Canada, J. Geophys. Res., 85, 6636-6648, 1980.

Tabata, S., On the accuracy of satellite-observed sea surface temperatures, Oceanography from Space (Editor: J.F.R. Gower), Plenum Publishing Corporation, New York, N.Y., 145-157, 1981.

TABLE 1

Statistics and related data associated with NOAA-7 field calibration. Temperatures are in ^{o}C. SST = sea surface temperature.

SATELLITE ORBIT NUMBER	DATE 1982	REGRESSION ANALYSIS SLOPE	TEMPERATURE AT COUNT 100 EQUAL TO 110	STANDARD ERROR OF ESTIMATE	NO. OF OBSERVATIONS	OBSERVED SST RANGE	DATE OF SST 1982	SST OBSERVATION PLATFORM
4510	8 May	-0.28	12.57 9.77	0.30	34	1.5	4-5 May	Research Ship (RS)
		-0.43	15.02 10.72	1.01	11	4.9	8 May	Shore stations (SS)
		-0.31	13.06 9.96	0.59	45	4.9	4-8 May	RS & SS
6373	17 Sept.	-0.46	12.95 8.35	1.12	30	6.2	17 Sept.	RS
		-0.39	13.63 9.73	1.20	6	6.5	17 Sept.	SS
		-0.46	13.01 8.41	1.12	36	8.4	17 Sept.	RS & SS
6529	28 Sept.	-0.36	14.51 10.91	0.63	171	4.4	28-30 Sept.	RS
		-0.50	15.45 10.45	1.35	10	5.4	28 Sept.	SS
		-0.37	14.58 10.88	0.68	181	5.4	28-30 Sept.	RS & SS
7305	22 Nov.	-0.39	14.65 10.75	0.44	67	2.5	24-25 Nov.	RS
		-0.24	11.84 9.44	0.67	13	1.8	22 Nov.	SS
		-0.45	15.29 10.79	0.51	80	4.4	22-25 Nov.	RS & SS
7553	10 Dec.	-0.12	11.54 10.34	0.36	69	2.3	3-5 Dec.	RS
		-0.17	10.56 8.86	0.69	9	2.0	10 Dec.	SS
		-0.38	13.90 10.10	0.50	78	4.1	3-10 Dec.	RS & SS

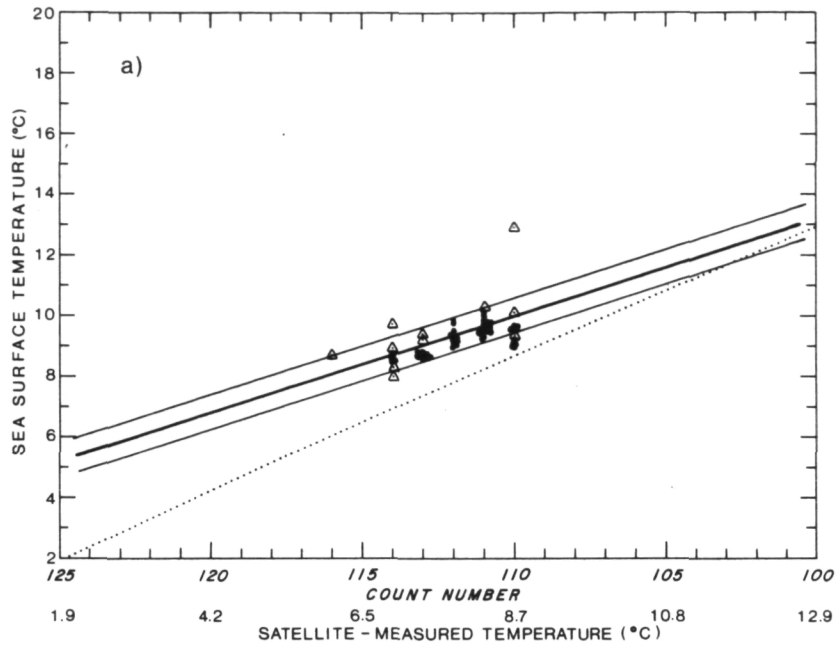

Figure 1. Plots of shipborne-shore station SST (^{o}C) against satellite-derived observations. Details and statistics associated with the above data are shown in Table 1. Triangles denote shore-station data. The two lines about the heavier regression line represent the standard error of estimate. The dotted line denotes the radiometer calibration data for 1 April 1983.

a. 8 May 1982
b. 17 September 1982
c. 28 September 1982
d. 22 November 1982
e. 10 December 1982

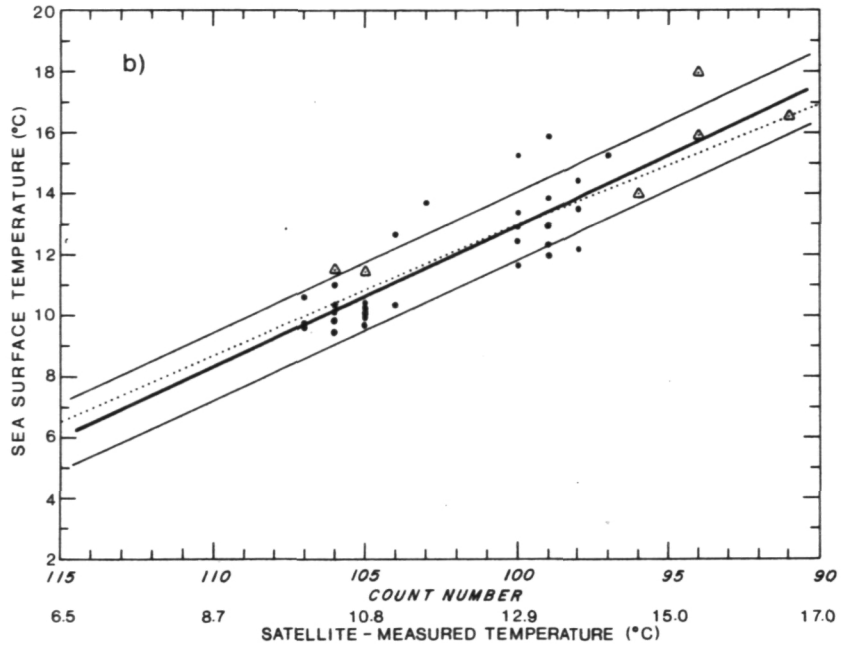

Figure 1b

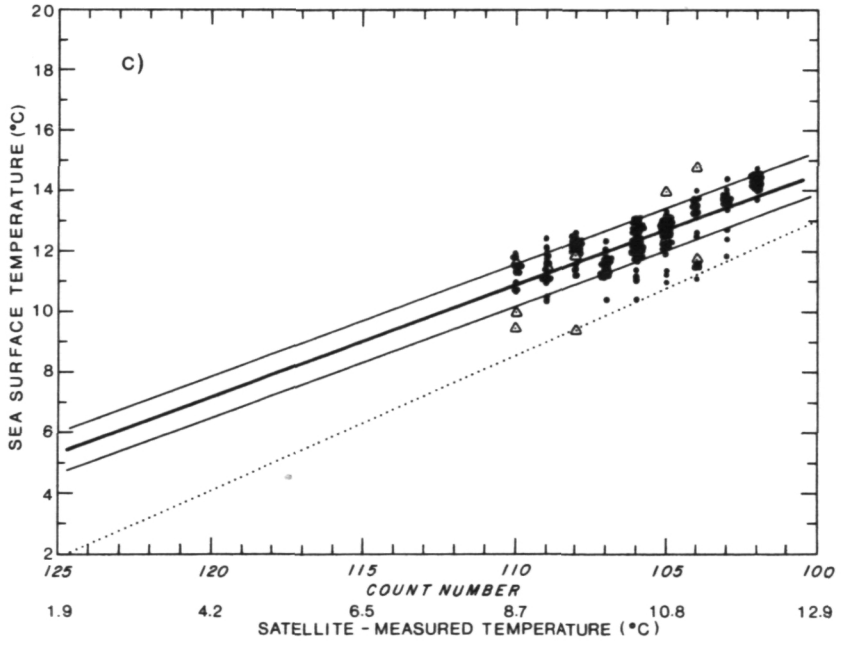

Figure 1c

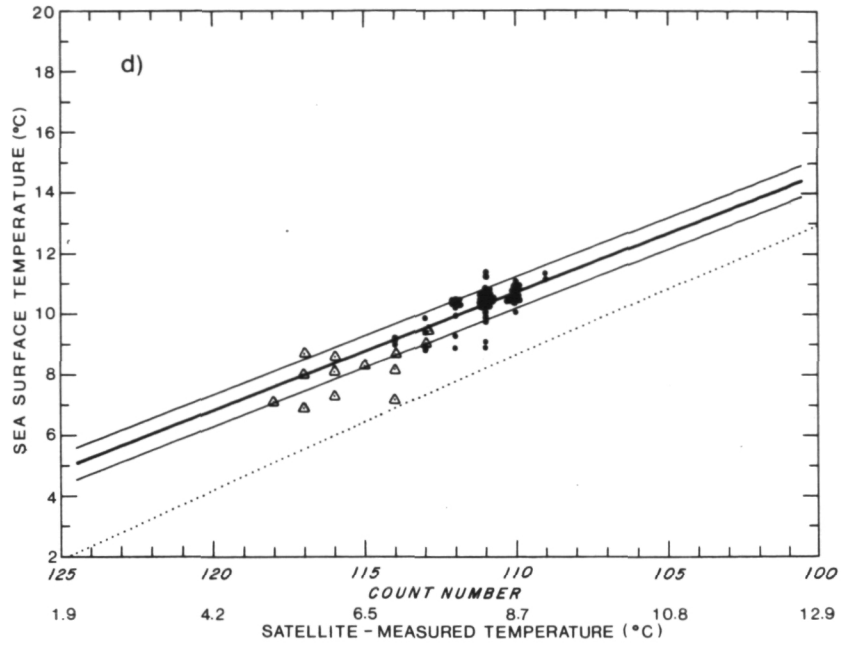

Figure 1d

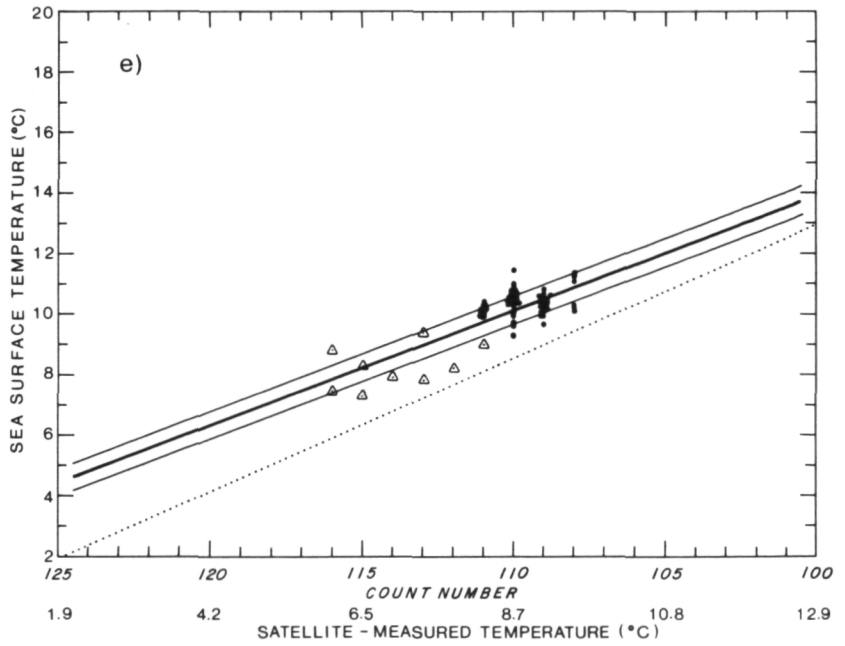

Figure 1e

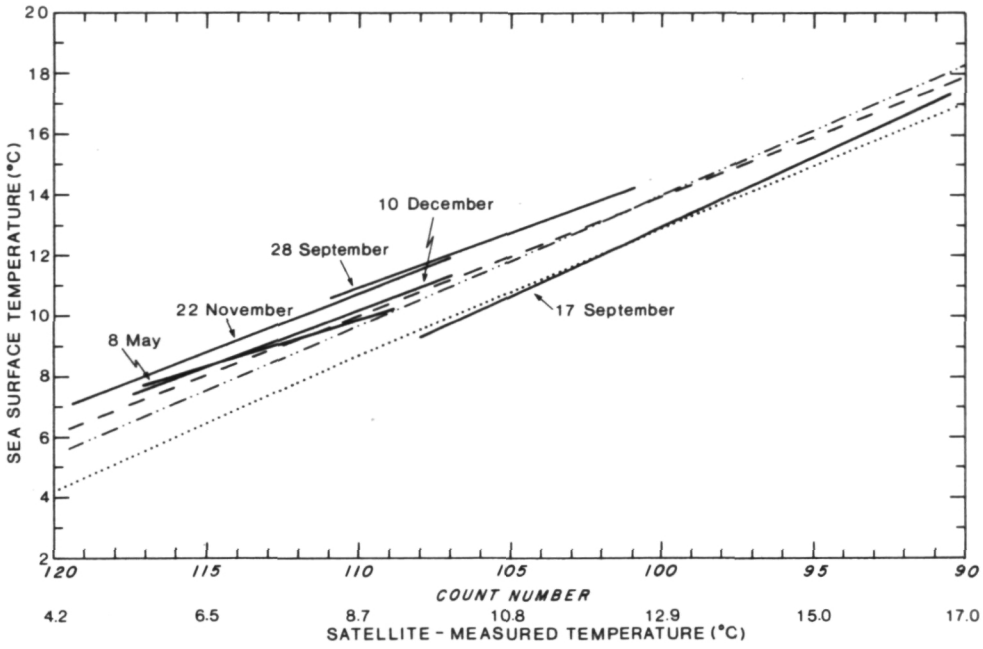

Figure 2. Field-calibration curves for data of 8 May, 17 September, 28 September, 22 November and 10 December 1982. The dotted line represents the radiometer calibration curve while the dot-dashed line represents this curve shifted one degree upward. Dashed line denotes the mean field-calibration curve based on May-December data.

INFRARED MEASUREMENTS OF SST - SHIP-SATELLITE COMPARISONS IN THE NORTH ATLANTIC, AND FUTURE DEVELOPMENTS

D T Llewellyn-Jones
P J Minnett
A M Zavody

Rutherford Appleton Laboratory, Chilton, Didcot, Oxfordshire, U.K.

Abstract

An atmospheric transmittance model, based on calculations of molecular absorption and aerosol scattering, has been used in deriving SST regression coefficients for satellite measurements both from AVHRR and the Along-Track Scanning Radiometer (ATSR) now being designed for the ERS-1 satellite.

The results of NOAA-7 validation exercises, undertaken in order to test the transmission model, are presented, and brief descriptions of ATSR and ERS-1 are given.

The urgent needs for improved cloud clearance procedures and accurate surface measurements are highlighted.

1. Introduction

Objective:

Experimental verification of atmospheric transmission models used for ATSR performance analysis and algorithm development.

Instrument Used:

AVHRR/2 on NOAA-7
CHS 3, 4, 5 for SST
CH 1 for cloud clearance
1 km resolution at Nadir in North East Atlantic (Dundee Receiving Station)
4 km resolution at Nadir in Tropics (NOAA 'Global area cover').

Simulations:

To compare performance of A - multi-channel retrievals
B - A+ along-track scanning
C - B+ μ-wave radiometry

Radiation: emitted by sea; emitted, absorbed and scattered by atmosphere; reflected by sea.

Molecular Absorption:	line-by-line calculations plus up-to-date atmospheric transmission models for water vapour "continuum".
Atmospheric Profiles:	globally representative radiosonde set (NOAA).
Particles:	confined to lowest 1 km, modelled with Mie theory.

256 layers in atmosphere to height 20 km (40 km)
59 radiosonde profiles with SST = T $\pm$ 0, 2, 4K

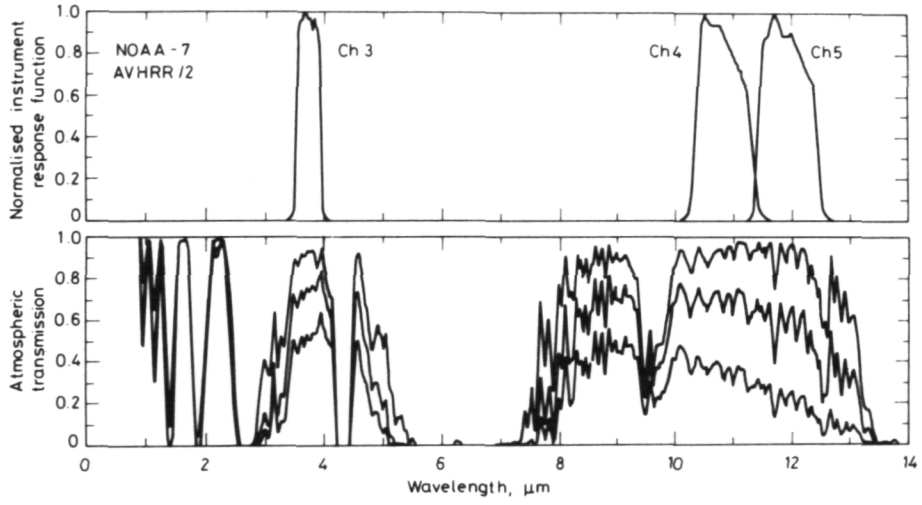

Fig. 1. Theoretical spectra of atmospheric transmission, at nadir, in the infrared region at 1 to 15 μm wavelength. The three spectra correspond to different amounts of precipitable water (7 mm - polar, 29 mm - temperate, 54 mm - tropical). Aerosol effects are not included in these spectra. The response functions of channel 3 (3.7 μm), channel 4 (11 μm) and Channel 5 (12 μm) of the AVHRR/2 on the NOAA-7 satellite are shown, and indicate the "atmospheric windows" used. The different dependence of atmospheric transmission on water vapour amounts in each "window" permits an estimate of the atmospheric effect in SST measurement by multichannel methods.

SST Retrieval Algorithms:

- Use line by line calculations of atmospheric transmission/emission.
- Global and regional subsets of NOAA radiosonde profiles.
- Linear regression.
  $SST = C0 + C1\ T1 + C2\ T2 + \ldots\ldots$
- Airmass dependence taken into account
- Cloud clearance by three possible methods.
- Spatial resolution of retrievals:
  50 x 50 pixels
  2280 km swath-width.

Airmass Dependence

- Atmosphere correction is non-linear function of airmass.
- Effect of neglecting it is significant (up to 2K).
- Specific regression coefficients derived for five air-masses:
  1.0, 1.25, 1.5, 1.75, 2.0
  Corresponding zenith angles:
  0°, 36.9°, 48.2°, 15.2°, 60°
- SST values for air masses 1-2 (ie 2280 km swath for NOAA-7) derived by linear interpolation between SST values corresponding to nearest airmasses.
- No apparent systematic dependence of SST scatter upon airmass.

Cloud Cover:

Three methods used:-

1. Truncated normal distribution (11 um histogram)
2. Spatial coherance (3 x 3 pixel sub-arrays used rejecting those with standard deviation 0.1 K) (2 x 2 also used).
3. Visible threshold.

- Good agreement found between these (except TND always warmer).
- Statistically significant systematic dependence upon number of cloud-free pixels.
- 3.7 μm channel (ch 3) not suitable as substitute for visible in threshold technique.
- Conclusion: advisable not to rely on one only!

2. Ship-Satellite Comparisons - Two Case Studies

Case Study 1 (Aug-Oct 81):

"Split-Window" SST Retrievals

- 53 Ship-satellite comparisons.
- AVHRR/2 (NOAA-7) ch 4 and 5.
- Research vessels only for surface measurements.

- Satellite values over 50 x 50 pixel array on which ship is centred.
- Each ship observation within 2½ hours of overpass.
  - North Atlantic
  - Tropics

Standard deviation: 0.58 K
Mean difference : -0.13 K

The results of this limited study, described in detail in Ref 1 were obtained using regression coefficients applicable specifically to the North Atlantic. When global coefficients are used, (either RAL or MCSST) a similar value of standard deviation is obtained, but the mean difference increases and changes sign.

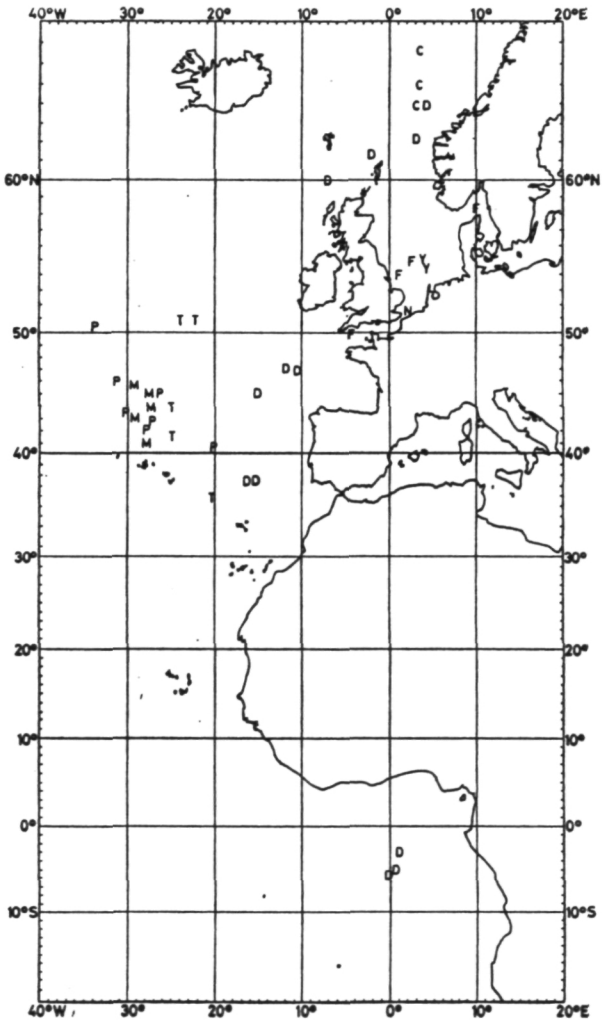

Fig. 2. The positions of the research vessels (each indicated by a letter) at the time of the ship-satellite comparison.

Case Study 2 (March 1982):

- 28 ship-satellite comparisons.
- XBT and drift buoys for surface measurements.
- SST retrievals and cloud clearance as in case study 1.
- Comparison of three "split-window" algorithms.
  - (i) RAL (Ref 1)
  - (ii) MCSST
  - (iii) Secant approximation (Ref 2).
- Results:

(i) statistics of SST (sat) - SST (in situ)

Algorithm	Mean	Sd	rmsd
RAL	-0.34 K	0.40 K	0.52 K
MCSST	-0.44 K	0.52 K	0.67 K
Secant	-0.15 K	0.42 K	0.44 K

For a sample of this size, the differences between these values are not statistically significant, except in the case of the low bias (-0.15 K) of the secant approximation.

(ii) cloud clearance is the most problematical aspect of SST retrieval. In this study the effects of the cases with 20% cloud-free pixels dominate any residual dependence on airmass or SST (see Fig. 3).

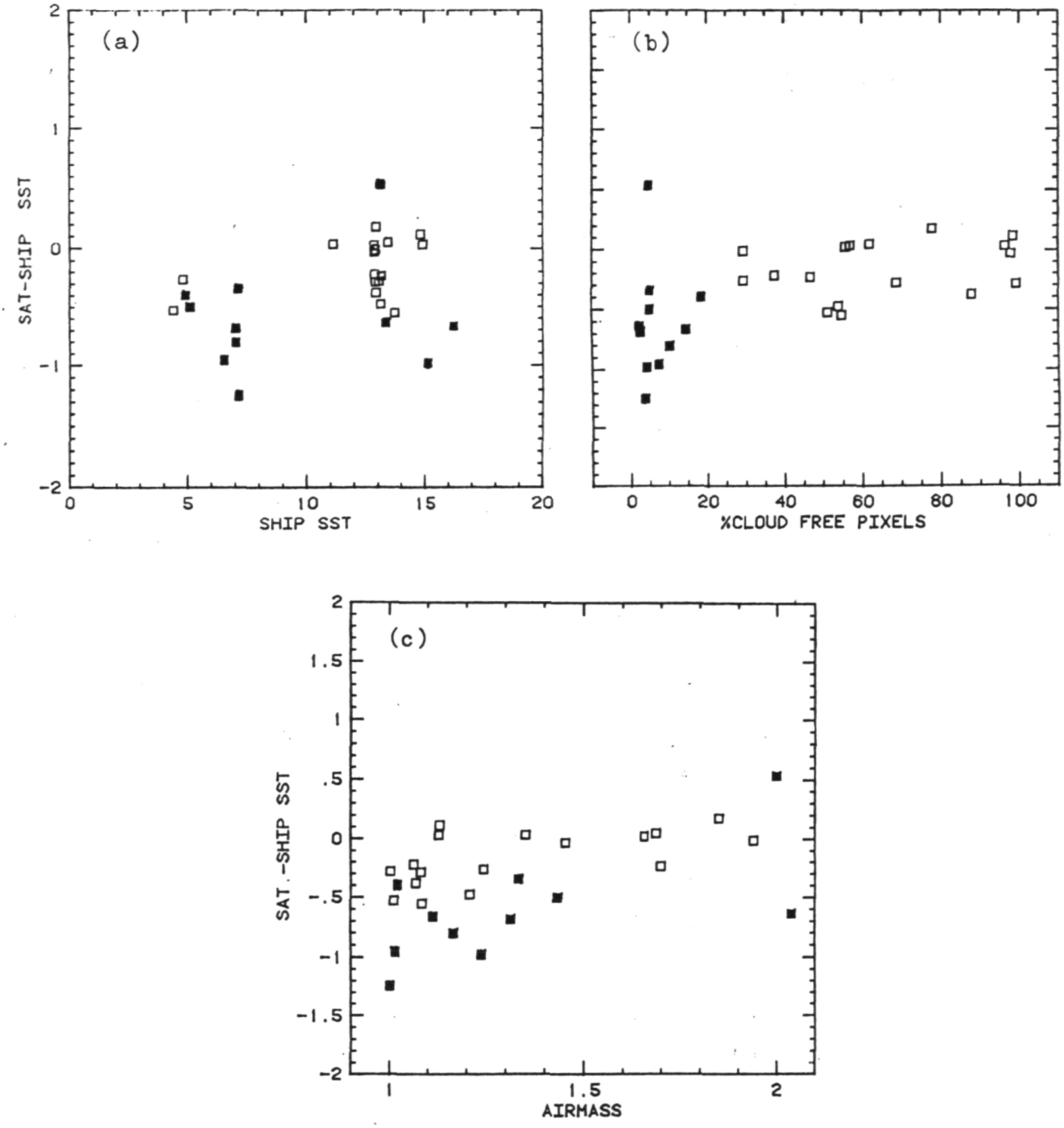

Fig. 3. The differences between the satellite and in situ measurements of SST are shown as functions of a) in situ SST, b) cloudiness c) airmass, for the retrievals using the RAL algorithm. The filled-in symbols indicate those cases where 20% of the pixels in the 50 x 50 array were free of cloud. Similar plots for the MCSST and Secant algorithms show the same results, but reflect the individual statistics given in the table.

3. Triple - / Split-Window Comparison

Limited Comparison of Night Time Satellite SST for 17 & 25 September 1981

Difference between split and triple window SST values:

Standard deviation: 0.15 K
Mean : 0.23 K

Questions: Why such good correlation? (presumably atmosphere very stable and clear).
Why the relatively high systematic discrepancy? (instrumental or modelling?).

4. Conclusions of Comparison Work

- Airmass dependence should be taken into account and can be easily and reliably implemented.
- Cloud clearance is a serious problem. No one method is infallible, new methods should be investigated.
- No clear improvement when comparing triple window with split window values, contrary to simulation results.
- No clear improvement in scatter when comparing global and regional algorithms.

These could be explained by inadequacy of surface data.

ie:

Is the usefulness of this kind of comparison limited by the quality of the "ground truth" data sets?

Future Work To Include

- Utilisation of alternative representative radiosonde data sets, more appropriate to regional requirements and taking into account seasonal variations (in collaboration with UK Meteorological Office).
- Systematic error budget evaluation.
- Possible use of radiometric "ground truth".
- Development of regional algorithms and possibly seasonal.
- Application of findings to ATSR algorithm development.

5. ATSR - Sea Surface Temperature for ERS-1

ERS-1, the European Space Agency's first remote-sending satellite, is due for launch in 1988. It consists of a SEASAT-like suite of microwave radars (Synthetic Aperture Radar, Wind and Wave Scatterometer, Radar Altimeter) plus a scientific payload (announcement of opportunity packages) which includes the Along-Track Scanning Radiometer (ATSR).

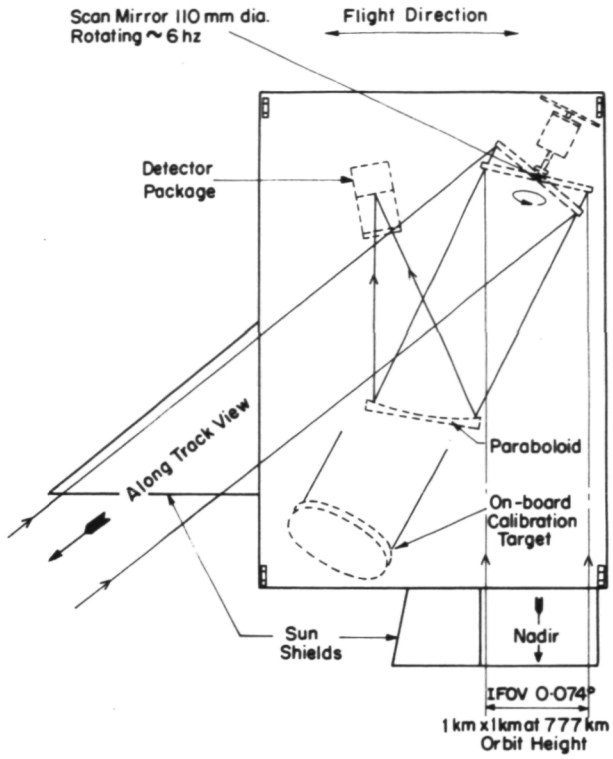

Fig. 4. Along-Track Scanning Radiometer Scientific Payload for ERS-1

ATSR is a sensitive infrared radiometer designed to demonstrate that Global Sea Surface Termperature can be measured on an operational basis with an accuracy better than $\pm$ 0.5 K, as required for effective modelling of ocean/atmosphere heat exchange processes which are major driving elements in Global Climate Models.

This level of accuracy is achieved by viewing the same area of the Earth's surface at two angles, and in three infrared wavebands, centred on 3.7, 11, and 12 μm.

This choice of wavelengths is the same as that of the highly successful AVHRR/2 instrument currently flying in the operational NOAA-7 satellite and achieving SST accuracies $\lesssim$0.8 K.

ATSR is expected to obtain even higher accuracy because the "two angle" view involves different atmospheric paths and gives a direct measurement of the "atmospheric correction" to the surface radiance.

The performance of ATSR has been simulated using a sophisticated atmospheric transmission model based on molecular absorption theory, and taking into account aerosol contamination. On the basis of these simulations an improvement of about a factor of two in SST measurement accuracy over AVHRR/2 is expected — resulting in global SST values accurate to $\pm$ 0.3 - 0.4 K.

ATSR also incorporates a two-channel nadir-looking microwave radiometer which will measure the total vertical column water vapour content of the atmosphere below the satellite. This will improve the accuracy of the SST retrievals and also provide an effective tropospheric range correction for the radar altimeter on ERS-1.

ATSR is being built by a consortium consisting in the UK of the Rutherford Appleton Laboratory, Oxford University Atmospheric Physics Department, University College London's Mullard Space Science Laboratory, and the Meteorological Office, and in France the Centre de Recherches en Physique de L'Environement Terrestre et Planetaire, who are building the microwave radiometer.

References

1. Llewellyn-Jones D T, P J Minnett, R W Saunders and A M Zavody. 1984. Satellite multichannel infrared measurements of sea-surface temperature of the North East Atlantic Ocean using AVHRR/2. To be published.

2. McClain E P and C W Walton. 1983. Satellite zenith angle corrections for satellite measurements. Unpublished manuscript.

NOAA-7 MULTICHANNEL SEA SURFACE TEMPERATURE (MCSST) WITHIN THE GULF OF MEXICO REGION

Jeffrey D. Hawkins

Naval Ocean Research and Development Activity
NSTL Station, Mississippi 39529

Abstract

NOAA-7 multichannel infrared (IR) data over the Gulf of Mexico were processed for retrieval of sea surface temperatures (SST). Full resolution (1.1 km) calibrated imagery easily allowed the detection of false SST gradients due to atmospheric (i.e., water vapor) sources. These anomalous features were aligned with clouds associated with atmospheric frontal systems. False gradients as large as 2.0 - 2.5°C were apparent after first inspection. These values were further substantiated after using NESS MCSST atmospheric correction algorithms.

The absolute values derived from the MCSST algorithms were then compared with high quality (XBT) surface truth. This was made possible by very precise image navigation, where 1-3 pixel accuracy was obtained. Thus, excellent matchups of IR pixels with surface truth spot observations were possible. These comparisons were made for several images using different XBT data sources. Consistent biases of about -0.9°C and standard deviations of $\sim$0.5°C were obtained. These accuracies allowed further quantitative work on Loop Current characteristics to follow.

Loop Current temporal changes were detailed by processing MCSST images for selected times during the winter of 1981-1982. The dynamic nature of the Loop Current system was clearly evident. Warm and cold eddies, cool intrusions (meanders), and warm jet-like features were detected. They agreed in principle with earlier NORDA studies using GOES-E imagery. However, the NOAA-7 full resolution data allows the determination of accurate SST gradients. A better understanding of the thermal contrasts in the Gulf of Mexico and how they relate to XBT sub-surface data results.

INVESTIGATION OF THE APPLICABILITY OF THE MULTIPLE-CHANNEL TECHNIQUE ON INLAND WATER BODIES

A. R. Condal, H. V. Le, G. J. Irbe
Atmospheric Environment Service
Downsview, Ontario Canada

Abstract

In this paper we report on the applicability of the multiple-channel method to data obtained in inland waters. Because this technique was developed from data obtained in deep ocean areas, an assessment for accuracy against temperatures obtained by a single channel method and buoys was performed. Results stress the importance of the effect of air-water temperature difference. Temperatures are less reliable when unusual conditions, e.g., a very hot air mass, are present in the region.

Introduction

Sea Surface Temperatures (SST) of the Great Lakes have been produced at the Atmospheric Environment Service (AES) in Downsview, Ontrio, since 1975. The present analysis is based on digital infrared data from the Advanced Very High Resolution Radiometer (AVHRR) on NOAA's operational polar satellites. The data are rectified, but minor distortions, caused by orbital perturbations, remain in the data. The atmospheric attenuation correction is performed by radiative transfer calculations, using the Low Resolution Transmission (Lowtran) model of Selby et al., 1976 (currently up-dated LOWTRAN 5, described by Kneizys et al., 1980), and local radiosonde data for water vapour distribution in the atmosphere. This method has performed very well (rms difference of 0.6°C from temperatures measured by buoys, Irbe et al., 1981), but its use is restricted to areas where radiosonde data are regularly available and is not appropriate for implementation in a fully automated image analysis system. To improve this situation and provide to the users of our facilities AVHRR data in which temporal as well as multi-spectral analysis of the satellite's radiances can be performed, a computer assisted image system has been developed in which the images are first registered to within $\mp$ 1 image pixel and then calibrated in function of % albedo (visual channels) and temperature (infrared channels). An optional atmospheric attenuation correction by use of the Multiple-Channel Method (MCM) as presented by McClain (1981) is also possible to apply to the infrared data. Specifically, the split-window (ch 4/5: 11 and 12 μm) correction algorithm can be applied to the NOAA-7 data. Dual and triple window algorithms are not considered because of the systematic noise present in the channel 3 (3.8 μm) of the NOAA-7 satellite.

It is the main purpose of this paper to report on the applicability of the MCM technique to data obtained in Lakes Superior and Erie.

Because this technique was developed mainly from data obtained in deep waters, we present an assessment for accuracy against temperatures obtained by our single channel method and buoys.

The AVHRR Resampled Data

In order to perform any sort of quantitative analysis, the images are remapped onto a fixed earth coordinate system eliminating image distortions induced by the sensor's scanning geometry and satellite yaw, roll, and pitch. This is done by use of ground control points (GCP). GCP's designation is an interactive display function. Each successive GCP is used to develop a time series for the satellite's attitude and altitude. This process is repeated until the time series converges to within the desired limits (normally 8 - 10 GCPs are required). Once these correction parameters have been computed, the computed transformation algorithm is applied to the input image to produce the geometrically corrected output image. Inputs to the system are: i) the latitude and longitude of each GCP, ii) the size (in km) of the basic element in the resampled data, iii) the dimensions of the area under consideration. Overlay comparisons of equivalent channels from different satellite orbits indicate a $\mp$ 1 image pixel accuracy in the resampled data.

Resampled data can be displayed by a pseudo-color transformation in which channels 1, 2 and 4 are assigned to the primary colors (red, green, and blue) or by means of contour plots. Figure 1a presents a black and white reproduction of a pseudo-color picture for Lake Superior (23-June-1982). Figure 1b presents the temperature map (split-window: 4/5 μm) for the same data. Temperature contours have been drawn at 2°C intervals, but closed contours (which are set by the noise level in the data) could still be drawn at the 0.°8°C level. Our sample includes clear-skies NOAA-7 data from the spring to the fall of 1982 and spring of 1983. Winter data were not considered as buoy temperatures for the winter season were not available.

For the purpose of the analysis, the data were divided into day and night passes and a direct comparison of the split-window temperatures against the single channel temperatures and buoy temperatures were made.

Discussion

Results obtained up to this moment indicate that the magnitude of the atmospheric correction depends critically on the difference in temperature between the lake surface (T_L) and the moistest layers of the atmosphere (T_a). When $T_L \sim T_a$, a situation encountered mostly in the night passes, the atmosphere re-emits almost the same amount of energy as it absorbs. If $T_a > T_L$, the re-emission overcompensates for the absorption and there is a net gain of infrared energy. For a given mass of

absorbing gas, an increase in $T_a - T_L$ means that the gas becomes a radiation source which is increasingly distinct from the water surface. The application of the split-window method to inland waters thus requires first the acquisition of a good number of cases with large $T_a - T_L$, in order to generate the optimal split-window algorithm for these conditions. Lake temperatures derived by use of present algorithm are unreliable when unusual conditions, e.g., a very hot air mass, are present in the region.

References

Selby, J.E.A., E.P. Shettle and R.A. McClatchey, 1976. Atmospheric transmittance from 0.25 to 28.5 μm: Supplement LOWTRAN 3B (1976); AFGL-TR-76-0258, Environm. Res. Papers, No. 587, Air Force Geophysics Laboratory, Hanscom AFB, Mass.

Kneizys, F.X., et al., 1980. Atmospheric transmittance/Radiance: Computer Code LOWTRAN 5; AFGL-TR-80-0067, Environm. Res. Papers, No. 697, Air Force Geophysics Laboratory, Hanscom AFB, Mass.

Irbe, J.G., R.K. Cross and A. Saulesleja, 1981. Remote Sensing of surface water temperature on the Great Lakes and off the Canadian east coast; NAFO Sci. Coun. Studies, 4: 31-39, Northwest Atlantic Fisheries Organization, Dartmouth, Canada.

McClain, E.P., 1981. Operational implementation of AVHRR-only multichannel sea surface temperature products; report from S/RE1 - E. Paul McClain, Princ. Scientist, ESL and Chairman, NESS Sea Surface Temperature Research Panel (SSTRP), NOAA/NESS, Washington, D.C.

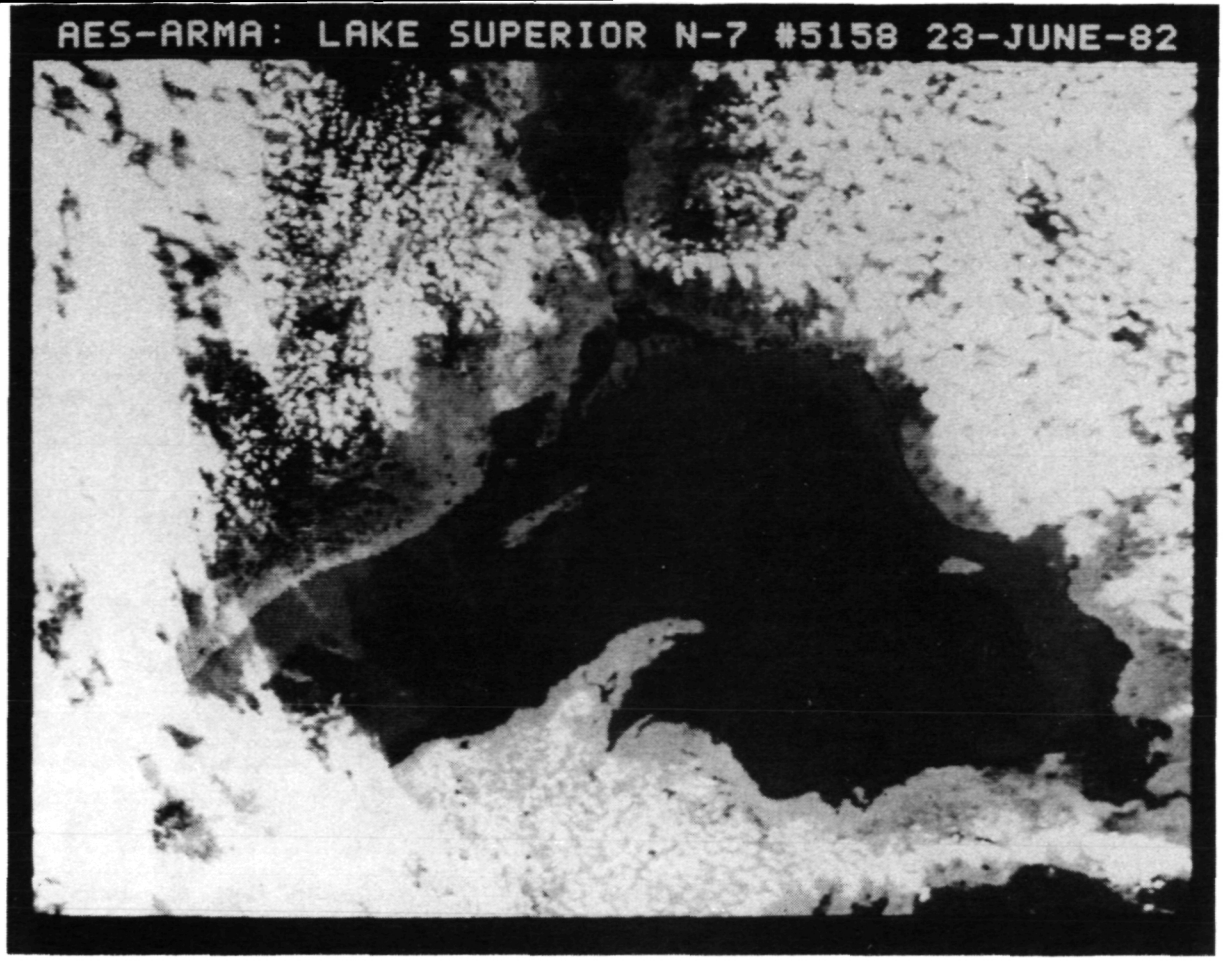

(a)

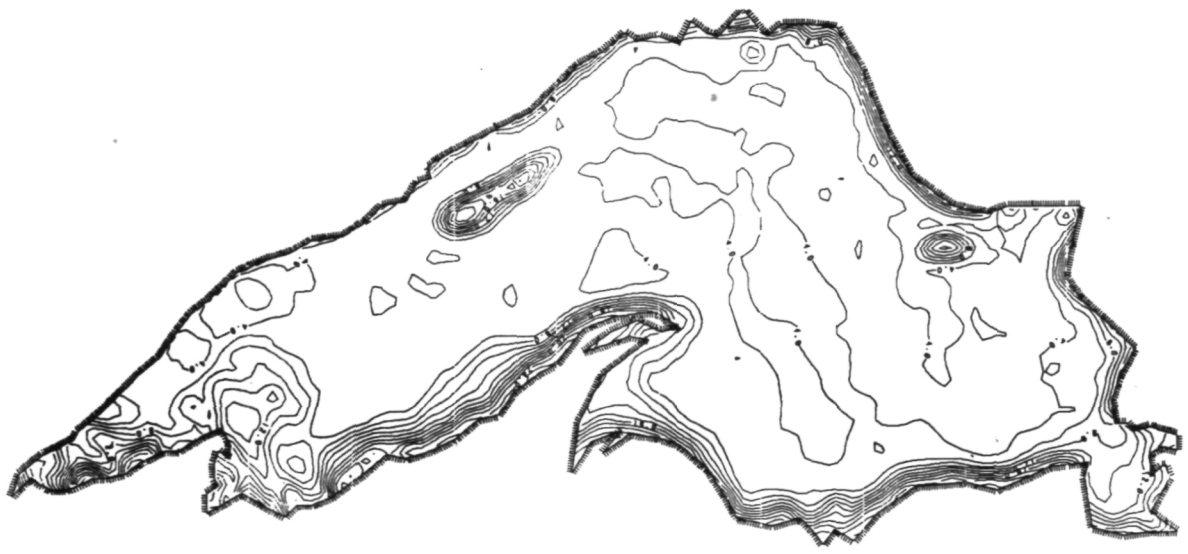

(b)

Figure 1a: NOAA 7 AVHRR resampled image
Figure 1b: Temperature map of the same data

COMPARISON OF SHIP AND SATELLITE SST IN THE KUROSHIO - OYASHIO REGION

Andrew C. Vastano*

Robert L. Bernstein†

*Department of Oceanography
Texas A&M University
College Station, Texas 77843

†Scripps Institution of Oceanography
University of California, San Diego
La Jolla, California 92093

Abstract

Two NOAA-6 daytime AVHRR images for May 20-21, 1981 were processed with a multi-channel algorithm to produce SST estimates for the region of intense mesoscale activity between the Kuroshio and Oyashio fronts northeast of Japan. A comparison was made between the remotely-sensed SST values and sixteen XBT SST measurements spanning May 18-23. The pairs yield an rms scatter of 0.8°C about a mean bias of 0.6°C (satellite warmer). Pair spatial separations have an rms scatter of 9.9 km about a mean of 17.2 km.

Discussion

The perturbed portion of the Tohoku Area northeast of Japan is a mixing zone between the Kuroshio Extension and the Oyashio Front. Intense mesoscale activity characterizes this zone and the joint application of AVHRR imagery and hydrographic measurements has been used to examine the relationship between surface and subsurface features (Vastano and Bernstein, submitted). A contoured map of SST was produced from two daytime NOAA-6 passes on May 20-21, 1981 in the course of this investigation. Full resolution (∿1.5 km) thermal infrared sensings were processed with a multi-channel algorithm (Bernstein, 1982) that yielded radiometrically calibrated and atmospherically corrected SST estimates. The irregularly spaced individual SST values for each pass were combined, spatially interpolated to a 25 km grid, and contoured at a 1°C contour interval. This analysis is superimposed on the 11 μm (ch 4) image for 21 May shown in Figure 1. The surface temperature range is greater than 18°C, spanning the subartic Oyashio waters above 42°N to the Kuroshio Extension south of 38°N. A primary seven degree front is clearly defined extending northeastward from 38°N-40°N. Two major mesoscale features are well-resolved; a jet with paired vortices centered at 39°30′N, 144°30′E and an eddy between the first and second Oyashio Intrusions at 40°50′N, 147°30′E. These mesoscale perturbations along this front are not resolved in the environmental reports for this region.

Surface-acquired measurements were obtained in the study region during a five day interval (May 18-23) encompassing the two passes that contributed to

the contoured SST map. An interrogation of the FNWC archives revealed that observations by Japanese research vessels and TRANSPAC ships presented an opportunity to compare XBT and satellite SST, and estimate the accuracy of the contour map. Individual XBT and satellite SST values were selected from the archive and the irregularly spaced data provided by the processing algorithm under the constraints of the five-day interval and a maximum 25 km separation. Twenty such pairs were found. Four SST pairs obtained with XBTs taken on 18 May resulted in temperature differences ranging from 3.4 to 4.9°C in the vicinity of the primary front. These pairs were eliminated from the accuracy computation on the basis of the 2-3 day time lapse between XBT-satellite pattern acquisition and satellite observed surface pattern advection during 20-21 May. Figure 2 presents a scatter diagram of ship and satellite SST for the remaining sixteen pairs. These exhibit an rms scatter of 0.8°C about a mean bias of 0.6°C with the satellite estimates warmer. Pair spatial separations have an rms scatter of 9.9 km about a mean of 17.2 km. These accuracy estimates are consistent with results derived from a larger data set reported by Bernstein (1982).

Acknowledgements

The image processing and analyses were carried out at the Satellite-Oceanography Facility, Scripps Institution of Oceanography, La Jolla, California. A.C. Vastano was supported by National Science Foundation grant OCE80-26037. R.L. Bernstein was supported at Scripps Institution of Oceanography, University of California at San Diego by J. Sherman, NOAA SEASAT Office, under contract MO-A01-78-00-4329.

References

Bernstein, R.L., 1982. Sea surface temperature estimation using the NOAA-6 satellite AVHRR Radiometer. J. Geophys. Res., 87, 9455-9465.

Vastano, Andrew C. and Robert L. Bernstein, submitted. Mesoscale features along the First Oyashio Intrusion. J. Geophys. Res.

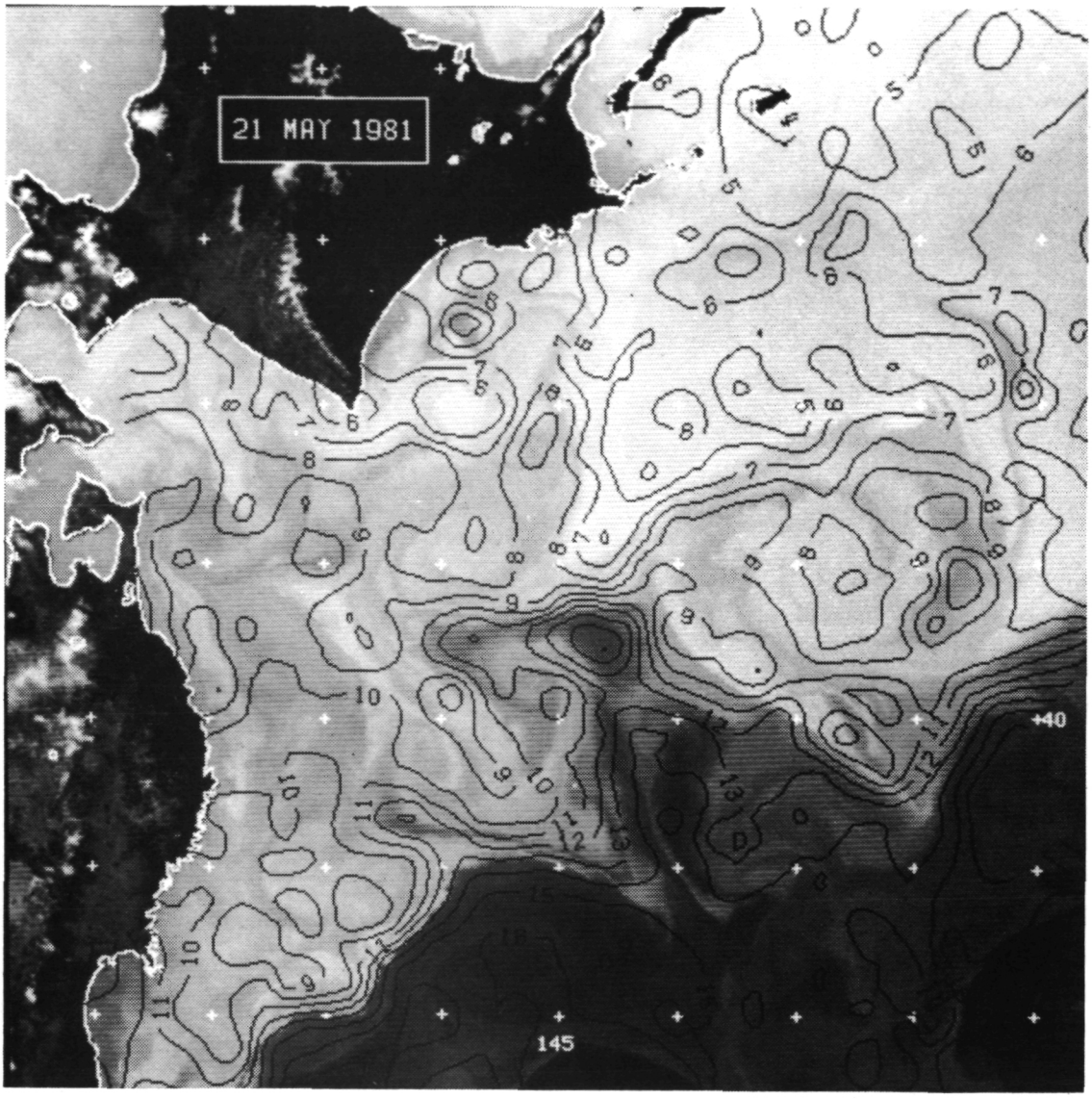

Fig. 1. Contoured, satellite-derived sea surface temperature distributions overlayed on the NOAA-6 thermal infrared image for May 21, 1981.

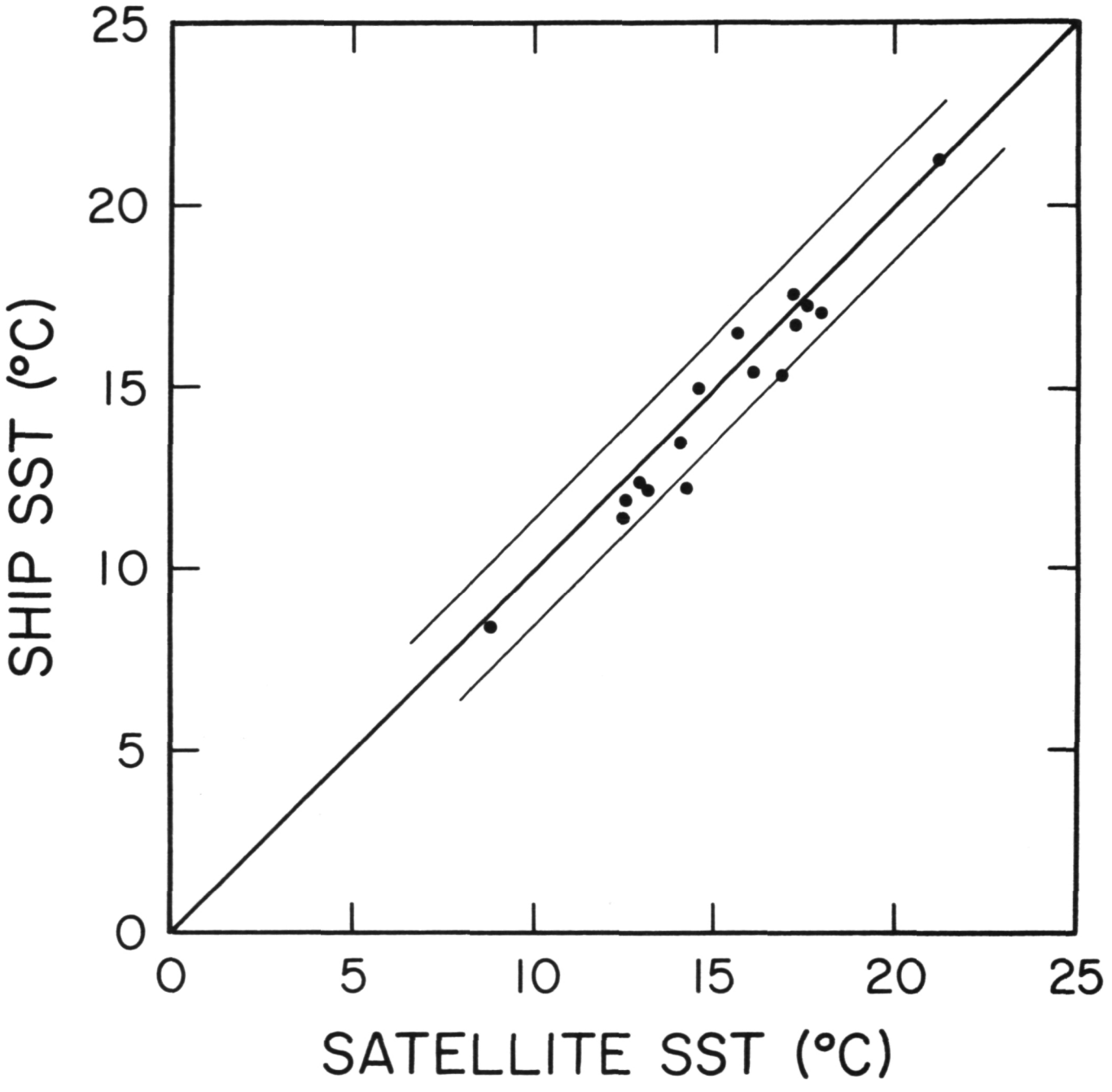

Fig. 2. Scatter diagram of ship and satellite-derived SST pairs for the period May 18-23, 1981.

SUMMARY OF A TWO-SATELLITE METHOD FOR MEASUREMENT OF SST INCLUDING COMPARISONS WITH GROUND TRUTH AND MCSST VALUES

Ronald J. Holyer

Naval Ocean Research and Development Activity

NSTL Station, Mississippi 39529

ABSTRACT

Multispectral SST techniques (MCSST) are the most common means of making IR atmospheric corrections via differential absorption. However, differential absorption can be approached on a geometrical (path length) basis as well as on a multispectral basis. A two-satellite (GOES and NOAA polar orbiter) implementation of the geometrical differential absorption concept will be presented. Two-satellite SST (TSSST) results are compared with ground truth and with MCSST values. In addition to accuracies comparable to the MCSST values, the TSSST method is shown to be relatively insensitive to atmospheric aerosols which have adverse effects on MCSST accuracy. The 0.5 deg C digitization interval in the GOES data is shown to be the limiting factor in the usefulness of the present TSSST methodology. However, the promise shown here creates interest in the upcoming ESA satellite ERS-1 with its Along-Track Scanning Radiometer which will provide two 10-bit AVHRR-quality looks at the same point from different angles.

A TECHNIQUE FOR CALCULATING SEA SURFACE TEMPERATURES WITH HIGHER SPATIAL RESOLUTION FROM NIMBUS-7 SMMR RADIANCES

Per Gloersen
Goddard Laboratory for Atmospheric Sciences
NASA/Goddard Space Flight Center
Greenbelt, Maryland 20771

A technique is described for obtaining global displays of sea surface temperatures (SSTs) from the Nimbus-7 Scanning Multichannel Microwave Radiometer (SMMR) with spatial sampling intervals of approximately 50 km rather than the 150 km spacing normally used for such retrievals. In order to permit comparison with the other SST information being generated for the SST Workshop II, the technique is illustrated using a composite global SMMR data set for December 1981. For the special purposes of this investigation, a rudimentary SST retrieval algorithm and a sampling interval of 50 km were chosen. The results in the latitude band from 40N to 40S were found to be in qualitative agreement with in-situ data, insofar as such comparisons were attempted, and with data obtained in December 1981 from another spacecraft instrument (AVHRR) observing in the thermal infrared. More detailed comparisons are reserved for the Workshop. The data were organized into five six-day periods and separated into ascending and descending orbital nodes. The minimum SST was selected for each pixel between these day/night pairs for each six-day period as well as for the entire month. For the purpose of estimating the geophysical variability of the SSTs in each pixel during the entire month, the maximum difference between all of the weekly and the monthly minimum SSTs was calculated and is shown for each pixel. This investigation confirms that instrument noise does not preclude sensible SST calculations on these time and space scales. Determining the cause of the observed week-to-week variations in the isotherms must await implementation of an improved algorithm and comparison with independent sets such as those available from NORPAX.

METEOROLOGICAL CONDITIONS AND SMMR-DERIVED SEA SURFACE TEMPERATURES IN THE NORTH PACIFIC

Sue Ann Bowling

Geophysical Institute
University of Alaska
Fairbanks, Alaska 99701

SMMR-derived sea surface temperatures should have considerable advantages in areas of persistent cloud cover where thermal infrared temperatures are rarely available and biased toward anticyclonic conditions. We set out to use the SEASAT SMMR data set to compare sea surface temperature changes with meteorological conditions in the Gulf of Alaska, and with anomalies in the general circulation throughout the North Pacific. Seasonal changes show up nicely, but small-scale changes are often masked by the coarseness of the resolution, cross-track bias, and the fact that meteorological factors which could affect sea surface temperature may also directly influence the microwave intensity received at the satellite. Examples of possible meteorological effects on sea surface temperatures will be shown.

Sea Surface Temperatures Retrieved from HIRS/MSU

J. Susskind

NASA/Goddard Space Flight Center
Greenbelt, Maryland 20771

The techniques used to retrieve November 1979 sea surface temperatures from HIRS2/MSU data were basically identical to those described in the Workshop I Report. The only differences occurred in the selection of data to be processed and sent to JPL. Two factors tended to make the November 1979 fields of sea surface temperature anomalies appear noisier than the January 1979 fields described in Susskind et al 1982. First, there were many gaps in the November satellite data we recieved from NOAA/EDIS, including an eight day gap between November 10 and November 17. Considering the numerous missing days and orbits, the data contained only 15 days of effective data. In addition, the fields were analyzed at JPL on a 2° x 2° grid rather than the 4° x 5° grid used at GLAS. Therefore, to increase the number of soundings, we analyzed the data in both the clearest and second clearest 125 x 125 km quadrant of each 250 x 250 km area, rather than just in the single clearest quadrant as described in the Workshop I Report. In addition, to reduce noise, some retrievals which passed the internal consistency checks for a single retrieval were discarded either as being partially over land or inconsistent with other retrievals in their vicinity for the month. A retrieval was considered inconsistent if its deviation from the Reynolds Climatology, interpolated to its location, differed by more than two standard deviations from the mean value of this quantity in a box 4° x 4° surrounding the retrieval. This procedure removed about 8% of sea surface temperature retrievals. In order to assess the fields, we compared the HIRS2/MSU sea-surface temperature anomaly fields with those given by the NMC analysis for November 1979, which utilized data from both ships and

bouys and AVHRR sea-surface temperatures. We looked at both RMS differences of sea-surface temperature anamolies and also correlations of the two anomaly fields. These comparisons were done in different regions and at the 2° x 2° grid and 4° x 5° grid. In addition, we prepared a smoothed analysis on the 2° x 2° grid, obtained by averaging the anomaly in each 2° x 2° grid box with the average of the anomalies in all the eight 2° x 2° grid points surrounding the point. These results are shown below for the North Pacific Ocean and North Atlantic Ocean.

		2° x 2° unsmoothed	2° x 2° smoothed	4° x 5° unsmoothed
North Pacific 0 - 55°N	Mean (GLAS-NMC)	.18	.21	.18
	RMS (GLAS-CLIM)	.86	.71	.63
	RMS (GLAS-NMC)	.90	.78	.64
	Correlation	.31	.35	.53
North Atlantic 0 - 55°N	Mean (GLAS-NMC)	.15	.16	.05
	RMS (GLAS-CLIM)	1.28	1.23	.96
	RMS (GLAS-NMC)	1.16	1.06	.56
	Correlation	.44	.51	.81

In computing the correlations shown above, we subtracted the global mean difference from climatology from the observation in each region, rather than the regional mean, which we felt was real signal. For example, the average North Atlantic Ocean is biased warm in both the HIRS and NMC analyses. It is seen from the above table that small scale noise exists on the 2° x 2° grid but this noise is considerably reduced by smoothing as evidenced by decreasing RMS differences and increasing correlations.

REFERENCE

Susskind, J., J. Rosenfield, D. Reuter and M. T. Chahine, 1982: The GLAS Physical Inversion Method for Analysis of HIRS2/MSU Sounding Data, NASA Technical Memorandum 84936, November 1982

SEA SURFACE TEMPERATURES FROM THE NIMBUS-7 SMMR

A. S. Milman
Systems and Applied Sciences Corporation
Riverdale, MD

T. T. Wilheit
NASA/Goddard Space Flight Center
Greenbelt, MD

Introduction

The algorithms used to derive SST's from the Nimbus-7 SMMR data were described in the report of Workshop I (Ref. 1). The algorithm that worked best is called Version IV (called SMMR D in that report); that version was extended to include the data for November and December, 1981. Special features of the algorithm that apply to this time period are briefly described; after that, the SMMR data are compared with ship data and data from AVHRR.

It will be shown that the ship data are not of sufficiently high quality to assess the accuracy of the SMMR data. The AVHRR data are of sufficient quality; the comparison of SMMR with AVHRR data will show that the rms error in the monthly average SST anomaly from SMMR is less than 0.78 C.

Version II of the SST algorithm is derived from models of the microwave emission from the earth; Version IV adds a correction to that algorithm of the form

$$T = T' + \sum a_i t_i \equiv T' + k_{iv} \tag{1}$$

where T is the Version IV SST, T' the Version II SST, the a_i are constants, and the t_i are measured parameters of the instrument; these parameters may be measured brightness temperatures, temperatures of components of the instrument, or crystal currents. The values of a_i were found by least-squares fitting to minimize the difference between T and climatology. The climatology used was that of Robinson and Bauer (Ref. 2).

Because of the requirements of this workshop, the data for November and December, 1981, were analyzed out of sequence from the rest of the SMMR data. An examination of these data showed that the performance of the instrument had changed since 1979. For example, the day-night difference in some of the antenna temperatures had increased, and the effects of differences in the instrument temperatures had increased. It was found necessary, for this time period, to change the coefficients that multiply the brightness temperatures, as well as to find different coefficients for the instrument variables. For November and December, 1981, the correction is given by

$$\begin{aligned} k_{iv} = {} & -0.2328(V+H)_{6.6} - 0.5191(V-H)_{6.6} \\ & + 0.1348(V+H)_{10.7} + 0.5830(V-H)_{10.7} \\ & - 0.0987(V-H)_{18} + f(\{t_i\}) \end{aligned} \tag{2}$$

where k_{iv} is defined in equation 1; V and H are the vertically and horizontally polarized brightness temperatures at the frequency denoted by the subscript; and $f(\{t_i\})$ is a linear function of five of the temperatures measured in the SMMR instrument.

Comparison with Ships

Figures 1 through 6 are maps of SST anomalies from SMMR and from ships. Let T_s, T_f, T_c, and T_r be the SST's measured from SMMR, ships, the climatological value of the SST, and the true value of the SST, respectively. Let $\delta T_s = T_s - T_c$, $\delta T_f = T_f - T_c$, and $\delta T_r = T_r - T_c$ be the SST anomalies measured by SMMR and by ships, and the true SST anomaly. The maps show the anomalies δT_s and δT_f; this is done to remove the large-scale temperature gradient in the north-south direction.

The ship reports used here were obtained from NMC; they were not screened as carefully as the ones that were used in Workshop II. All ship reports were used unless they were more than 10°C from climatology. The ship SST's were handled by first substracting T_c for the appropriate location and time of year from each ship report. The values of δT_f were averaged onto either a 2° by 2° grid of cells—maps of the whole globe—or a 1° by 1° grid for maps of the Northern Pacific only. The ship data were then smoothed by taking a weighted mean with contiguous cells.

$$\langle \delta T_f \rangle = \frac{1}{w} \sum w_{ij} n_{ij} (\delta T_f)_{ij} \qquad i,j=-1,\ldots 1 \qquad (3)$$

where w is the sum of the weights; $w_{ij} = 0.40$ if $i=j=0$; and $w_{ij} = 0.075$ otherwise; n_{ij} is the number of ship reports in the $(i,j)^{th}$ cell.

Because of the problems with land contamination, SST's are only calculated in ocean areas at least 600 km from land. Unless otherwise stated, only night-time SMMR data have been used.

Figure 1 shows the SMMR SST anomalies for the Northern Pacific. The SMMR data have been smoothed in this map in the same way the ship data were. Figure 2 shows the difference between SMMR and the ship data, and Figure 3 shows the ship SST anomalies.

The most noticeable feature in these three figures is the band of high SMMR SST's around the northern rim of the Pacific. These SMMR SST's are wrong; the ship reports are too dense for the error to lie with the ship data. The effect is seen in other winter months, and is probably due to the SMMR SST's being affected by the presence of winter storms. A later version of the SMMR SST algorithm has been developed to correct this problem; it will be discussed elsewhere.

At Workshop II, this error in the SMMR SST's drew a considerable amount of criticism. However, this region is <u>not</u> representative of the SMMR data as a whole. In Workshop II, ship data were used only if there were at least five ship reports in a 2° by 2° cell; this restriction limited the ship data to the region north of 20° N latitude. Comparison of Figures 1, 2, and 3 shows that there is fairly good agreement between the features seen in the Pacific between 20° S and 30°N; the ship data are rather sparse, however, over most of that region.

Given three presumably independent estimates of the SST (SMMR, ships, and climatology), they can be compared to get estimates of the errors in the SMMR and ship SST's, and of the true deviation of SST from climatology. Let σ_s and σ_f be the errors in the SMMR and ship SST's; let σ_c be the standard deviation of δT_r, the true SST anomaly. Let σ^2_{s-c} and σ^2_{f-v} be the variances of δT_s and δT_f; and let σ^2_{sc} be the covariance of σT_s with δ_r.

The relationship between the measured quantities (σ^2_{s-c}, σ^2_{f-c}, and σ^2_{s-f}) and the errors can be written

$$\sigma^2_{s-c} = \sigma^2_s + \sigma^2_c + 2\sigma^2_{sc}$$

$$\sigma^2_{f-c} = \sigma^2_f + \sigma^2_c$$

$$\sigma^2_{s-f} = \sigma^2_f + \sigma^2_s \; . \qquad (4)$$

It is assumed that there is no correlation between the ship errors and the true SST anomaly.

These questions can be solved for the values of the errors in the SMMR and ship measurements, and the value of σ^2_c. The result is

$$\sigma^2_c + \sigma^2_{sc} = 1/2(\sigma^2_{s-c} + \sigma^2_{f-c} - \sigma^2_{s-f}) = \sigma^2$$

$$\sigma^2_s + \sigma^2_{sc} = \sigma^2_s - \sigma^2$$

$$\sigma^2_f - \sigma^2_{sc} = \sigma^2_f - \sigma^2 \; . \qquad (5)$$

From the nature of the SST tuning, one would expect that $\sigma^2_{sc} \leq 0$; i.e., SMMR should underestimate the magnitudes of the anomalies. (Think about an algorithm that defined T_s to be T_c.) Then the result of ignoring σ^2_{sc} is to overestimate the error in the ship measurement, and to underestimate the error in SMMR and underestimate σ^2_c.

Table 1 shows the results of the error partitioning for the data shown in Figures 1 to 3. The "equatorial" region is between 20° S and 20° N latitudes. These numbers were calculated giving unit weight to each SMMR observation; in the next Section, results are shown where the average SST anomaly in each 2° by 2° cell is given unit weight.

The results shows that the SMMR error is quite large in the north--which can be confirmed by glancing at Figure 2--but, in the equatorial region, the SMMR error is 0.98 C, while the ship error is 1.11 C. Aside from the problem of sparse coverage by ships in the equatorial and southern waters, the SMMR data seem to be more reliable than the ship data in equatorial areas. This is partly because the gross errors in the nighttime SMMR data are pretty well confined to the northern region. The value of 0.55 C for σ_c in the equatorial region is about the same as was obtained at Workshop II from intercomparisons of SMMR, ship, AVHRR, and climate data (the values ranged from 0.34 to 0.54 C). The lower value

of σ_c for the northern data is probably caused by the large systematic error in the SMMR data (i.e., $\sigma^2_{sc} < 0$).

Figures 4, 5, and 6 show, for the whole globe, δT_s, $(T_s - T_f)$, and δT_f. Here, the ship data have been smoothed, but the SMMR data have not. The SMMR data can be seen to have systematic errors in the North Atlantic and the equatorial region of the Atlantic; in the South Atlantic, the agreement between SMMR and ships is rather good. The error partitioning results for the whole globe are given in Table 2. The relative size of the ship error increases from north to south as the frequency of the ship observations decreases. Figure 7 shows the number of ship reports in each 1° by 1° cell. In the ship analysis at the June JPL Workshop, it was recognized that individual ship reports are rather unreliable. In that analysis, only ship data were used when there were at least five ship reports in a 2° by 2° cell. Although the cell size in Figure 7 is 1° by 1°, it shows how few ship reports are available south of 30° N.

The maps of the North Pacific region were included specifically to facilitate the comparison of small-scale features in the SMMR and ship SST's. There are some large-scale errors in the SMMR SST's north of 30° N, but another question to ask is whether or not smaller-scale features are seen in the SMMR SST's.

Relative to the surrounding water, small features are seen in both SMMR and ship SST maps (Figures 1 and 3) at the approximate locations given in Table 3. There are, of course, other features, some of which are seen on one map, but not on the other.

Note particularly the area around Hawaii (Table 3, item 6). There are several small features seen both by SMMR and ships in that area; that region is one where there are many shipping routes. Many other common features can be found in the SMMR and ship SST maps if one takes into account the large-scale tendency for SMMR to overestimate the SST in the north.

Comparison with AVHRR

After Workship II, The AVHRR SST data for December, 1981, were received on magnetic tape. This section describes a comparison between the SMMR and the AVHRR SST's.

Figure 8 is a map of the SST anomalies from the AVHRR data; data from regions within 600 km of large land masses have been excluded. No smoothing has been done except for averaging the data into 2° by 2° cells. Comparing Figure 8 with Figure 4, it can be seen that the SMMR SST anomalies are indeed too high in the North Pacific, as was also shown from the ship comparison. However, there is fairly good agreement between the features seen by SMMR and AVHRR in the rest of the world's oceans.

A statistical comparison was made between SMMR, AVHRR, and climatology. The comparison was done only for data between 50° S and 45° N latitudes; it has already been shown that the SMMR data are unreliable outside this range.

For this comparison, three separate SMMR products were used: daytime data only, nighttime data only, and a combined day and night product. To arrive at this combined product, it was reasoned that the SMMR data are sometimes wrong

because of calibration errors that repeat from day to day--or from night to night--but are different between day and night. Where the day and night SST's are very different, the most likely one to be right is the one that is closer to climatology.

First, maps were made of the monthly mean SST anomaly from daytime and nighttime data separately; the day and night anomalies were averaged for each 2° by 2° cell using the expression

$$T_{D\&N} = \frac{1}{(g_D + g_N)} (g_D T_D + g_N T_N) \qquad (6)$$

where the subscripts D and N refer to day and night; D&N refers to the combined product; T_D or T_N is the SMMR SST anomaly; and g_D and g_N are weights given by

$$g = (\delta T)^{-2} \qquad |\delta T| > 1$$

$$g = 1 \qquad |\delta T| < 1. \qquad (7)$$

Table 4 gives the result of the error partitioning for the comparison between SMMR and AVHRR. Each SMMR record is given unit weight; only nighttime data were used. In the equatorial and southern regions, the estimated errors for SMMR are the same as from the ship comparison (Table 2). For the northern region, the estimated error is lower, since data were excluded north of 45° N. (Table 4 also shows the result when all of the data are used.) A similar analysis done at Workshop II gave an overall estimate of the error in the AVHRR data of 0.62 C; this is about the same as the estimate for the northern and southern regions shown here; in the equatorial region, the error is smaller.

Another way to make the comparison is to consider not each individual SMMR measurement, but to look at the average SST anomaly in each 2° by 2° cell in the map. In this case, the comparison can be made for daytime, nighttime, and the D&N product separately. Table 5-a shows the average and standard deviation for the three possible pairwise comparisons between SMMR, AVHRR, and climatology. The rms difference between the D&N SMMR product and climate is 0.74 C; the rms difference from AVHRR is 0.78 C. Table 5-b gives the same information for the comparison of SMMR and ship data. The difference in the two estimates of σ^2_{s-c} is due to the difference in the spatial coverage of AVHRR and ships; the SMMR data for these comparisons were used only there are AVHRR data (Table 5-a) or ship data (Table 5-b) available.

Table 6-a gives the estimated errors for SMMR and AVHRR, and for σ_c, using day, night, or D&N data separately. Because of the way the D&N product was derived, there is certainly some (negative) correlation between the SMMR SST's and δT_r (i.e., $\sigma^2_{sc} < 0$). In this case, σ_s will be underestimated, while the error in AVHRR will be overestimated (cf. Equation 5). The value of $\sigma_s = 0.56$ C given in Table 6-a should be treated as a lower limit; on the other hand, the error in the SMMR SST's cannot be larger than the rms difference between SMMR and AVHRR (0.78 C, from Table 6-a). The comparison with AVHRR data--unlike the comparison with ship data--provides maps and statistics that are of uniform quality and cover the entire globe.

Table 6-b gives the same information when ship data are used instead of AVHRR data. Comparison of Tables 6-a and 6-b shows that the values of σ_s and σ_c do not change much, but that the error in the AVHRR data is much smaller than the error in the ship data.

Conclusions

The results of Workshop II showed that there were serious problems with the SMMR SST's in the Northern Pacific and Northern Atlantic; a systematic comparison of SMMR with ship data was not made at that workshop for other regions. The data presented here show that the SMMR SST's compare favorable with the ship SST's for the equatorial region--where infrared techniques for measuring SST will have their worst problems with clouds--and in the Southern Hemisphere. The comparison of the SMMR and AVHRR data allowed both regional statistical analyses and also the production of maps in identical formats for comparison of the SST features.

Shortly after the conclusion of Workshop II, the development of a better SST algorithm was started. This new algorithm--called Version IV.1--reduces considerably the error in the northern ocean areas. The Version IV SST's were usually too high in the northern winter months, and the pattern of the error seemed to coincide with regions of persistantly high wind speed in the winter months. Version IV.1 seems to have corrected for that.

There is a fundamental difference in the nature of the errors in the SMMR and ship SST's. The ship errors are not correlated, except in the case where one ship has a thermometer that is systematically wrong. The spatial correlation scale for the ship errors is very small. On the other hand, the random errors in the SMMR data are small, while there are large-scale (1000 to 10 000 km) errors that--for Version IV, at least--are sometimes several degrees. One of the authors (TTW) has developed an objective analysis scheme that combines ship and SMMR SST anomalies in such a way that these different errors are greatly reduced.

Comparison of the SMMR and AVHRR data (Figures 4 and 8) as well as the ship data (Figure 6) shows that both satellite products are in general agreement with each other in many areas and with the ship data, except for the regions of high SMMR SST anomaly noted above, and for the tendency for SMMR to underestimate the SST anomaly in the North Atlantic between about 0° and 30° N (cf. Figure 5). These same problems with the SMMR SST's appear in the SMMR data during most winter months; the cause of this problem is the lack of adequate calibration of the SMMR instrument. That this is primarily a calibration problem can also be seen from comparing Figure 4 (nighttime SST anomaly) with Figure 9 (D&N SMMR): there are calibration problems both with the daytime and nighttime SMMR data, but they appear in different places.

The statistical analyses show that the AVHRR SST's have a smaller rms error than the ship SST's (compare Tables 2 and 4); at least in the Equatorial Pacific and the southern regions (cf. Tables 1 and 2), the SMMR SST's also have a smaller rms error than the ship observations. Of course, both satellites provide more extensive coverage of the equatorial and southern oceans that ships do.

Acknowledgement

The authors thank Dr. E. P. McClain for his helpful discussion of the AVHRR data.

References

1. Satellite-Derived Sea Surface Temperature: Workshop I, E. Njoku, editor, JPL Publication 83-34 (1983).

2. A Comparison of Sea Surface Temperature Climatologies, R. W. Reynolds, (to appear in JCAM March, 1983).

Tables

Table 1. SMMR and ship errors for the Northern Pacific. Only nighttime data were used; both SMMR and ship data were smoothed.

	SMMR σ_s (C)	ship σ_f (C)	σ_c (C)	average no. ships per cell
northern	1.45	0.94	0.35	5.6
equatorial	0.98	1.11	0.55	1.6

Table 2. SMMR and ship errors for the whole globe. Only nighttime data were used; the ship data were smoothed.

	SMMR σ_s (C)	ship σ_f (C)	σ_c	average no. ships per cell
northern	1.55	0.72	0.18	22.6
equatorial	1.03	0.94	0.52	3.8
southern	1.26	1.54	0.60	2.4

Table 3. Some common features in SMMR and ship SST's.

feature	latitude	east longitude	
1	35	210	
2	25	150	
3	15	220	
4	45	180-200	
5	30	195	
6	22	205	note surrounding area

Table 4. SMMR and AVHRR errors for the whole globe from 50° S to 45° N. Only nighttime SMMR data were used.

	SMMR σ_s (C)	AVHRR σ_f (C)	σ_c (C)
northern	1.38	0.60	0.40
equatorial	1.06	0.25	0.45
southern	1.30	0.63	0.56
. . . . .			
all northern SMMR data	1.49	0.54	0.47

Table 5-a. Differences between SMMR, AVHRR, and climate. The average SST in each 2° by 2° cell is given unit weight. Data are used from the whole globe between 50° S and 40° N.

	SMMR - climate avg (C)	SMMR - climate sd (C)	AVHRR - climate avg (C)	AVHRR - climate sd (C)	SMMR - AVHRR avg (C)	SMMR - AVHRR sd (C)
daytime	0.2	1.08	-0.1	0.72	0.3	1.01
nighttime	0.0	1.07	-0.1	0.72	0.0	1.11
D&N	0.1	0.74	0.1	0.72	0.1	0.78

Table 5-b. Same as above, but with ship data.

	SMMR - climate avg (C)	SMMR - climate sd (C)	ship - climate avg (C)	ship - climate sd (C)	SMMR - ship avg (C)	SMMR - ship sd (C)
daytime	0.1	1.20	0.0	1.14	0.1	1.42
nighttime	0.0	1.06	0.0	1.16	0.1	1.38
D&N	0.0	0.78	0.0	1.11	0.0	1.17

Table 6-a. Comparison of SMMR, AVHRR, and climate, giving the average SST in each 2° by 2° cell unit weight. Data are used from the whole globe between 50°S and 40° N.

	SMMR σ_s(C)	AVHRR σ_f (C)	σ_c (C)
daytime	0.91	0.43	0.58
nighttime	0.96	0.55	0.47
D&N	0.56	0.54	0.48

Table 6-b. Same as above, but the comparison is with ship data.

	SMMR σ_s (C)	ship σ_f (C)	σ_c (C)
daytime	1.04	0.98	0.60
nighttime	0.92	1.03	0.52
D&N	0.62	1.00	0.47

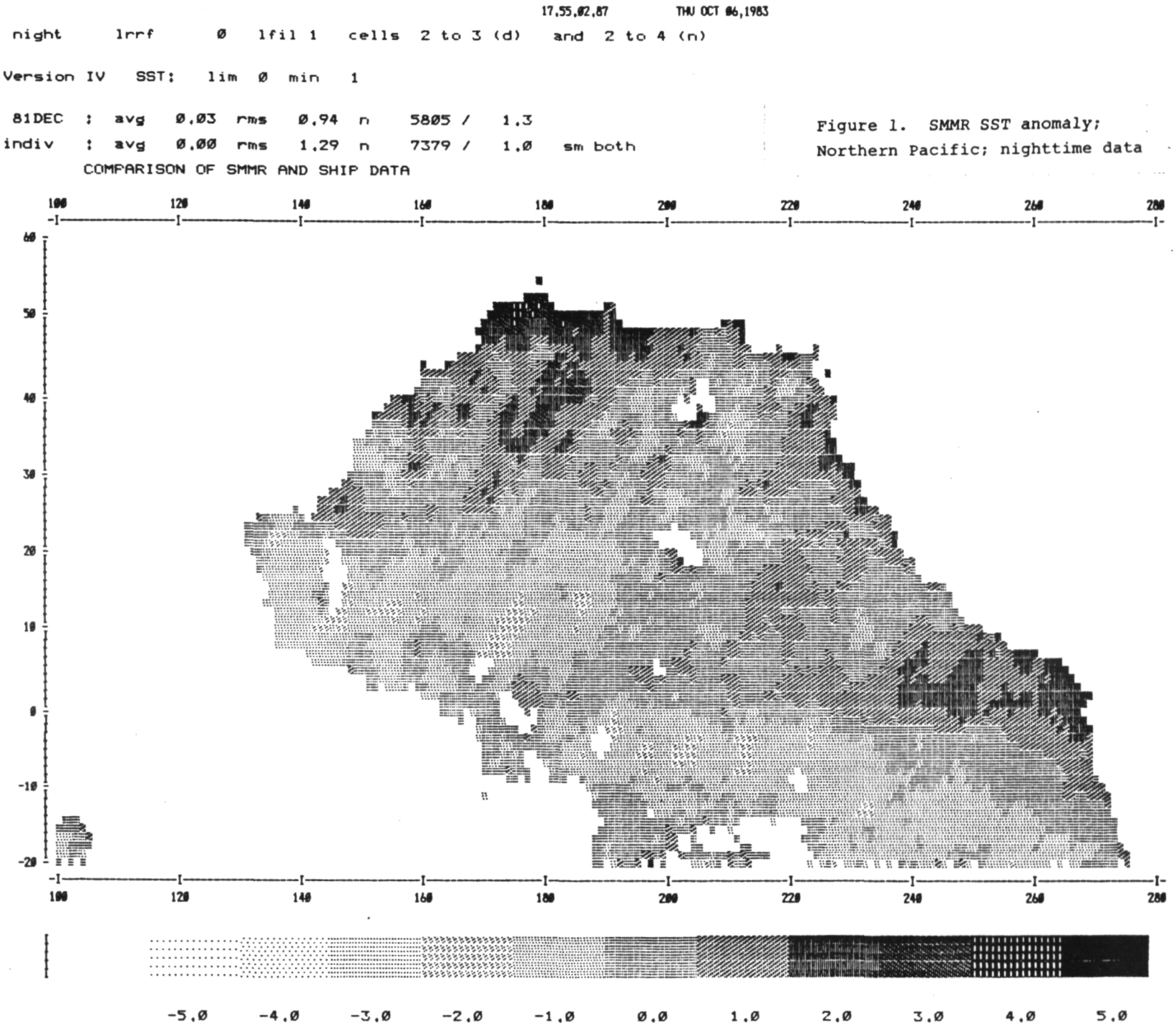

Figure 1. SMMR SST anomaly; Northern Pacific; nighttime data

night lrrf 0 lfil 1 cells 2 to 3 (d) and 2 to 4 (n)

Version IV SST: lim 0 min 1 diff S-F

81DEC : avg 0,63 rms 1,40 n 3595 / 2,1

indiv : avg 0,59 rms 1,70 n 4495 / 1,0 sm both

COMPARISON OF SMMR AND SHIP DATA

Figure 2. SMMR SST minus ship SST; Northern Pacific; nighttime SMMR data.

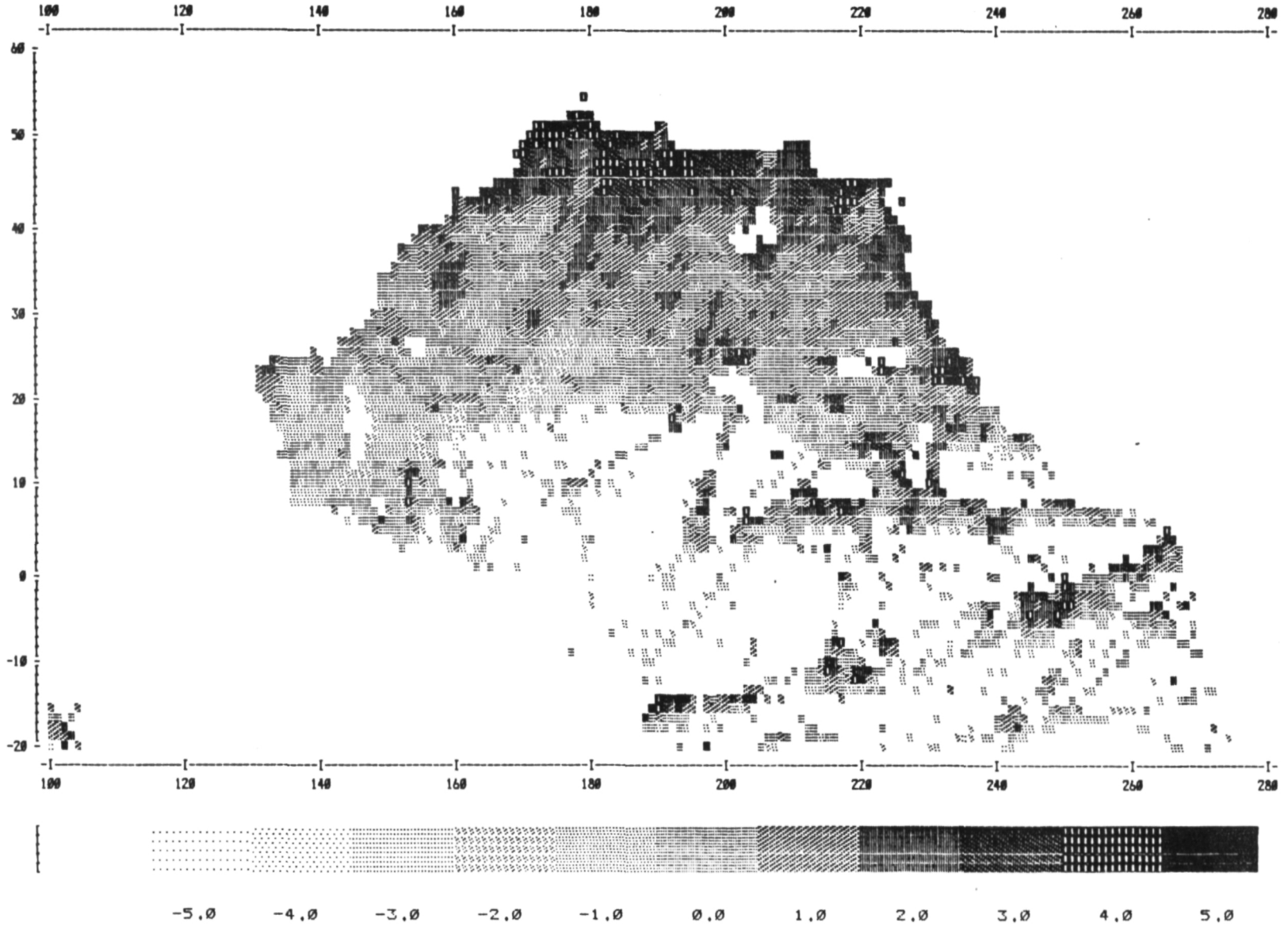

night lrrf 0 lfil 1 cells 2 to 3 (d) and 2 to 4 (n)

Version IV SST: lim 0 min 1 diff F-C

81DEC : avg -0.42 rms 1.14 n 3595 / 2.1
indiv : avg 0.59 rms 1.70 n 4495 / 1.0 sm both

COMPARISON OF SMMR AND SHIP DATA

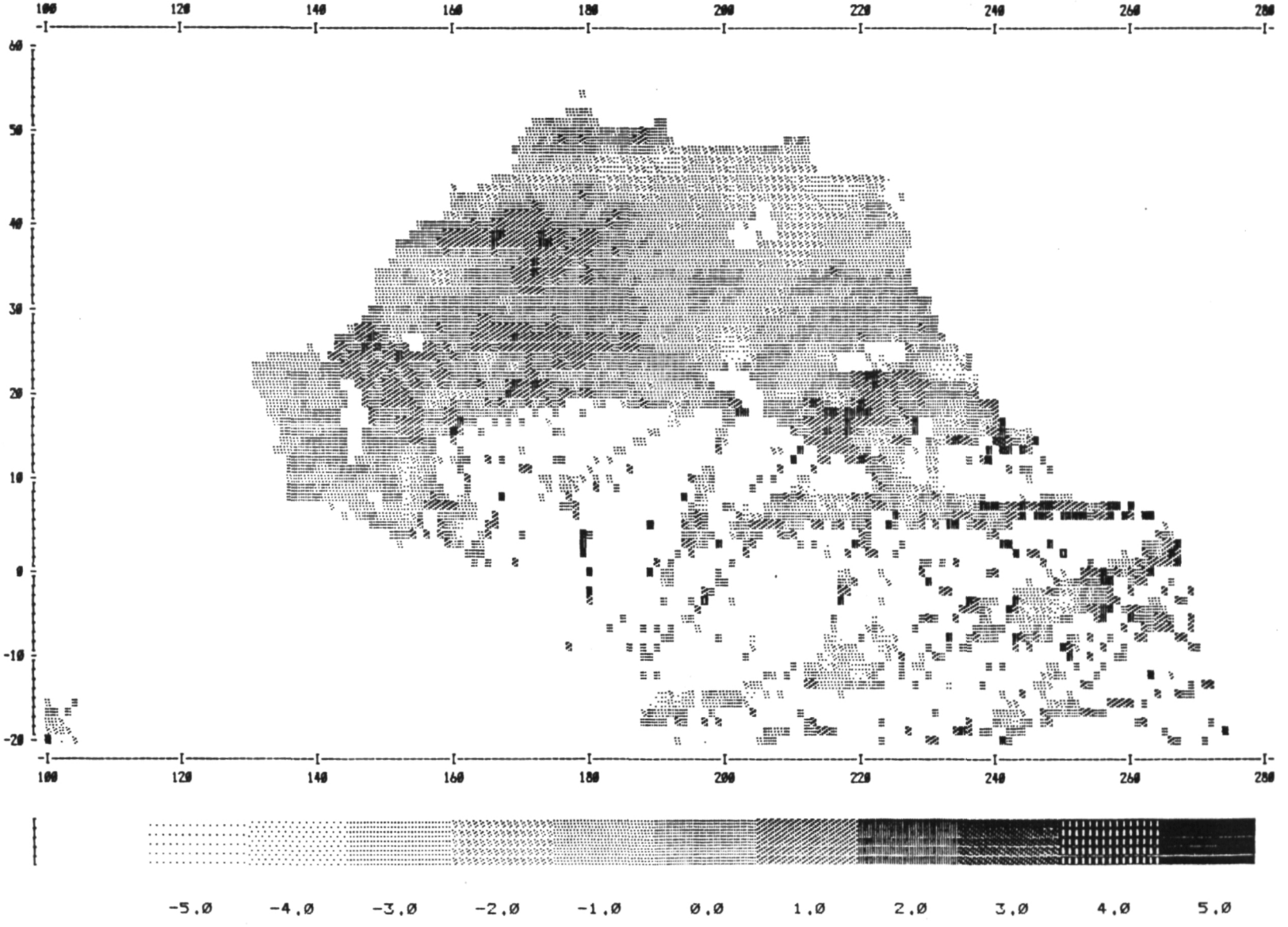

Figure 3. Ship SST anomaly; Northern Pacific.

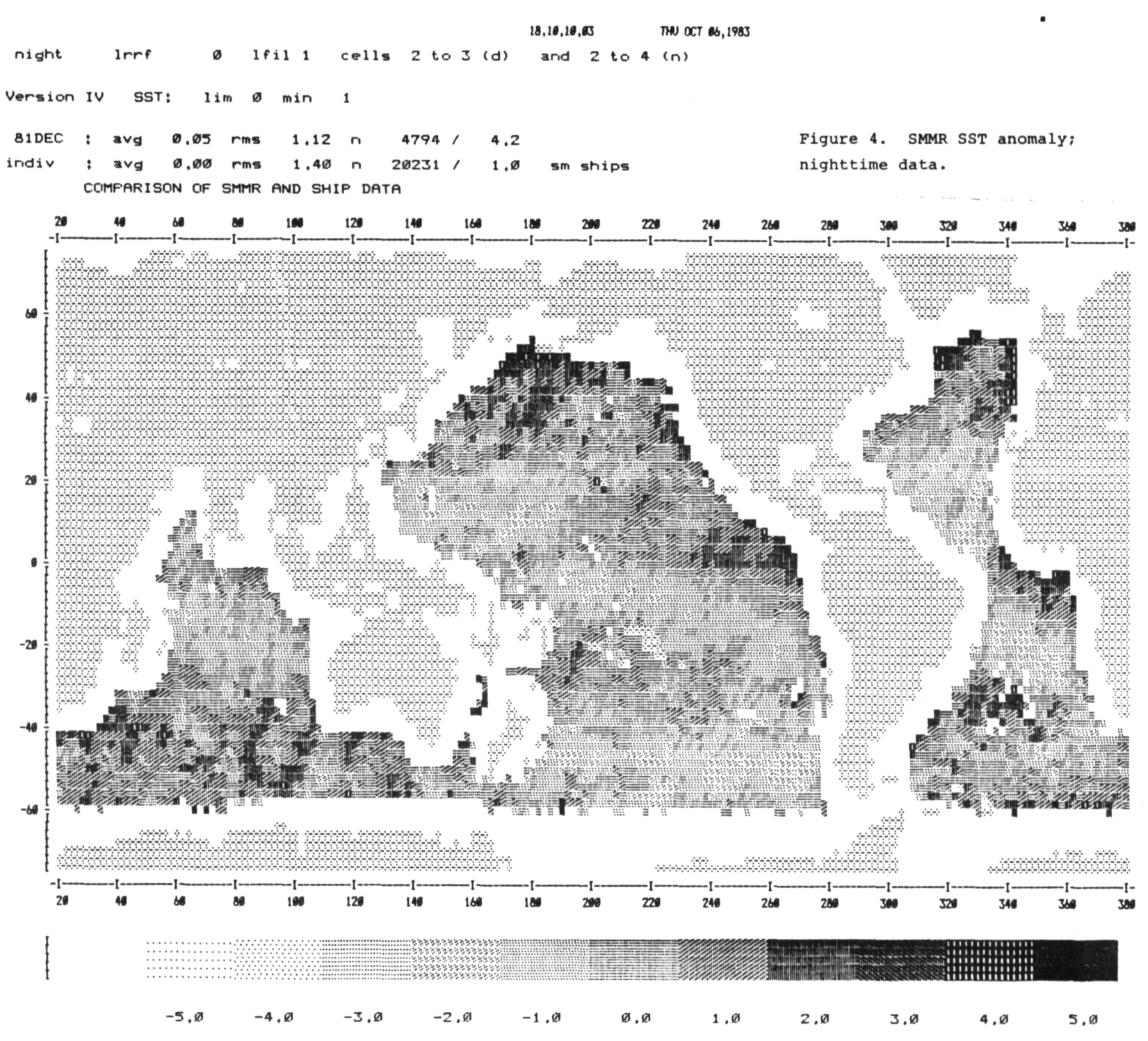

Figure 4. SMMR SST anomaly; nighttime data.

night lrrf 0 lfil 1 cells 2 to 3 (d) and 2 to 4 (n)

Version IV SST: lim 0 min 1 diff S-F

81DEC : avg 0,18 rms 1,53 n 3330 / 6,1

indiv : avg 0,14 rms 1,73 n 14226 / 1,0 sm ships

COMPARISON OF SMMR AND SHIP DATA

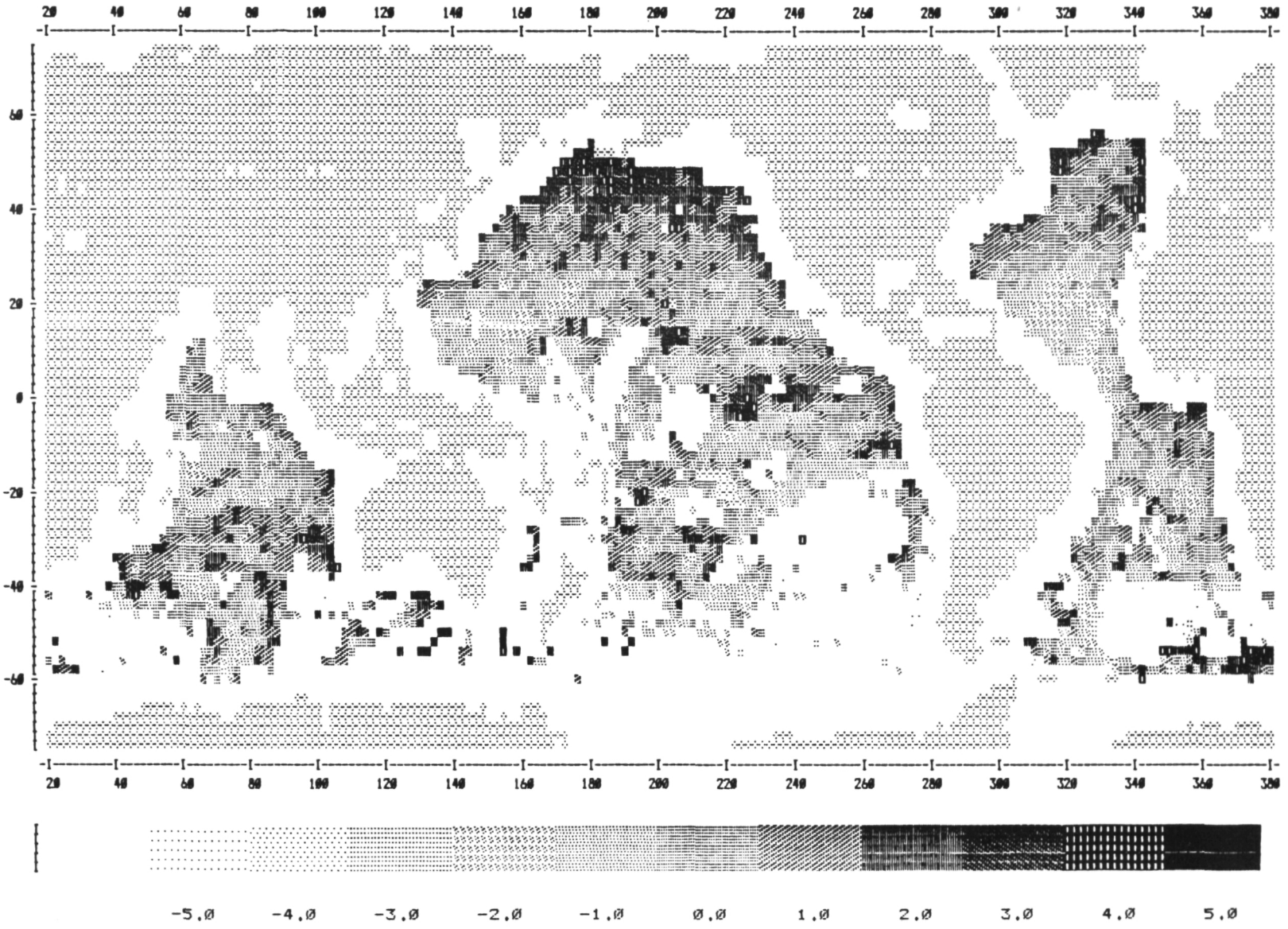

Figure 5. SMMR SST minus ship SST; nighttime SMMR data.

night lrrf 0 lfil 1 cells 2 to 3 (d) and 2 to 4 (n)

Version IV SST: lim 0 min 1 diff F-C

81DEC : avg -0,05 rms 1,24 n 3330 / 6,1

indiv : avg 0,14 rms 1,73 n 14226 / 1,0 sm ships

COMPARISON OF SMMR AND SHIP DATA

Figure 6. Ship SST anomaly.

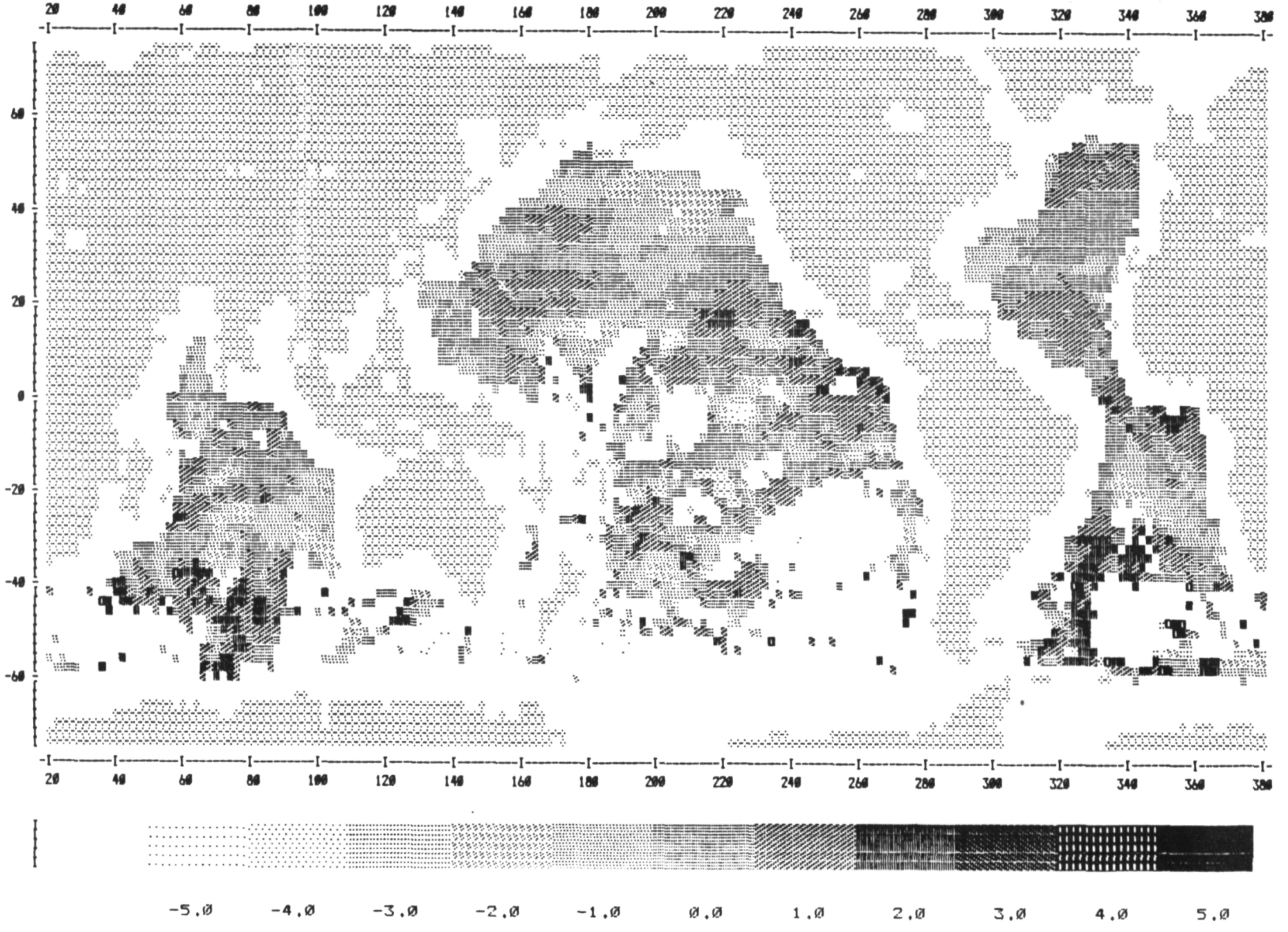

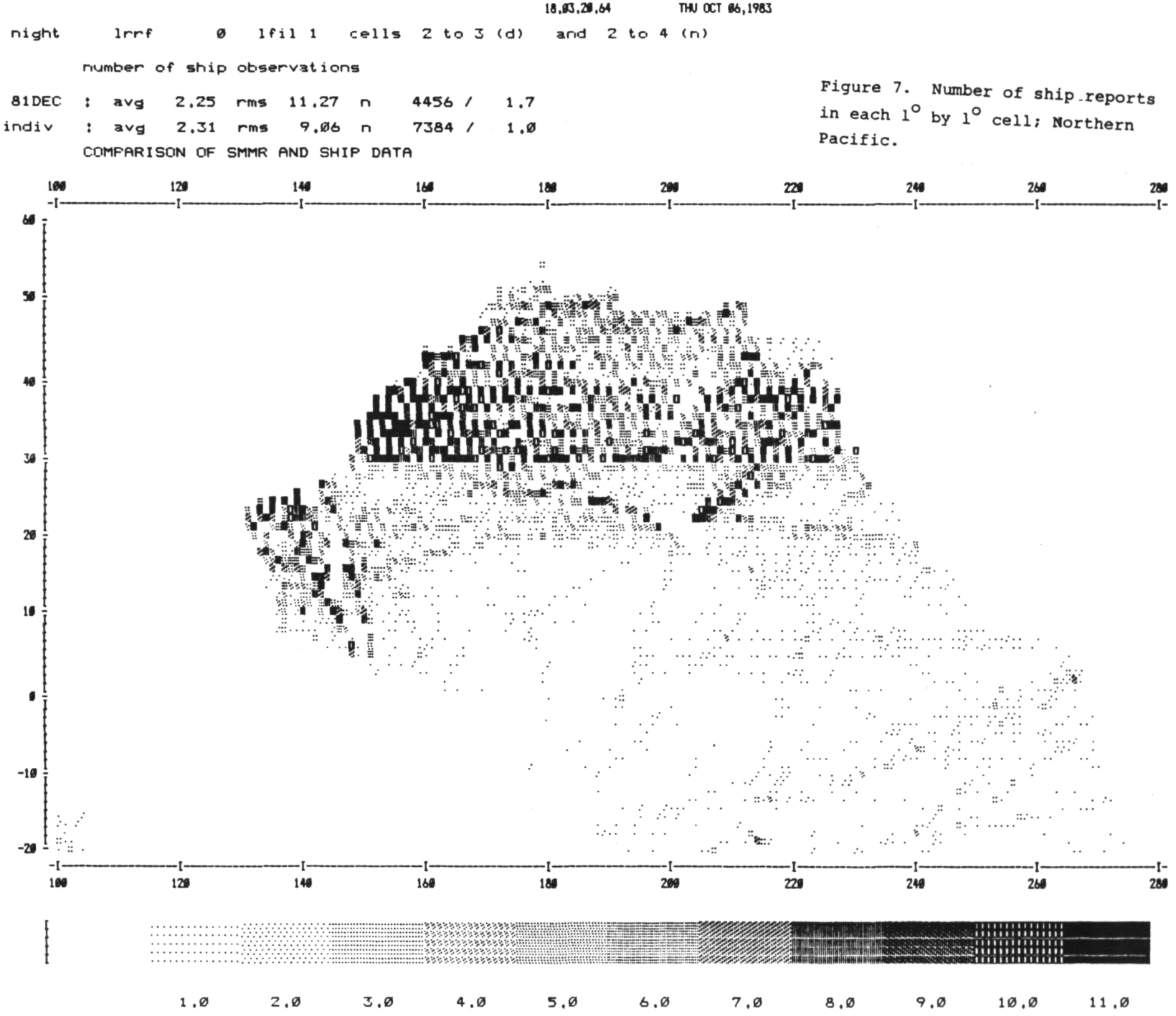

Figure 7. Number of ship reports in each 1^{o} by 1^{o} cell; Northern Pacific.

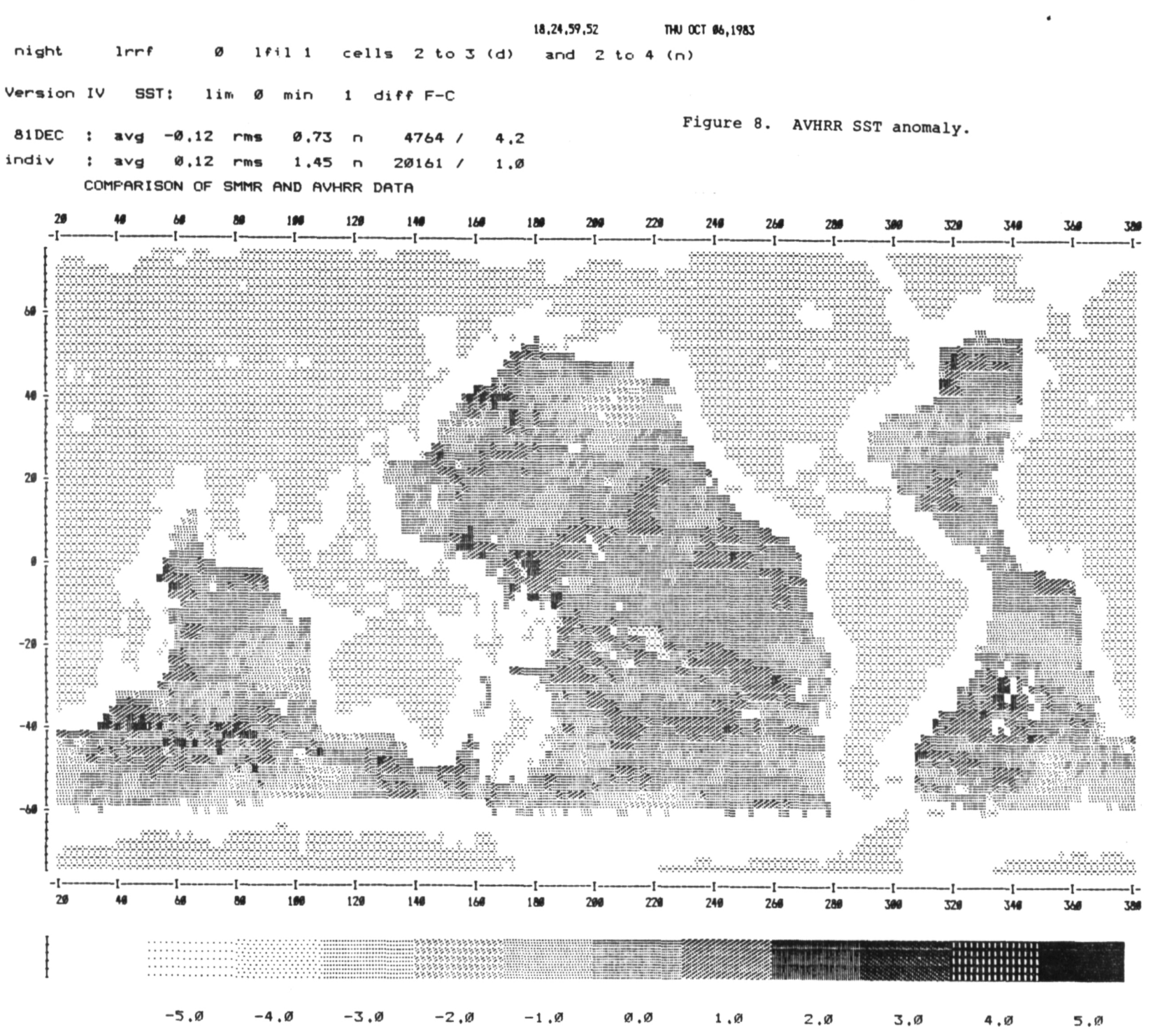

Figure 8. AVHRR SST anomaly.

d & n lrrf 0 lfil 1 cells 2 to 3 (d) and 2 to 4 (n)

Version IV SST: lim 0 min 1

81DEC : avg 0.14 rms 0.79 n 4563 / 0.0

indiv : avg 0.13 rms 1.40 n 34285 / 1.0

COMPARISON OF SMMR AND AVHRR DATA

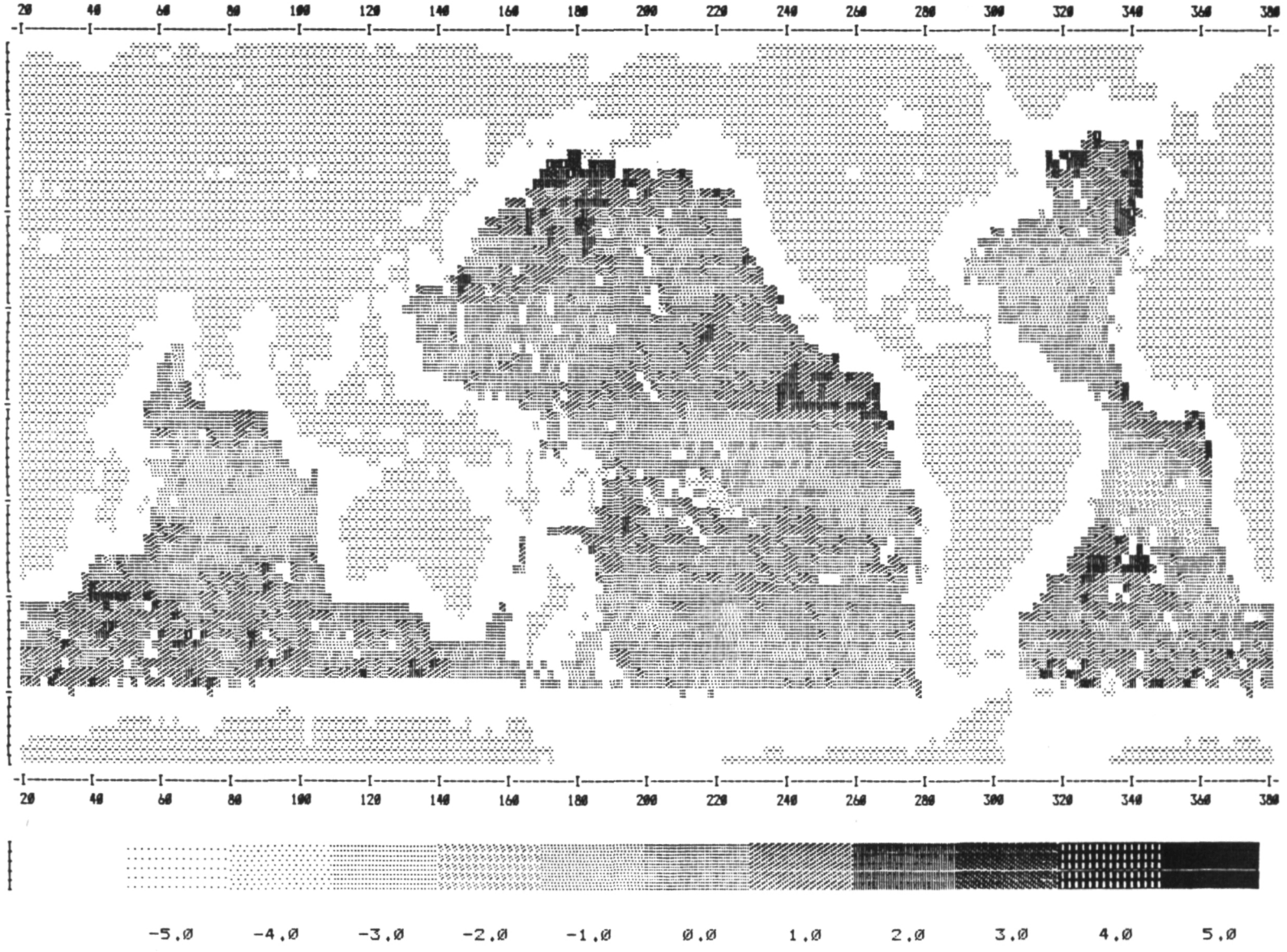

Figure 9. SMMR SST anomaly; D&N product.

ESTIMATION OF SEA SURFACE TEMPERATURE FROM NIMBUS-7 SMMR

Prabhakara, C., I. Wang* and D. Short
Goddard Space Flight Center, Greenbelt, Maryland 20771
*Computer Sciences Corporation, Silver Spring, Maryland 20910

Abstract: The sea surface winds and atmospheric water vapor and liquid water affect the microwave brightness in the 6.6 GHz channel of SMMR. Remote sensing of SST from this channel requires techniques to minimize errors introduced by these variables. In this study a method, that takes into consideration the polarization ratio $T^V_{6.6}/T^H_{6.6}$ as a discriminator, is developed to minimize the errors due to surface winds and liquid water in the atmosphere. Correction for atmospheric water vapor absorption is properly incorporated in the estimation of SST.

Introduction: The ability of the microwave radiation to propagate through thin clouds or fog with little attenuation improves considerably our capability to remotely sense the sea surface temperature (SST) on a global basis. As the clouds are generally opaque in the infrared, remote sensing of SST from infrared observations requires cloud free viewing conditions. This restricts the number of useful IR observations to about 15% between 10°N to 10°S and at high latitudes as shown by Pischell and Banks (1983, Private communication) from Advanced Very High Resolution Radiometer (AVHRR) measurements having a spatial resolution of ~ 1 km. Microwave remote sensing of SST can supplement this missing information.

Method: Amongst the five spectral channels in the Scanning Multichannel Microwave Radiometer (SMMR), flown on Nimbus 7, the one at 6.6 GHz is most transparent to the water vapor and liquid droplets in the atmosphere. The sea surface emissivity at 6.6 GHz is nearly independent of the sea surface temperature. Further the 6.6 GHz brightness temperature measurements of SMMR in the vertical polarization are affected less by the atmospheric constituents as compared to the horizontal polarization measurements (Prabhakara et al, 1982). For these reasons in this study the SMMR measurements at 6.6 GHz in the vertical polarization are used to remotely sense the SST.

Surface winds increase the sea surface emissivity in the microwave region and thereby increase the brightness temperature measured at the top of the atmosphere. However such an increase in the horizontal polarization is larger than that in the vertical polarization. As a result the polarization ratio R

$$\text{where } R = T^V_{6.6}/T^H_{6.6} \qquad (1)$$

decreases with increase in surface wind speed (Wilheit, 1979).

Liquid water and to a lesser extent water vapor in the atmosphere also decrease this ratio and depolarize the microwave radiation at 6.6 GHz. The sun glint, if it is present, also decreases this ratio. Thus in general by examining the polarization ratio and choosing data that give a high R value it is possible to select microwave measurements that are affected minimally by the liquid water in the atmosphere, the surface

wind and sun glint. SST can be derived from such observations with small corrections.

Because of the difficulties involved in calibrating raw SMMR observations, some residual errors of a systematic nature remain in the final calibrated brightness temperature measurements (Milman and Wilheit, 1983). These calibration errors differ between night and day, from channel to channel, and as a function of the cross track scan position. In order to derive SST measurements from SMMR data it is therefore necessary to correct for some of these systematic errors. In this study we have made two simple explicit corrections to the SMMR data at 6.6 GHz. A constant value of 16.2° C is added to SST data derived from 6.6 GHz vertical polarization measurements during December 1981. Secondly an attempt is made to reduce the difference between the day and night observations explicitly. From the nature of these corrections one can see that the basic calibration, which depends on the intrinsic characteristics of SMMR, is not changed.

The polarization ratio R (See Eq. 1) derived from SMMR data will also be affected by the calibration errors. For this reason an empirical procedure is developed to select the SMMR data that yield a large value of R.

From an examination of the SMMR data for the month of December 81 it is found that the zonally averaged minimum brightness temperature over the oceans at 6.6 GHz (vertical polarization) varies as a function of latitude as shown in Fig. 1A. As can be seen from the figure, this minimum differs between night and day. The minimum brightness at a given latitudinal belt is assumed to represent nearly calm surface wind condition and absence of significant liquid droplets in the atmosphere. The ratio R as a function of latitude, for night and day, corresponding to these minima is computed. In Fig. 1B R obtained in this manner is shown. From this figure we notice that this value of R does not go below 1.7 during day and 1.72 at night. On the basis of this finding it is assumed that the SMMR 6.6 GHz data giving R value greater than 1.7 during day and greater than 1.72 during night, represent atmospheric and sea surace conditions suitable for retrieval of SST. Corrections for water vapor absorption to such data is made and then SST is derived. The water vapor information needed to make this correction is retrieved from the 18 and 21 GHz SMMR measurements (Prabhakara et al 1982).

To illustrate that the values of R chosen for night and day are reasonable we show in Fig. 2 graphs of R vs $T_{6.6}^{V}$ for night and day observed by SMMR close to 53° N and 145°W. This figure shows that as $T_{6.6}^{V}$ increases, generally R decreases. The threshold of R, 1.7 for day and 1.72 for night, as can be seen from the figure eliminates from SST retrieval a considerable number of SMMR observations that are affected by atmospheric and surface conditions.

It is obvious from Fig. 1A that the SST derived from day and night SMMR measurements, as explained above, will have a systematic bias that has opposite behavior in the northern and sourthern hemispheres. This latitudinally dependent bias is reduced explicitly such that the day and night measurements agree with one another.

In addition to the screening of the data on the basis of R values a spatial filter is applied to eliminate large noise in the data. This

filter eliminates SST data that differ by more than 2°C with respect to the average of an area 2° latitude x 6° longitude surrounding a given point.

In Fig. 3 the December 81 global map of the SST derived from night and day measurements of SMMR is shown to illustrate the overall capability of the method described in this paper.

The estimation of SST made from SMMR data in this study is not influenced by any statistical techniques or by fine tuning to correct for calibration errors. Such a method is helpful to assess the basic quality of SMMR measurements for the purpose of estimating SST.

References:

Milman, A. and T. Wilheit, (1983)
"Sea surface temperatures from the Nimbus-7 Scanning Multichannel Microwave Radiometer."
Appendix A: Satellite-Derived Sea Surface Temperature: Workshop-1 Report; J. P. L. Publication 83-84, Jet Propulsion Laboratory, Pasadena, California.

Prabhakara, C., H. D. Chang, and A. T. C. Chang, (1982)
"Remote sensing of precipitable water over the oceans from Nimbus-7 microwave measurements" Jour. of App. Met., Vol. 21, pp 59-68.

Wilheit, T. T., (1979)
"A model for the microwave emissivity of the ocean's surface as a function of wind speed"
IEEE Transactions on Geoscience Electronics, Vol. G-E, No. 4, pp. 244-249.

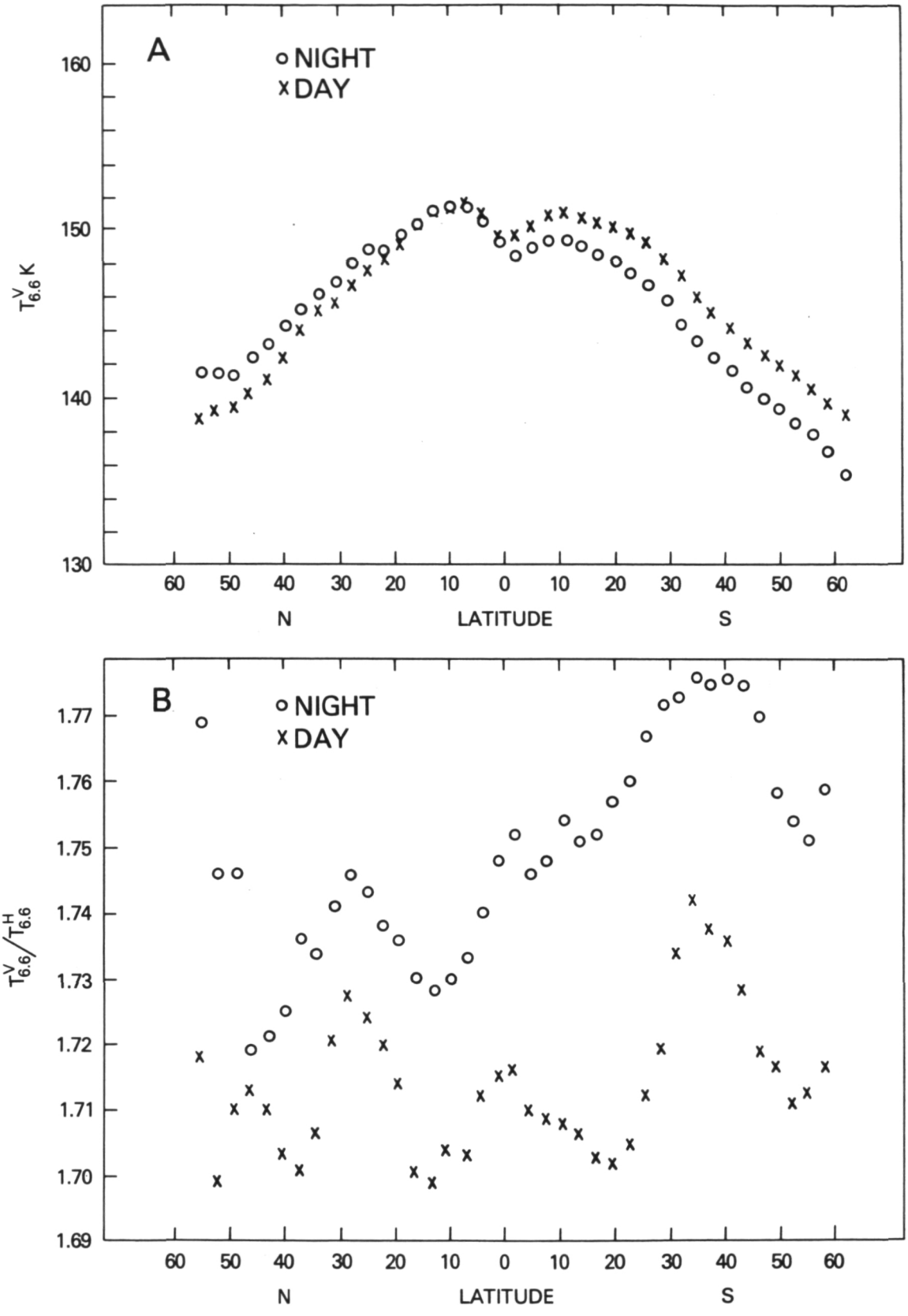

Fig. 1A. Zonal mean variation of $T^V_{6.6}$ as a function of latitude for night and day.

B. Polarization ratio variation with respect to latitude for night and day.

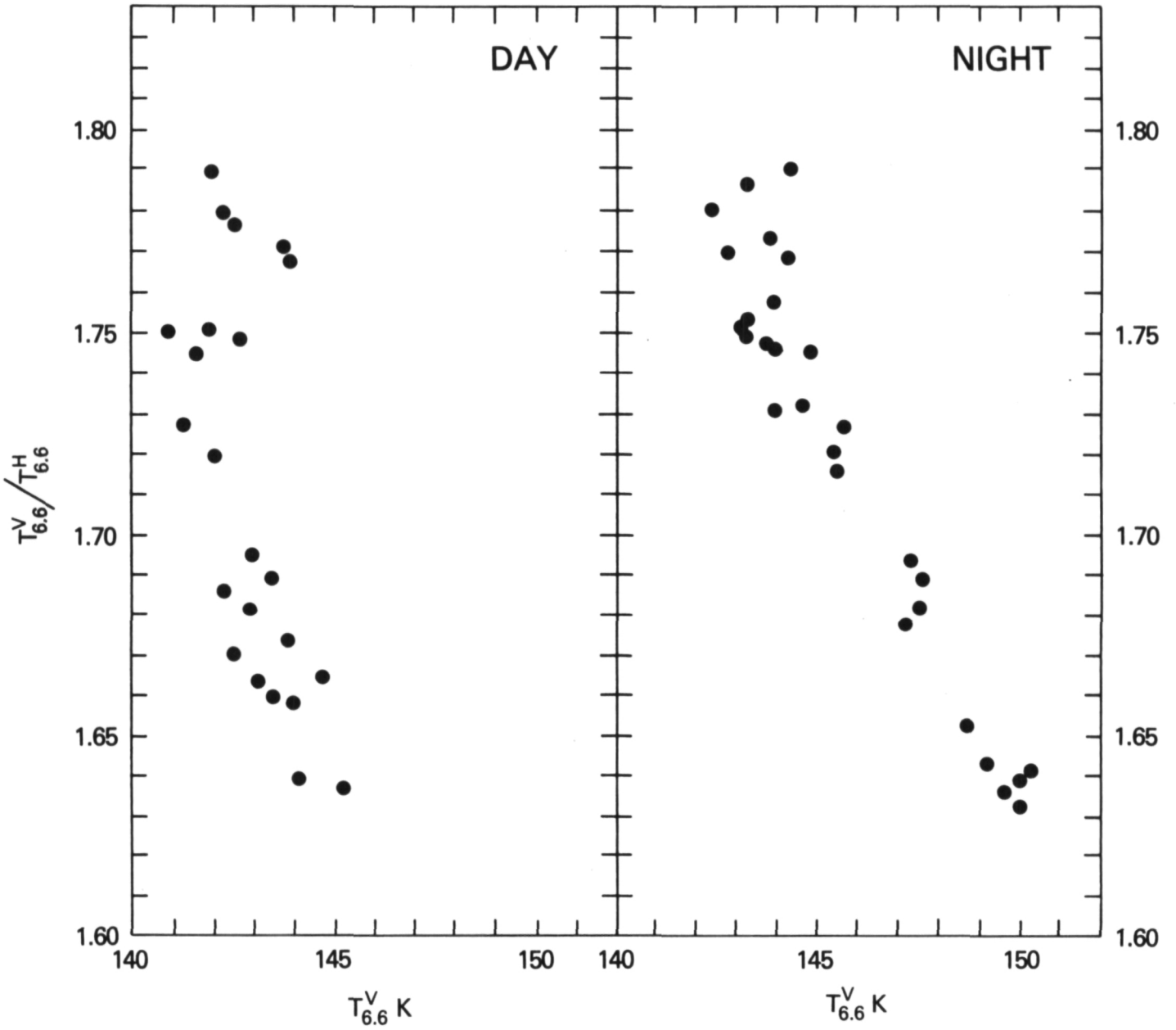

Fig. 2. Polarization ratio as a function of $T^V_{6.6}$ during day and night near 53°N and 145°W.

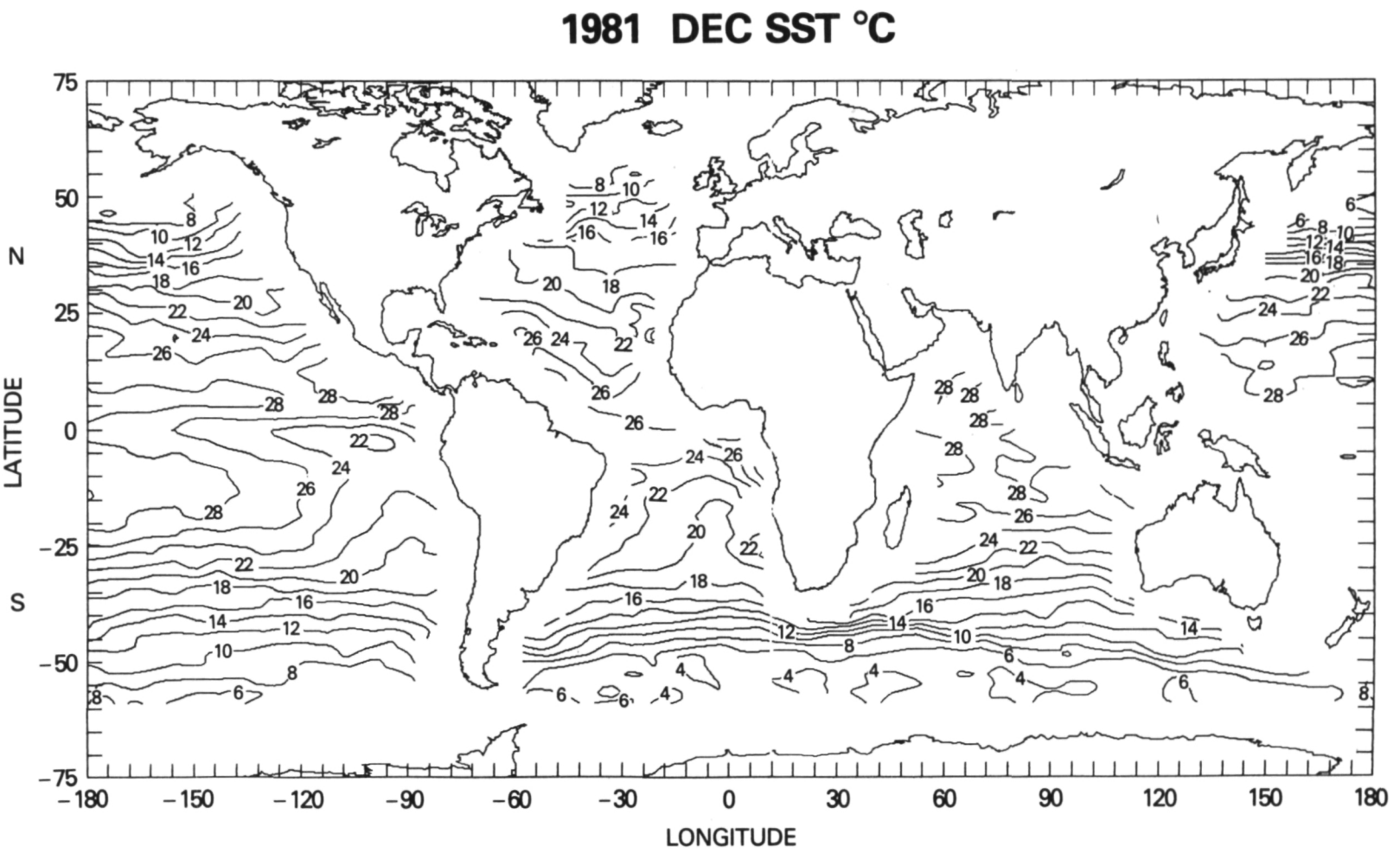

Fig. 3. Combined night and day Nimbus-7 SMMR measured sea surface temperature.

NIMBUS-7 SMMR-DERIVED SEA SURFACE TEMPERATURES:

COMPARISONS WITH THE SEASAT SMMR

Eni G. Njoku
Indu R. Patel

Jet Propulsion Laboratory
4800 Oak Grove Drive
Pasadena, CA 91109

Abstract

Nimbus-7 SMMR data were processed from raw data to sea surface temperatures at JPL to enable performance comparisons between Seasat and Nimbus-7 SMMR instruments. Data were analyzed at antenna temperature, brightness temperature, and geophysical levels, for September 1978 (Seasat) and December 1981 (Nimbus). Results show calibration and polarization coupling differences between the two instruments that vary between channels. Largest differences occur at the 21 GHz frequency. By adjusting the SMMR channel biases, Seasat algorithms can be applied to Nimbus data to obtain sea surface temperatures of comparable accuracy to those derived using Nimbus-specific algorithms.

1. Introduction

The Scanning Multichannel Microwave Radiometer (SMMR) operates at five frequencies: 6.6, 10.7, 18, 21 and 37 GHz, each with horizontal and vertical polarization, for a total of ten independent data channels. The SMMR was flown on two satellite missions: Seasat (June 28 - October 10, 1978) and Nimbus-7 (October 24, 1978 - present). Since the missions did not overlap, no direct comparisons of sensor performance could be made. The two SMMR instruments were identical in design, but pre-launch calibration tests and in-orbit engineering assessments showed significant differences in component losses, effects of sensor heating, polarization coupling, and overall calibration between the two instruments. The purpose of this study is to examine some of these instrument differences and their effects on the SMMR ability to measure sea surface temperature.

The Pacific ocean was chosen as the region for study between 55°S to 55°N and 100°E to 290°E. Measurements of sea surface temperature (SST) from the SMMR on Seasat were discussed previously by Njoku and Swanson (1983). Figure 1(a) shows Seasat monthly-averaged SST contour map for August 1978. Figure 1(b) shows the SST anomaly map formed by subtracting August climatological SSTs from the SMMR-derived values. The August climatology is that of Levitus (1977). Notable in Figure 1(b) are warm SST anomalies in the northwest and south Pacific. The south Pacific anomalies were due to a Seasat retrieval algorithm bias at cold ocean temperatures (below $\sim$10°C).

(a)

(b)

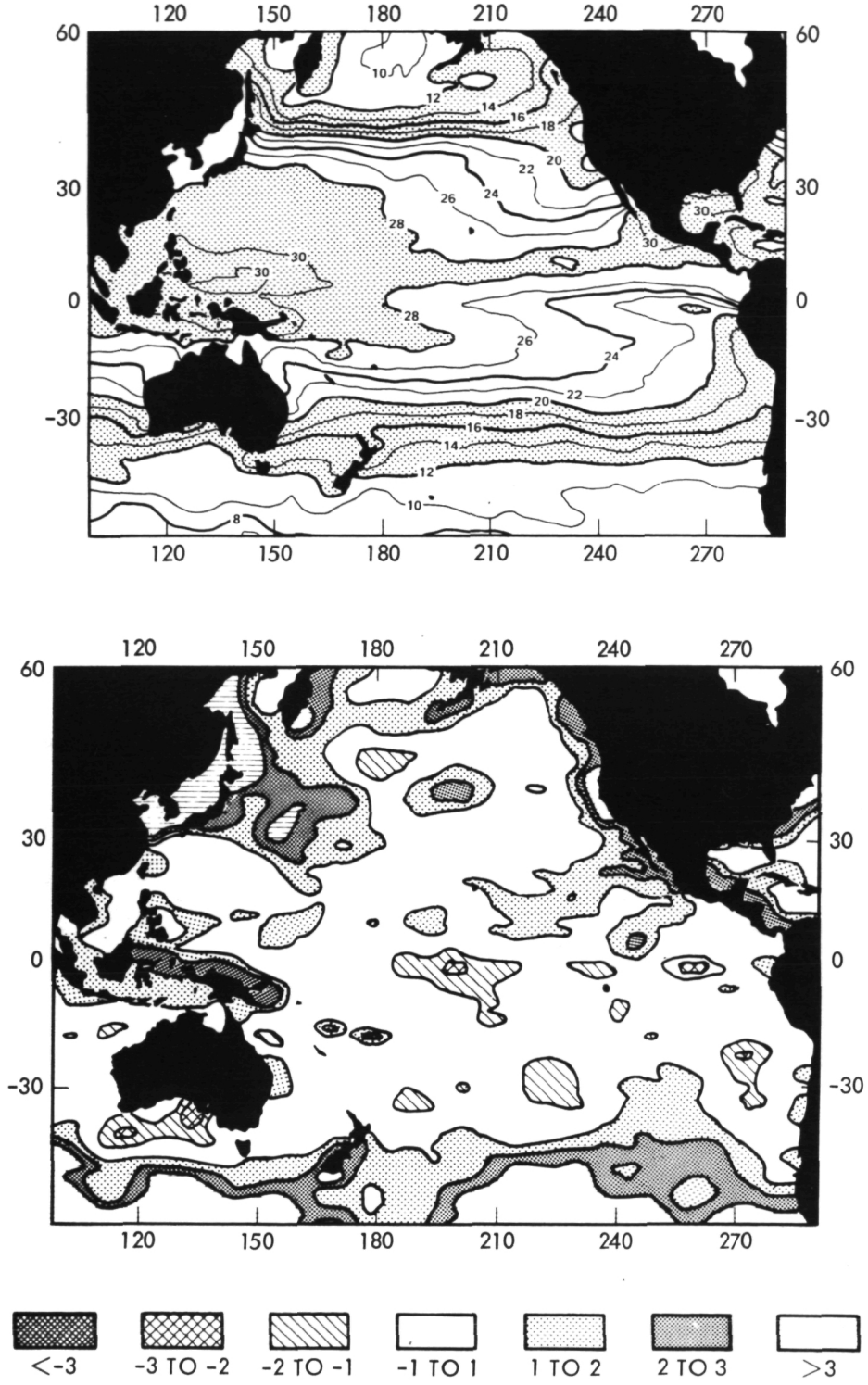

Figure 1. Seasat SMMR Sea Surface Temperature Measurements for August, 1978: (a) Monthly averaged SST contour map, (b) Monthly averaged SST difference from climatology.

For an indirect but quantitative comparison between the two SMMRs, a mid-ocean region was selected: 50°S to 50°N, 180° to 230°E (North and South Pacific). In this region, histograms of 2° latitude by 2° longitude monthly-averaged brightness temperatures were generated for all ten SMMR channels. The Seasat histograms were generated for the month of September 1978, while Nimbus histograms were generated for December 1981. December 1981 was used for Nimbus since it is the month for study in SST Workshop-II. (Future Nimbus SMMR studies in Workshop-III will include July 1982, which can be more directly compared for seasonal compatibility with Seasat SMMR data of July, 1978.) Due to the seasonal difference between August, 1978 and December, 1981 some differences in the monthly brightness temperature histograms are to be expected for geophysical and not instrument-related reasons. However, these differences have been minimized by using data equally from northern and southern hemispheres.

Comparisons of the ten-channel brightness temperature histograms indicate bias differences between the Seasat and Nimbus instruments. By adjusting the bias levels of the Nimbus brightness temperatures the Seasat SST retrieval algorithms were applied directly to the Nimbus data, to investigate the portability of geophysical algorithms from one sensor to the other. The difference in antenna beam earth-incidence angles between Seasat and Nimbus-7 (48.8° versus 50.2) will contribute slightly to the brightness temperature biases.

2. Data Processing

Nimbus SMMR data were processed from the raw (TAT tape) level. The data were calibrated to antenna temperatures using the Nimbus project SMMR calibration algorithm obtained from the NASA (Goddard Space Flight Center). The ten channels of SMMR data were then interpolated along-scan and along-track to coincide with locations of the 37 GHz vertical data points. Data sample locations for a short section of the swath are shown in Figure 2, (alternate half-scans only). Twenty-seven useful data points are shown sinusoidally distributed across each half-scan. With all ten channels co-registered, polarization coupling effects can be straightforwardly corrected.

As discussed by Njoku (1980) the SMMR antenna causes coupling between horizontal and vertical polarizations at each frequency. In addition coupling may be caused by polarization-switch leakages. Thus, the measured antenna temperatures are related to the true brightness temperatures by equations of the form:

$$T_{A_p} = T_{B_p}\left[a_{pp}\cos^2\phi + a_{pq}\sin^2\phi + (a_{pp}\,a_{pq})^{1/2}\sin 2\phi\cos\beta_p\right] + T_{B_q}\left[a_{pp}\sin^2\phi + a_{pq}\cos^2\phi - (a_{pp}\,a_{pq})^{1/2}\sin 2\phi\cos\beta_p\right] \quad (1)$$

where p = v (vertical) and q = h (horizontal), or vice-versa, and is the antenna scan angle which oscillates between ±25°. (Space-viewing but not earth-viewing antenna sidelobes have been accounted for in these

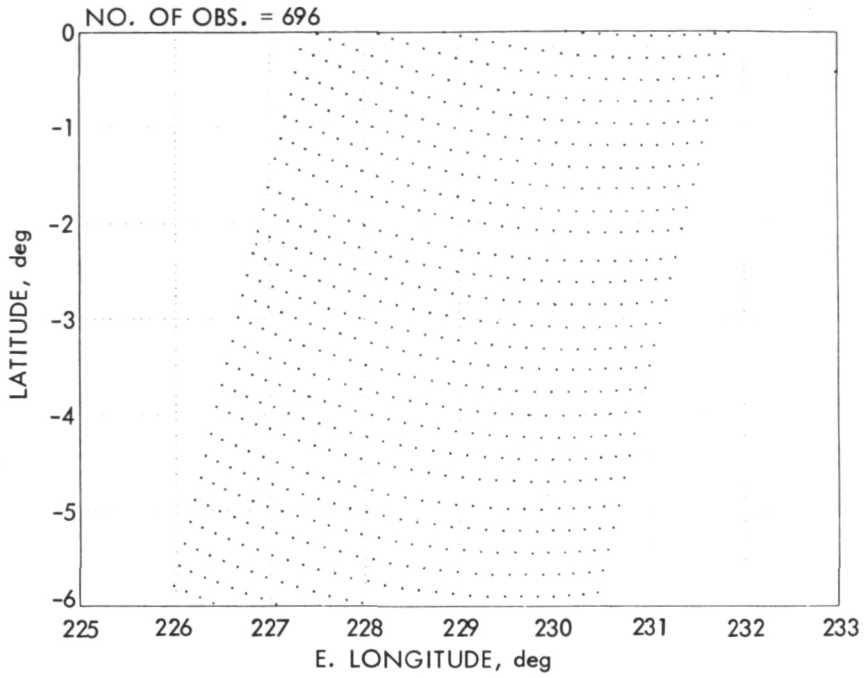

Figure 2. Locations of 37 GHz Vertical Data Samples (to which all channels were interpolated) in short section of Nimbus SMMR swath

equations). The constants a_{pp} and a_{pq} are co- and cross-polarization coefficients respectively ($a_{pq} = 1 - a_{pp}$), and cos β_p is a phase factor. Ideally, a_{pq} is very small, and cos β_p is zero. Non-zero cos β_p results in asymmetry of the measured antenna temperatures about the center scan position ($\phi = 0$) when viewing a scene of supposedly uniform brightness.

Although the a_{pp} and a_{pq} coefficients were measured prior to launch, unknown losses may have occurred. In addition the cos β_p factors were not measured prior to launch. Hence these coefficients had to be fine-tuned empirically post-launch. This was done by averaging SMMR antenna temperature measurements at individual scan positions, over fixed ocean regions for a large number of orbits. This procedure approximately averaged out meteorological noise and provided an approximately uniform brightness scene. Figure 3 shows resulting antenna temperature curves illustrating a good case of symmetry (10.7 GHz horizontal) and a poor case (21 GHz vertical). These curves were fitted to the theoretical expression given in (1) by empirical adjustment of the coefficients. Once determined, these coefficients were used unchanged for further data processing since they are instrument-related and not geophysics-dependent. This procedure is similar to that discussed by Gloersen et al. (1980).

(a)

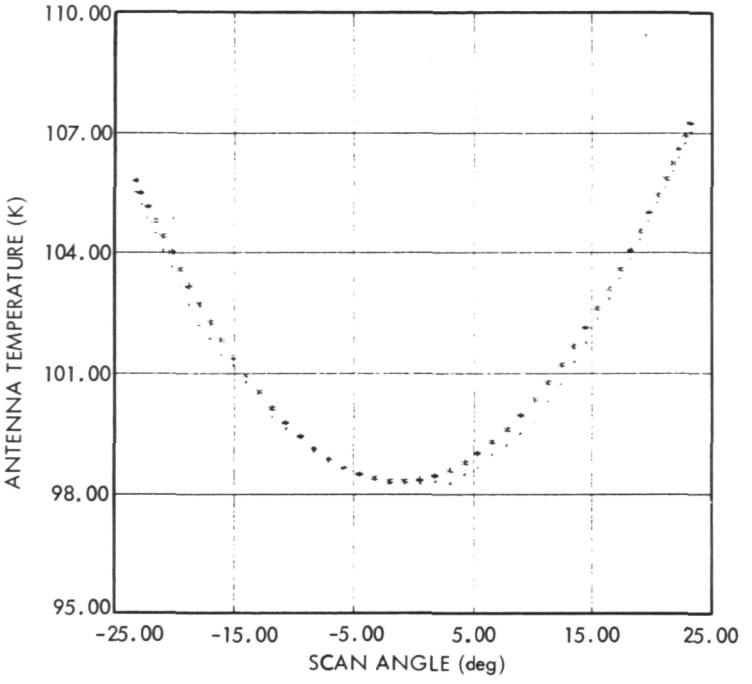

(b)

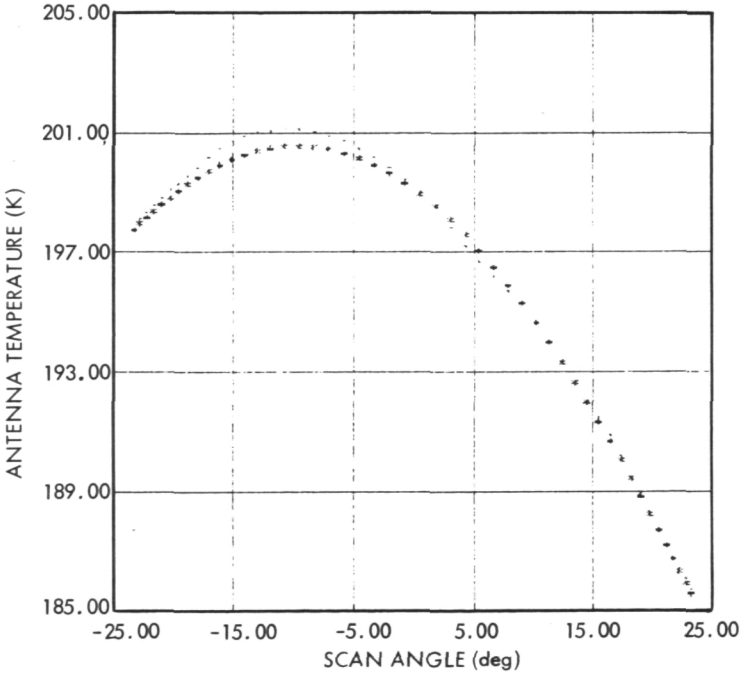

Figure 3. Measured Antenna Temperature Data (dots) and Theoretical Curve Fits using Equation (a) (asterisks) Illustrating Cross-scan Asymmetry: (a) 10.7 GHz horizontal, (b) 21 GHz vertical.

The results of these fits are shown in Figure 3 for the two channels illustrated (10.7 H and 21 V).

Once the coefficients have been empirically determined, Equation (1) can be used to compensate the antenna temperatures for polarization coupling, and hence obtain brightness temperatures (which are correct except for effects of antenna side lobes). Figure 4 shows the extent of the asymmetry correction required for each Nimbus SMMR channel, in terms of total cross-track brightness temperature difference. Also shown are values previously obtained in similar manner for the Seasat SMMR. The Nimbus cross-track asymmetries are more severe than Seasat's, particularly at 6.6, 18 and 21 GHz. Although the 21 GHz vertical channel shows a serious anomaly, the 6.6 GHz vertical cross-track bias is more serious for sea surface temperature accuracy. Even though these biases are corrected in the processing algorithms, one might expect better geophysical parameter retrieval accuracies from the Seasat SMMR on the basis of Figure 4.

3. Brightness Temperature Results

Nimbus SMMR brightness temperatures, corrected for polarization coupling but not antenna sidelobes, were computed as described above for Pacific Ocean nighttime data in the month of December 1981. To reduce the data volume, data were binned into 1° by 1° cells between 55°S to

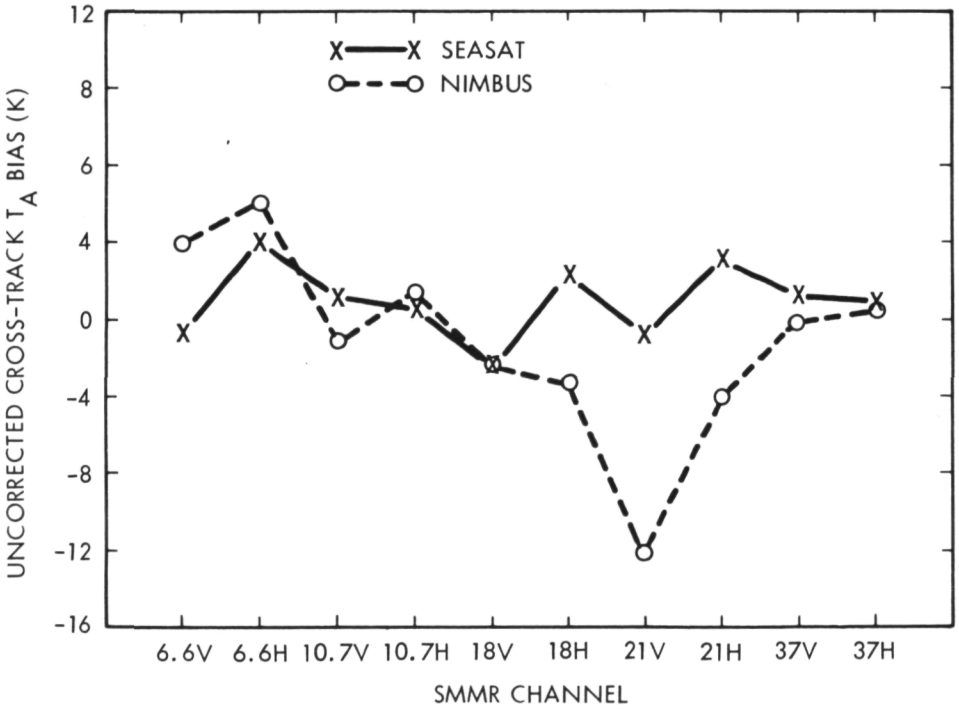

Figure 4. Total Cross-Track Brightness Temperature Correction Required per Channel for Nimbus-7 and Seasat SMMR.

55°N and 100°E to 290°E. Histograms were then made of these data between the longitudes of 180° and 230°E, to cover both north and south latitudes equally, and to keep as far from land as possible (see Figure 1). Similar histograms were made using Seasat SMMR data from September 1978. Sample histograms are shown in Figure 5. The Nimbus and Seasat histograms for all channels have similar standard deviations, but in some cases have significantly different shapes and mean values. Figure 6 plots the differences between histogram means for the ten channels.

The differences between Seasat and Nimbus brightness temperature means shown in Figure 6 cannot be relied upon as purely instrument-related since monthly-averaged ocean features do change significantly from month to month. However, these changes cannot accout for more than a small part of the effects seen in Figure 6. Thus, differences in instrument losses and calibration are the primary factors. These brightness temperatures need to be evaluated over other regions, including land, to make firm conclusions about the consistency of the biases.

4. Sea Surface Temperatures

As mentioned earlier, differences between histogram shapes and means can reflect geophysical as well as instrument-related biases. To test this further, it was assumed that the biases were purely instrumental, and bias offsets shown in Figure 6 were added to the Nimbus SMMR brightness temperatures to bring them into line with the Seasat mean values. As a final step, the Seasat geophysical algorithm (JPL, 1981) was applied to the bias-adjusted Nimbus brightness temperatures to derive sea surface temperature. The equation used was:

$$SST = -230.0 + 2.303\ T_{BGV} - 1.106\ T_{BGH} - 0.042\ C - 0.116\ V\ (°C)$$

where cloud liquid water C (mg/cm^2) and water vapor V (g/cm^2) were estimated using the higher frequency channels (18, 21 and 37 GHz). The 10.7 GHz channels were not used, hence compensation for surface roughness came primarily from the 6.6 GHz horizontal channel while the 6.6 GHz vertical channel provided sensitivity to surface temperature. The limit check on the brightness temperatures was performed to screen out a few obviously erroneous data points, otherwise no other data filtering was performed.

The results are shown in the SST contour plot and SST anomaly contour plot, Figures 7(a) and (b). These show that the major SST features of the Pacific ocean have been identified. However, two significantly anomalous features are visible. First, there is a latitudinal trend in the SMMR SST from cold in the south latitudes to warm in the north. This trend was observed in previous Nimbus SMMR results (Wilheit and Milman, 1983) and was explained as an instrument calibration drift. Wilheit and Milman subsequently made an empirical correction for this effect in their processing algorithm. Secondly, a large warm anomaly occurs in the northwest Pacific. Comparisons with ship and AVHRR anomaly maps indicate that this is an artifact of the SMMR and not a real SST warming in this region. In a separate study, this has been explained by the presence of storms in the region (see elsewhere in the workshop report).

(a)

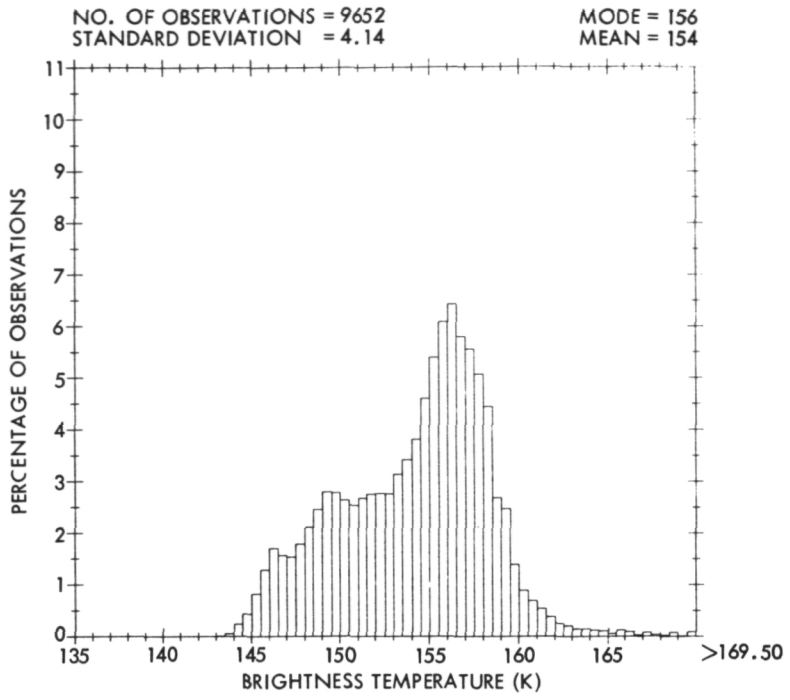

(b)

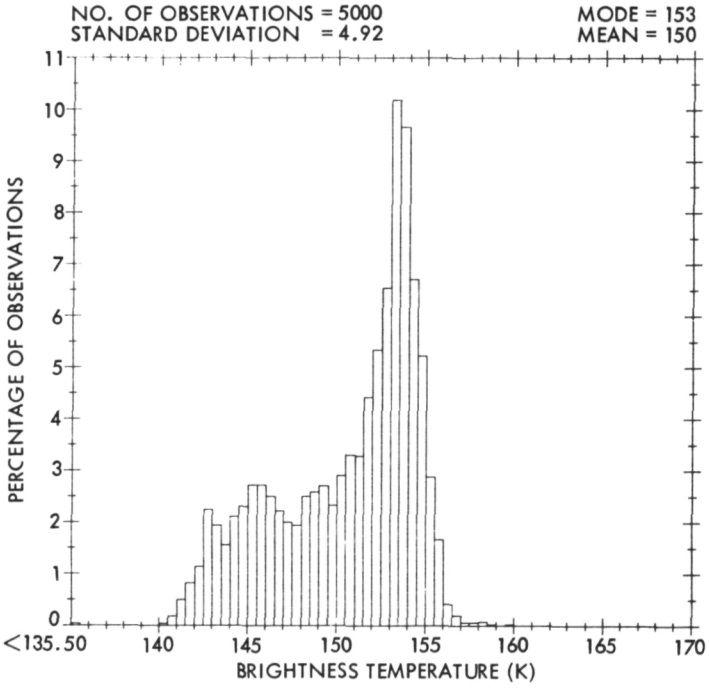

Figure 5. Histograms of Brightness Temperature in Central Pacific Ocean for the 6.6 GHz Vertical Channel: (a) Seasat SMMR, September, 1978; (b) Nimbus SMMR, December, 1981.

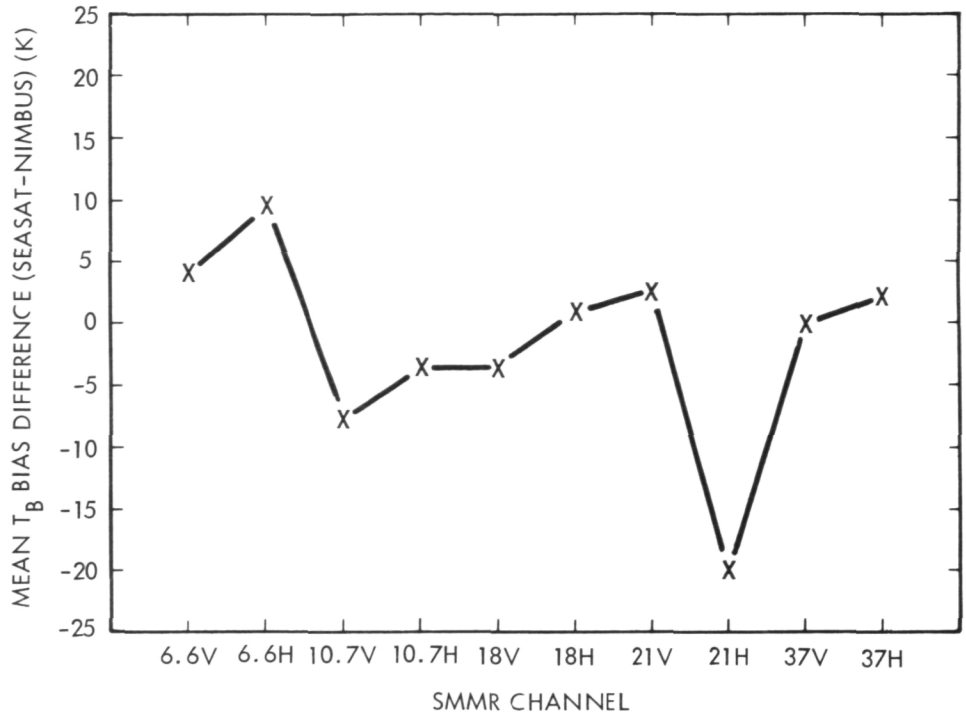

Figure 6. Brightness Temperature Histogram Mean Differences (Seasat Minus Nimbus).

5. Conclusions

This paper has presented preliminary results from a study of Seasat and Nimbus SMMR data in the Pacific ocean. Although, different months were used conclusions can be drawn from this work as follows: (1) Polarization coupling is more pronounced in Nimbus than in Seasat SMMR and is especially bad at 21 GHz vertical. (2) Significant differences in ocean brightness temperature occur between Seasat and Nimbus SMMRs which are related to instrument losses and calibration. (3) Once these bias offsets are accounted for, SST algorithms can be applied interchangeably between SMMR sensors. (4) More detailed study may be required to learn the exact causes of the instrumental biases.

6. References

Gloersen, P., D. J. Cavalieri, and H. V. Soule, "An alternate algorithm for correction of the SMMR polarization radiances using Nimbus-7 observed data", NASA Tech. Memo. #80672, Goddard Space Flight Center, Greenbelt, MD, 1980.

JPL, "SMMR Mini-Workshop IV (Appendix)", Publication #622-234, Jet Propulsion Laboratory, Pasadena, CA, 1981.

(a)

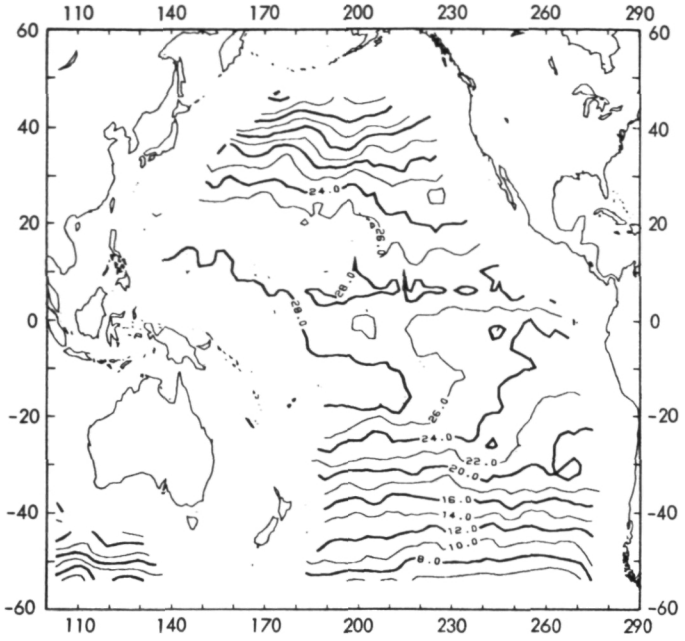

(b)

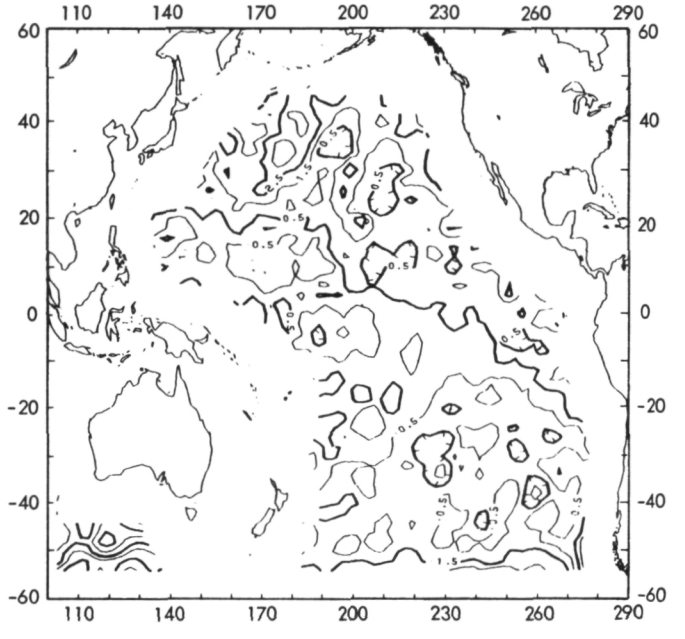

Figure 7. (a) Pacific Ocean SST Contour Map for December, 1981 using Seasat Algorithms Applied to Nimbus SMMR Data. (b) SST Anomaly Map for Same Month and Region, Obtained by Differencing the Reynolds December Climatology from SMMR SST.

Levitus, S. and A. H. Oort, "Global analysis of oceanographic data", Bull. Amer. Met. Soc., 58, 1270-1284, 1977.

Milman, A. and T. Wilheit, "Sea surface temperatures from the Nimbus-7 SMMR", Satellite-Derived Sea Surface Temperature: Workshop-I, Publication #83-34, Jet Propulsion Laboratory, Pasadena, CA, 1983.

Njoku, E. G., "Antenna pattern correction procedures for the Scanning Multichannel Microwave Radiometer (SMMR)", Boundary-Layer Meteorol., 18, 79-98, 1980.

Njoku, E. G. and L. Swanson, "Global measurements of sea surface temperature, wind speed, and atmospheric water content from satellite microwave radiometry", Mon. Wea. Rev., (accepted), 1983.

APPENDICES

APPENDIX A
ADDENDUM TO THREE-WAY ERROR PARTITIONING ANALYSIS

S. Pazan (SIO)

In the first workshop (Ref. 1) application of 3-way error partitioning allocated the smallest errors to climatology. This is obviously an artifact of the method, but it is related to something which may be more fundamental than the "error" as defined by the partitioning scheme: the signal to noise ratio of each sensor. This can be seen as follows, starting with Appendix G of Ref. 1 and continuing with the same definitions.

$$\langle \varepsilon_1^2 \rangle = (D_{12} + D_{13} - D_{23})/2$$

$$\langle \varepsilon_2^2 \rangle = (D_{23} + D_{12} - D_{13})/2$$

if $T_1 = 0$ (climatology), then

$$D_{13} = \langle T_3^2 \rangle \; ; \; D_{12} = \langle T_2^2 \rangle \; ; \; D_{23} = \langle (T_3 - T_2)^2 \rangle$$

Therefore,

$$\langle \varepsilon_1^2 \rangle = \langle T_2 \, T_3 \rangle$$

$$\langle \varepsilon_2^2 \rangle = \langle T_2^2 - T_2 \, T_3 \rangle$$

$$\frac{\langle \varepsilon_2^2 \rangle}{\langle T_2^2 \rangle} = 1 - \frac{\langle \varepsilon_1^2 \rangle}{\langle T_2^2 \rangle}$$

$$\langle \varepsilon_1^2 \rangle = \langle T_2^2 \rangle - \langle \varepsilon_2^2 \rangle$$

We can show that if the error of the "climatology sensor" is less than or equal to the error of sensor 2, then the signal-to-noise ratio of instrument 2 exceeds a threshold value of 0.707. First, assume

$$1 \geq \langle \varepsilon_1^2 \rangle / \langle \varepsilon_2^2 \rangle = \frac{T_2^2}{\langle \varepsilon_2^2 \rangle} - 1 = \frac{1}{(S/N)_2^2} - 1$$

Then,

$$(S/N)^2 \geq 1/2 \text{ or } \left.\frac{\text{SIGNAL}}{\text{NOISE}}\right|_{\text{sensor\#2}} \geq 1/\sqrt{2}$$

Likewise, if the sensor 3 error is greater than the error of the "climatology sensor", the signal-to-noise of sensor 3 exceeds 0.707. A general expression for signal to noise is:

$$(S/N)_1 = \left(1 + \frac{\langle \varepsilon_1^2 \rangle}{\langle \varepsilon_i^2 \rangle}\right)^{-1/2} \quad ; \quad i = 2, 3$$

REFERENCE

1. Jet Propulsion Laboratory, "Satellite-Derived Sea Surface Temperature: Workshop-I," JPL Publication 83-34, Jet Propulsion Laboratory, Pasadena, CA, 1983.

APPENDIX B

SATELLITE-DERIVED SEA SURFACE TEMPERATURE WORKSHOP-II

June 22-24, 1983

Jet Propulsion Laboratory
(Building 180, Room 101)

FINAL PROGRAM

Wednesday, June 22: Investigator Working Sessions

09:00 Preliminaries
09:05 Introduction
09:15 Poster Summaries
09:45 Review of Global Data Sets - I (E. Njoku)
10:30 Break
10:50 Review of Global Data Sets - II (E. Njoku)
12:15 Lunch
13:30 Discussion Group: Atmospheric Corrections to IR Measurements (D. Hagan)
15:00 Break
15:15 Discussion Group (Contd.)
16:30 Wrap-up
18:00 Social Event

Thursday, June 23: Symposium Presentations

08:30 REGISTRATION
09:00 WELCOME (Dr. A. Albee, JPL Chief Scientist)
09:05 INTRODUCTION (E. Njoku)
09:10 SESSION ONE: AVHRR STUDIES - (1) (Chairman: T. Barnett)

1. Multichannel Sea Surface Temperatures from the AVHRR on NOAA-7 (E. P. McClain, NOAA/NESDIS)

2. Intercomparison of SST at 0^{o}, 110^{o}W: NOAA GLOBAL analysis versus In Situ Observations (D. Halpern, NOAAA/PMEL)

3. Satellite Sea Surface Temperature Estimation in the Eastern Tropical Pacific Ocean (R. L. Bernstein, SeaSpace and P. Pullen, NOAA/PMEL)

4. Accuracy of NOAA-7 Observed SST in the Northeast Pacific Ocean (S. Tabata, Inst. of Ocean Sci., Canada)

5. NOAA-7 Ship satellite Comparisons in the Eastern Atlantic (D. Llewellyn-Jones, P. Minnett and A. M. Zavody, Rutherford-Appleton Lab., England) -- POSTER PAPER

10:30 - 10:50 BREAK
10:50 - 12:30 SESSION TWO: AVHRR STUDIES - (2) (Chairman: D. Hagan)

1. NOAA-7 Multichannel Sea Surface Temperature (MCSST) within the Gulf of Mexico Region (J. D. Hawkins, NORDA)

2. Investigation of the Applicability of the Multiple-Channel Technique on Inland Water Bodies (A. R. Condal, H. V. Le, and G. J. Irbe Atmos, Env. Service, Canada)

3. Mesoscale Features Along the First Oyashio Intrusion (A.C. Vastano, Texas A & M Univ., and R. L. Bernstein, SeaSpace)

4. Thermal Time-Series of Warm Core Ring 82B (O.B. Brown and R. Evans, Univ. of Miami)

12:30 - 13:45 LUNCH
13:45 - 15:05 SESSION THREE: OTHER TECHNIQUES (Chairman: T. Wilheit)

1. Summary of a Two-Satellite Method for Measurement of SST Including Comparisons with Ground Truth and MCSST Values (R. Holyer, NORDA)

2. Sea Surface Temperatures from the VAS (J. Bates, Univ. of Wisconsin)

3. A Technique for Calculating Sea Surface Temperatures with Higher Spatial Resolution from Nimbus-7 SMMR Radiances (P. Gloersen, NASA/SFC)

4. Meteorological Conditions and SMMR-Derived Sea Surface Temperatures in the North Pacific (S. Bowling, Univ. of Alaska)

15:05 - 15:25 BREAK
15:25 - 16:45 SESSION FOUR: GLOBAL SST COMPARISONS (Chairman: E. Njoku)

1. Summary of Global Comparison Approach (E. G. Njoku, JPL)

2. Summary of Available In Situ Data (S. Pazan, JPL/SIO)

3. Description of Satellite Intercomparison Data Sets (D. B. Chelton, Oregon State Univ.)

4. Satellite and In Situ SST Comparisons (R. L. Bernstein, SeaSpace)

*09:00 - 16:45 POSTER SESSION: GLOBAL SATELLITE SST RETRIEVALS

1. NOAA Satellite-Derived Operational SST Products (E. P. McClain, NOAA/NESDIS)

2. Measurement of Sea Surface Temperature from HIRS2/MSU Data (J. Susskind, NASA/GSFC)

3. Use of VAS Multispectral Data for Sea Surface Temperature Determination (J. Bates, Univ. of Wisconsin)

4. Sea Surface Temperatures from the Nimbus-7 SMMR (A. S. Milman, Systems & Appl. Sci., and T. T. Wilheit, NASA/GSFC)

5. Estimation of Sea Surface Temperature from the Nimbus-7 SMMR (C. Prahakara, NASA/GSFC, I. Wang, Comp. Sci. Corp., and D. Short, (NASA/GSFC)

6. Nimbus-7 SMMR-Derived Sea Surface Temperatures (E. G. Njoku, JPL)

(*Posters will remain on display through Friday, June 24)

18:30 - COCKTAILS AND HORS D`OEUVRES (CALTECH ATHENAEUM)

Friday, June 24: Round-Table Discussions, Future Prospects & Plans

08:45 - 09:00	RE-CONVENE	
09:00 - 10:30	SESSION ONE:	Review of Workshop Results--Satellite Sea Surface Temperature Accuracy (D. B. Chelton, Orgen State Univ., discussion leader)
10:30 - 10:45	BREAK	
10:45 - 12:00	SESSION TWO:	Oceanographic Requirements for Satellite SST Measurement (T. P. Barnett, Stripps Inst. of Oceanog., discussion leader)
12:00 - 13:00	LUNCH	
13:00 - 14:15	SESSION THREE:	Development of New Satellite Sensors and Techniques (E. G. Njoku, JPL, discussion leader)
14:15 - 14:30	BREAK	
14:30 - 16:00	WRAP-UP SESSION:	Agenda for Workshop-III

APPENDIX C

List of Workshop-II Participants

Name	Affiliation
M. Abbott	Jet Propulsion Laboratory, Pasadena, California
T. Barnett	Scripps Institution of Oceanography, La Jolla, California
J. Bates	University of Wisconsin, Madison, Wisconsin
R. Bernstein	SeaSpace, San Diego, California
M. Boswell	Royal Aircraft Establishment, Farnborough, England
S. Bowling	University of Alaska, Fairbanks, Alaska
A. Bratkovitch	Scripps Institution of Oceanography, La Jolla, California
J. Brown	Jet Propulsion Laboratory, Pasadena, California
O. Brown	University of Miami, Miami, Florida
M. Chahine	Jet Propulsion Laboratory, Pasadena, California
D. Chelton	Oregon State University, Corvallis, Oregon
D. Collins	Jet Propulsion Laboratory, Pasadena, California
A. Condal	Atmospheric Environment Service, Downsview, Ontario, Canada
P. Cornillon	University of Rhode Island, Narragansett, Rhode Island
R. Dixon	
R. Evans	University of Miami, Miami, Florida
L. Fu	Jet Propulsion Laboratory, Pasadena, California
C. Gautier	Scripps Institution of Oceanography, La Jolla, California
P. Gloerson	NASA/Goddard Space Flight Center, Greenbelt, Maryland
D. Hagan	Jet Propulsion Laboratory, Pasadena, California
D. Halpern	NOAA/Pacific Marine Environmental Laboratory, Seattle, Washington
J. Hawkins	Naval Ocean Research & Development Activity, NSTL Station, Mississippi
J. Hilland	Jet Propulsion Laboratory, Pasadena, California
D. Hogan	RCA Astro, Princeton, New Jersey
R. Holyer	Naval Ocean Research & Development Activity, NSTL Station, Mississippi
J. Huang	NOAA/Office of Climate & Atmospheric Research, Washington, D.C.
P. Hwang	NASA/Goddard Space Flight Center, Greenbelt, Maryland
G. Irbe	Atmospheric Environment Service, Downsview, Ontario, Canada
G. Kleppel	University of Southern California, Los Angeles, California
T. Liu	Jet Propulsion Laboratory, Pasadena, California
D. Llewellyn-Jones	Rutherford Appleton Laboratory, Chilton, England
P. May	Naval Ocean Research & Development Activity, NSTL Station, Mississippi
P. McClain	NOAA/National Environmental Satellite, Data, & Information Service, Washington, D.C.
A. Milman	Systems & Applied Sciences Corporation, Hyattsville, Maryland
E. Njoku	Jet Propulsion Laboratory, Pasadena, California
S. Pazan	Scripps Institution of Oceanography, La Jolla, California
R. Pieper	University of Southern California, Los Angeles, California
C. Prabhakara	NASA/Goddard Space Flight Center, Greenbelt, Maryland
H. Press	Jet Propulsion Laboratory, Pasadena, California

List of Workshop-II Participants (Continued)

Name	Affiliation
A. Rosenberg	RCA Astro, Princeton, New Jersey
H. Shin	University of British Columbia, Vancouver, B.C., Canada
M. Van Woert	SeaSpace, San Diego, California
A. Vastano	Texas A&M University, College Station, Texas
T. Wilheit	NASA/Goddard Space Flight Center, Greenbelt, Maryland
D. Wylie	University of Wisconsin, Madison, Wisconsin

NASA—JPL—Coml., L.A., Calif.